UNIVERSITY OF ALBERTA

Dynamic Simulation of an Utility Boiler's Natural-Circulation Circuit

BY

Ricky Leung

A THESIS
SUBMITTED TO THE FACULTY OF GRADUATE STUDIES AND RESEARCH
IN PARTIAL FULFILLMENT OF THE REQUIREMENTS FOR THE DEGREE OF
MASTER OF SCIENCE

DEPARTMENT OF CHEMICAL AND MATERIALS ENGINEERING

EDMONTON, ALBERTA
FALL, 1997

National Library of Canada
Acquisitions and Bibliographic Services
395 Wellington Street
Ottawa ON K1A 0N4
Canada

Bibliothèque nationale du Canada
Acquisitions et services bibliographiques
395, rue Wellington
Ottawa ON K1A 0N4
Canada

Your file Votre référence

Our file Notre référence

The author has granted a non-exclusive licence allowing the National Library of Canada to reproduce, loan, distribute or sell copies of this thesis in microform, paper or electronic formats.

L'auteur a accordé une licence non exclusive permettant à la Bibliothèque nationale du Canada de reproduire, prêter, distribuer ou vendre des copies de cette thèse sous la forme de microfiche/film, de reproduction sur papier ou sur format électronique.

The author retains ownership of the copyright in this thesis. Neither the thesis nor substantial extracts from it may be printed or otherwise reproduced without the author's permission.

L'auteur conserve la propriété du droit d'auteur qui protège cette thèse. Ni la thèse ni des extraits substantiels de celle-ci ne doivent être imprimés ou autrement reproduits sans son autorisation.

0-612-22625-5

Canada

UNIVERSITY OF ALBERTA

LIBRARY RELEASE FORM

Name of Author: RICKY LEUNG

Title of Thesis: Dynamic Simulation of an Utility Boiler's Natural-Circulation Circuit

Degree: Master of Science

Year this Degree Granted: 1997

Permission is hereby granted to the University of Alberta Library to reproduce single copies of this thesis and to lend or sell such copies for private, scholarly, or scientific research purposes only.

The author reserves all other publication and other rights in association with the copyright in the thesis, and except as hereinbefore provided, neither the thesis nor any substantial portion thereof may be printed or otherwise reproduced in any material form whatever without the author's prior written permission.

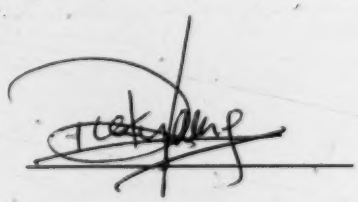

12812 158 Avenue
Edmonton, Alberta
T6V 1A1
Canada

DATE: Aug 26, 97.

UNIVERSITY OF ALBERTA

FACULTY OF GRADUATE STUDIES AND RESEARCH

The undersigned certify that they have read, and recommend to the Faculty of Graduate Studies and Research for acceptance, a thesis entitled **Dynamic Simulation of an Utility Boiler's Natural-Circulation Circuit** submitted by **Ricky Leung** in partial fulfillment of the requirements for the degree of **Master of Science**

Dr. K. Nandakumar

Dr. R.E. Rink

Aug 25/97

Dr. Biao Huang

To my parents Sam and Linda, my sisters Wincy and Vivian, and my wife Vicky

Abstract

The objective of the work described in this thesis is to build a first-principles based dynamic natural-circulation model for an utility boiler. Three models are developed in this thesis, namely a steady-state natural-circulation model from Kakaç *et.al.* (Kakaç, 1991), a transient natural-circulation model modified from the steady-state model, and the hydraulic flow network model based on Porsching *et.al.* (Porsching *et al.*, 1971). The steady-state model serves to examine the accuracy of Kakaç's method for simulating natural circulation. The transient circulation model, intending to improve the defficiency in simulation time of the steady-state model, is incorporated into a complete boiler model, including furnace, superheaters, steam drum, and economizer models which are developed by Chiu (Chiu, 1996). A comparatively detailed approach - the hydraulic flow network from Porsching *et.al.* (Porsching *et al.*, 1971) is examined to evaluate the feasibility to predict more accurate transient dynamics of the circulation.

Acknowledgement

I would like to sincerely thank Dr. Sirish Shah and Dr. Ray Rink for accepting me as their student. I would also like to thank my best friend, Alberta Chiu, for guiding and helping me to work on a variety of problems. Without his help and support I would not have gone that far for sure. I would like to thank my father and mother-in-laws for taking care of my family during my post-graduate studies. I would like to thank my two sister-in-laws who gave me a lot of happy times during my hard studies.

I would like to show my appreciation to my wife's hard work, contribution and support to me. I have to say that your support has ever been important and would never be replaced.

And above all I would like to express my deepest sense of gratitude to my family, my parents and my two sisters because without their love and sacrifices for me over the years, I would never have achieved anything.

Contents

1 Introduction **1**

1.1 Background 1

1.2 Scope and Objectives of Study 2

1.3 Structure of the Thesis 3

2 Description of Utility Boilers of Syncrude Canada Limited **5**

2.1 Introduction 5

2.2 The Components of the Utility Boiler 6

2.2.1 Furnace 6

2.2.2 Superheaters 10

2.2.3 Convective Generation Bank 10

2.2.4 Steam Drum 11

2.2.5 Mud Drum 13

2.2.6 Economizer 13

2.3 Steam Generation of the Utility Boiler 13

2.4 Conclusion 15

3 Two-Phase Flow and Heat Transfer **17**

3.1 Introduction 17

3.2 Two-Phase Flow 18

3.3 Pressure Drop of Two-phase Flow 19

3.3.1 The Homogeneous Flow Model 21

3.3.2 The Separated Flow Model 21

3.3.3 Frictional Pressure Drop 22

3.4 Two-phase Flow Void Correlation 24

3.5 Flow Boiling 27

3.6 Heat Transfer Correlation 28

3.7 Conclusion 34

4 Steam Generation Model Development **36**

4.1 Introduction 36

4.2 Natural Circulation 37

4.3 The Steady-State Natural-Circulation Model 39

4.3.1 Calculation of the Hydraulic Resistance of the Downcomers . 40

4.3.2 Determination of the Density of the Steam-Water Mixture . 41

4.3.3 Calculation of the Hydraulic Resistance of the Risers 41

4.3.4 Calculation of the Hydraulic Resistance of the Steam-Water Separator 45

4.4 Numerical Approach for Solving the Steady-State Model 45

4.5 Results and Discussions of the Steady-State Model 48

4.6 The Transient Natural-Circulation Model 54
4.7 Numerical Approach for Solving the Transient Model 55
4.8 Results and Discussions of the Transient Model 56
4.9 Conclusion 59

5 The Hydraulic Flow Network Model 69

5.1 Introduction 69
5.2 Basic Principles 70
5.3 The Implicit Integration Method for the Hydrodynamic Network System 72
5.4 Derivation of the Hydraulic Network's Formulations 78
5.5 Determination of Pressure and Temperature at Nodes 85
5.6 Node-link Representation of the Hydraulic Network Model 87
5.7 Heat Transfer Model for the Hydraulic Network Model 89
5.7.1 The Implicit Integration Method for the Heat Transfer Model. 96
5.8 The Programming Structure of the Hydraulic Flow Network 97
5.9 Simulation Setup for the Hydraulic Network Model 100
5.10 Results and Discussions of the Hydraulic Network Model 108
5.11 Conclusion 117

6 Conclusions 119

6.1 Recommendations 121

References 122

A Simulink Block Diagrams of the Dynamic Circulation Model 124

B The Derivation of the Homogeneous and Separated Flow Model 133

List of Figures

2.1 Schematic diagram of the UBO. 7

2.2 Schematic diagram of Furnace. 9

2.3 Schematic diagram of the steam drum structure. 12

2.4 The flue gas path in the UBO. 14

3.1 Flow pattern – co-current steam-water flow in a heated vertical tube. 20

3.2 Martinelli-Nelson two-phase friction factor for low quality region. . 23

3.3 Flow boiling in a vertical heated tube. 29

4.1 Circulation characteristic curves of a simple circuit. 49

4.2 Circulation characteristic curves of a complex circuit. 49

4.3 The flow chart of calculating the total circulation rate using bisection method. 50

4.4 The flow chart of calculating the local mass flow using bisection method. 51

4.5 The steam demand from the common header. 60

4.6 The total circulation rate of the steam generation circuit. 60

4.7 The circulation rate of the generation bank. 61

4.8 The steam generation rate of the generation bank. 61

4.9 The circulation rate of the front side walls. 62

4.10 The steam generation rate of the front side walls. 62

4.11 The circulation rate of the middle side walls. 63

4.12 The steam generation rate of the middle side walls. 63

4.13 The circulation rate of the rear side walls. 64

4.14 The steam generation rate of the rear side walls. 64

4.15 The circulation rate of the front wall. 65

4.16 The steam generation rate of the front wall. 65

4.17 The circulation rate of the rear wall. 66

4.18 The steam generation rate of the rear wall. 66

4.19 The circulation ratio of the overall circuit. 67

4.20 The steam quailty generated from the circulation circuit. 67

5.1 A noncritical link. 70

5.2 A critical link. 71

5.3 An 8-node network with 1 critical link. 77

5.4 The structure of the A matrix corresponding to the example network. 77

5.5 The pressure-specific internal energy diagram. 88

5.6 The pressure-specific internal energy diagram. 88

5.7 The schemetic diagram of the generation bank section. 90

5.8 The node-link representation of the generation bank. 91

5.9 The flow diagram for determining the heat transfer coefficient. . . . 94

5.10 The flow diagram of the hydraulic flow network. 101

5.11 The flow diagram of the Update.c algorithm. 102

5.12 The flow diagram of the CaldTw.c algorithm. 103

5.13 The flow diagram of the Calx.c algorithm. 104

5.14 The flow diagram of the CalPT.c algorithm. 105

5.15 The flow diagram of the Sethi.c algorithm. 106

5.16 The flow diagram of the CalTf.c algorithm. 107

5.17 The circulation flow response to the step increase of the flue gas inlet temperature. 111

5.18 The circulation flow response to the step decrease of the flue gas inlet temperature. 111

5.19 The pressure response at node 7 and 8 under a step increase of the inlet flue gas temperature. 112

5.20 The pressure response at node 7 and 8 under a step decrease of the inlet flue gas temperature. 112

5.21 The steam quality response to the step increase of the flue gas inlet temperature. 114

5.22 The steam quality response to the step decrease of the flue gas inlet temperature. 114

5.23 The circulation flow response to the step increase of inlet water enthalpy. 115

5.24 The circulation flow response to the step decrease of inlet water enthalpy. 115

5.25 The response of heat enthalpy at each node under a step increase of inlet water enthalpy. 116

5.26 The response of heat enthalpy at each node under a step decrease of inlet water enthalpy. 116

A.1 First level of the model. 125

A.2 Second level of the model. 126

A.3 Third level of the model. 127

A.4 Third level of the model. 128

A.5 Third level of the model. 129

A.6 Third level of the model. 130

A.7 Third level of the model. 131

A.8 Third level of the model. 132

List of Tables

3.1 The flow factor at different pressure for steam-water data. 26

4.1 Steam and circulation flow at individual circuitry of the steady-state model. 53

4.2 Parameters used to simulate the steady-state model at peak load conditions. 53

4.3 Simulation results of the steady-state model at peak load conditions. 53

4.4 Steam and circulation flow at individual circuitry of the transient model. 57

4.5 Simulation results of the transient model at peak load conditions. . 57

5.1 Measurements of the length and diameter of the links and the volume of the nodes. 89

5.2 The initial conditions of each node and link for the simulation. . . . 109

Nomenclature

A	Cross-sectional area for flow, m^2
C	Slip constant, $C = \alpha/\beta$
C_p	Specific heat at constant pressure, J/kgK
D	Diameter for a tube, m
f	Single-phase friction factor
g	Acceleration of gravity, m/s^2
G	Mass flux, kg/sm^2
h	Convective heat transfer coefficient, J/m^2K
h_d	Height of the downcomers, m
h_{Lo}	Single phase convective heat transfer coefficient, J/m^2K
h_{fg}	Heat of evaporation, kJ/kg
H_{ww}	Radiant heat from combustion, W
J	Jacobian matrix
k	Conductivity for water, W/m^2K
L	Length of a link, m^2
M	Mass of a node, kg
ΔM	Incremental mass of a node, kg
P	Pressure, MPa
ΔP	Pressure drop
Q	Volumetric flow rate, m^3/s
Q	Heat transfer, W
Re	Reynolds number
S	Slip ratio
t	Time, s
Δt	Time step
T	Temperature, K
T_w	Tube wall temperature, K
T_s	Saturation water temperature, K
T_{fi}	Inlet flue gas temperature to generation bank, K
T_{fo}	Exit flue gas temperature from generation bank, K
$\bar{v}$	Specific volume, m^3/kg
$\hat{u}$	Specific internal energy, kJ/kg

U	Internal energy of a node, kJ
ΔU	Incremental internal energy of a node, kJ
v'	Effective specific volume, m^3/kg
V	Volume, m^3, Velocity, m/s
V_o	Circulation velocity, m/s
W	Mass flow, kg/s
ΔW	Incremental mass flow, kg/s
x	Steam quality
dz	Incremental vertical elevation, m
Z	Vertical elevation, m

Greek

α	Void fraction
β	Volumetric quality, Volumetric flow ratio
λ	fictional coefficient
μ	Viscostiy of water, N/m
ξ	Loss coefficient
ρ	Density, kg/m^3
$\bar{\rho}$	Average density, kg/m^3
τ_o	Wall shear stress
χ_{tt}	Lockhart-Martinelli parameter
ψ	Helmholzt function
ϕ^2_{Lo}	Two-phase friction multiplier

Subscripts

d, dc	Downcomers
ec	Economizer section (subcool water)
ev	Evaporator section (saturation steam-water mixture)
i, j	Initial and terminal node
k	Link number for mass flow
f	Saturation liquid state
fg	Flue gas
g	Saturation vapor state
l	Liquid
m	Mixture of steam and water
md	Mud drum
s	Steam
se	Separator
sd	Steam drum
TPF	Two-phase friction

ν	Mass flow path
w, ww	Water wall

Superscripts

$n, n+1$	current and next time step

Chapter 1

Introduction

1.1 Background

An investigation, via modeling and simulation, of the Syncrude Canada Ltd. (SCL) steam/electrical system was proposed due to concerns regarding the stability of the local system under conditions of large transient excursion away from the previous operating point. The transient excursion is mainly caused by the operation of the large draglines during the loading phase at which tens of magawatts of power can be drawn. This significant power demand puts a detectable voltage transient onto the Alberta grid. As a result, the intertie power with Alberta grid is lost due to the protection of the rapid decay of electrical frequency. This phenomena will switch the power dependence to local power generation system and, at this time, the plant electrical load will be highly time varying. Under conditions mentioned, the numerous single-loop controllers can interact strongly and poor stability of the transient recovery has been observed. This may possibily lead to automatic boiler trip and cascading outage or to even complete plant shutdown.

The SCL steam generation system consists of five boilers, three utility boil-

ers (UB) and two carbon monoxide boilers (CB), connected in parallel to a common steam header which supplies steam to bitumen extraction and other plant processes, and for electric power generation by four turbogenerators. Therefore, a erratic variation in or a loss of steam generation would definitely affect the entire plant operation adversely, not only for economic impact but also for safety. Therefore, a dynamic simulation model which studies the steam and the electricity generation system under large transient conditions is essential before modifications for the local system are made to attain desired operating conditions.

1.2 Scope and Objectives of Study

The objectives of this study are to develop a dynamic model for the natural-circulation circuit of the utility boiler which will be combined with the remaining boiler components, such as furnace, superheaters, enconomizer and steam drum developed by Chiu(Chiu, 1996). The complete boiler model will be incorporated with the power generation and steam distribution system models, completing the entire system model.

A steady-state natural-circulation model will first be developed to establish the characteristics of natural circulation. Moreover, the steady-state model will also serve as a guideline to the development of the transient circulation model which is modified from the steady-state model. The transient model will be validated independently using data from reports of SCL. Then, the transient model will be incorporated with the rest of the overall model components. An examination

of the performance of the circulation circuits will be done to validate the steam generation capability.

Another approach, using the hydraulic flow network concept from Porsching *et.al.* for developing a dynamic circulation model, is examined to evaluate the accuracy of predicting the dynamic behavior of natural circulation. A more detailed study of two-phase heat transfer and transient circulation behavior during the change in heat input and subcooling in downcomers will be undertaken.

1.3 Structure of the Thesis

There are six chapters in this thesis. Chapter 1 provides the background for the initiation of the power generation system studies, the scope and objectives of the development for the dynamic circulation model, and the structure of the thesis.

Chapter 2 provides detailed descriptions of the structure of the utility boiler and the principles of steam generation.

Chapter 3 presents the theoretical background for the types of two-phase flow model. The determination of the pressure drop terms is also explained. The related heat transfer correlations used in modeling two-phase flow are fully presented.

Chapter 4 shows the development and validation of the steam generation model using Kackaç *et.al* (Kakaç, 1991) steady-state natural-circulation approach. The transient circulation model is also developed based on the steady-state model. This transient circulation model is validated independently and is incorporated

to the other utility boiler component models with which the performance of the model is analyzed.

Chapter 5 presents the development of the hydraulic flow network model, adopting generation bank as model. The heat transfer model is also developed to accurately study the feasibility of using this approach to predict natural circulation. The detailed derivations of all formulations and methods are shown in addition to analyzing the simulation under different proposed boundary conditions.

Chapter 6 provides concluding remarks and suggestions for future work.

Chapter 2

Description of Utility Boilers of Syncrude Canada Limited

2.1 Introduction

Boilers have evolved into complex and immense heat exchange machines. However, the fundamental function of a boiler unit is to convert water into steam for electricity generation and process applications. For different applications, there are various types of boiler designs characterized by their fuel types, operating pressures, steam-water circulation methods, fuel firing methods and heat transfer surface arrangements. The design objective is then to choose a proper boiler configuration capable of generating desired steam load under certain specific application requirements and restrictions, such as boiler sizes, reliability, fuel availability, environmental protection, and economic factors.

In the Mildred Lake Plant of Syncrude Canada Limited (SCL), there are three utility boilers operating in parallel to generate steam to the 6.6 MPa common header from which steam will be distributed to different process entities. The utility boilers are designed to operate at subcritical pressure [$< 22.1\ MPa$], to

circulate steam-water mixture using natural-circulation method, and to burn refinery gas as fuel. In addition, each utility boiler is designed to generate 94.5 kg/s steam as the normal peak load. The simulation of the utility boiler cannot be implemented without a thorough understanding of its physical structure. Therefore, this chapter will provide a detailed description of the structure of the utility boiler and explain how steam is generated.

2.2 The Components of the Utility Boiler

The utility boiler is a large and complex piece of heat exchange equipment. It is rather difficult to depict every detail of its structure. Therefore, a simplified schematic diagram of the utility boiler is used and shown in Figure 2.1. The utility boiler can be generally divided into sections as follows:

1. Furnace.
2. Superheaters.
3. Steam drum.
4. Mud drum.
5. Convective generation bank.
6. Economizers.

2.2.1 Furnace

Furnace is basically a big metal chamber lined with membrane panels of

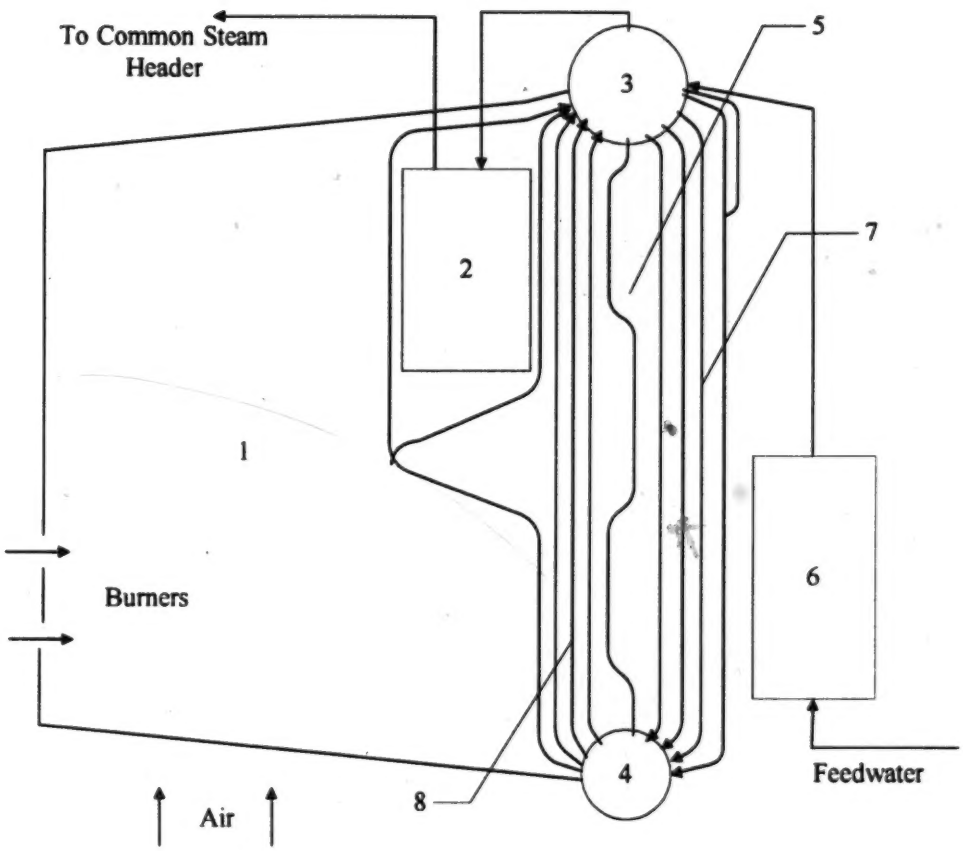

1. Furnace.
2. Superheaters.
3. Steam Drum.
4. Mud Drum.
5. Convective Generation Bank.
6. Economizer.
7. Downcomers.
8. Risers.

Figure 2.1: Schematic diagram of the UBO.

water tubes. It serves as a combustion chamber to produce hot flue gas and radiant heat for steam generation. A total of 482 membrane-panel water tubes of 0.0635 m outer diameter (OD) on 0.0762 m centers cover every surface of the furnace. The tube wall thickness is 0.00419 m. The water walls, besides generating saturated steam, play an important role to protect other metal parts, such as water feeders and boiler shell from temperature related failure. The adoption of membrane-panel water walls is due to their facility in construction and maintenance. They are prefabricated in pieces by manufacturer and fastened together on site using bolts and nuts, and welding. Therefore, if a specific area of tubes needs replacement, only that affected membrane panel is replaced, not the whole tube as in other design.

The water walls are geometrically divided into front wall, side wall and rear wall as shown in Figure 2.2. The front wall is the vertical part of the long water tubes running from mud drum to steam drum. The tubes then form the front wall, the floor, and the ceiling in the furnace. Similarly, the rear wall is composed of tubes running from mud drum to steam drum. However, the geometry of the rear wall is distinctive. It forms a slag screen to absorb remaining radiant heat from the furnace to protect the superheaters' tubes and a "nose" to protect feeders of the superheaters from intensive heat from the fire ball. The side walls can be divided into three sections on one side, total of six sections on both sides. Each section is connected to its own water feeders to which water is supplied from the mud drum. The two-phase mixture of each side wall section will go to the steam drum through the distributed headers and the risers.

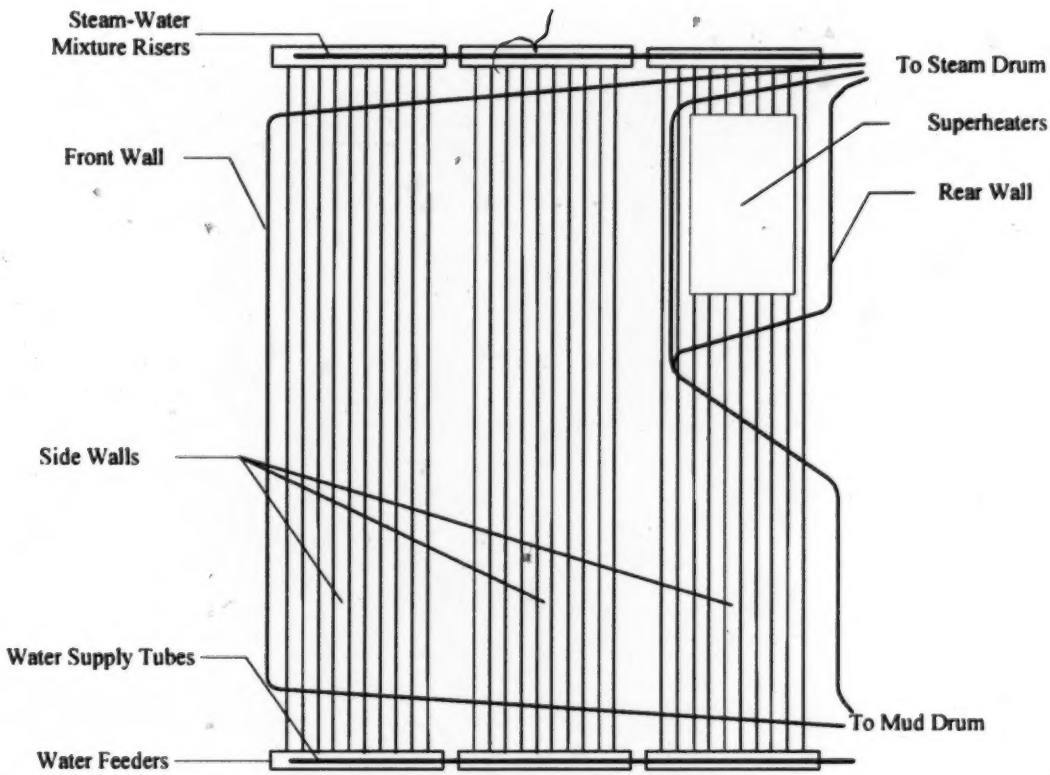

Figure 2.2: Schematic diagram of Furnace.

There are six horizontally placed burners arranged in two rows at the near bottom of the front wall as shown in Figure 2.1. The ignition is initiated by high voltage spark and high capacity natural gas in the combustion chamber where fuel and air are mixed to form an ignitable mixture. The system adopted to supply air and expel flue gas is called balanced draft, in which forced draft and induced draft fans are utilized. The forced draft fan is to provide atmospheric air from inside or outside of the Powerhouse for combustion and the induced draft fan is to draw flue gas from the boiler and discharge it to a common stack to maintain balanced draft

condition in the furnace. This particular system is designed for boilers operating in confinement (the situation in SCL) because it has operating pressure slightly lower than atmospheric pressure. Thus, flue gas containing hazardous elements will not leak out from cracks in the boiler shell.

2.2.2 Superheaters

There are two superheaters, primary and secondary superheaters, inside the UBO. They function to increase the heat content of the saturated steam leaving the steam drum to superheated steam. An interstage attemperation is applied to control the outlet superheated steam temperature. The attemperator manipulates high pressure feed water to desuperheat the superheated steam and thereby control temperature. Both superheaters are of continuous tube type and are supported by four headers. The superheaters receive heat by convection from the flue gas leaving furnace and a small amount by radiation from the fire ball. The outlet superheated steam then goes to the 6.6 MPa common header.

2.2.3 Convective Generation Bank

The purpose of the convective generation bank or boiler bank is to generate steam using convective heat of flue gas. The boiler bank is formed by bundles of aligned tubes which are connected between the steam drum and the mud drum. As shown in Figure 2.1, the boiler bank consists of two sections, risers and downcomers, each with eighty-one tubes. The front ten rows are heated risers and the rear eleven rows are heated downcomers. The boiler bank contains 1806 tubes which

are fabricated from 0.0635 m OD $\times$ 0.00343m MW tubing. All tubes are swaged at the mud and steam drum to 0.0508 m. The boiler bank enclosure is formed by the outer tubes of the boiler bank which are membraned as the water walls in the furnace.

2.2.4 Steam Drum

The steam drum, 11.89 m in length and 1.83 m in diameter, is a cylindrical tank with ellipsoidal ends, and the design maximum pressure is 7.93 MPa. It serves several functions as follows:

1. Separate the steam-water mixture by means of cyclones, and primary and secondary scrubbers.

2. Serve as mixing point for feedwater and recirculating boiler water.

3. Permit maintenance of boiler water impurities by blowdown operation.

The cyclones, which function to mechanically separate liquid water from saturated steam, are located on one side in the steam drum as shown in Figure 2.3. There are fifty-four cyclones arranged in two rows along the front side of the steam drum. The outer and inner row consists of twenty-eight and twenty-six cyclones respectively. The liner or the belly plate in the steam drum, which directs the steam-water mixture from the risers to the cyclones, covers the front ten rows of the boiler bank tubes. The primary and secondary scrubbers serve to further extract water from the saturated steam, so that the exit saturated steam has quality exceeding 99 %.

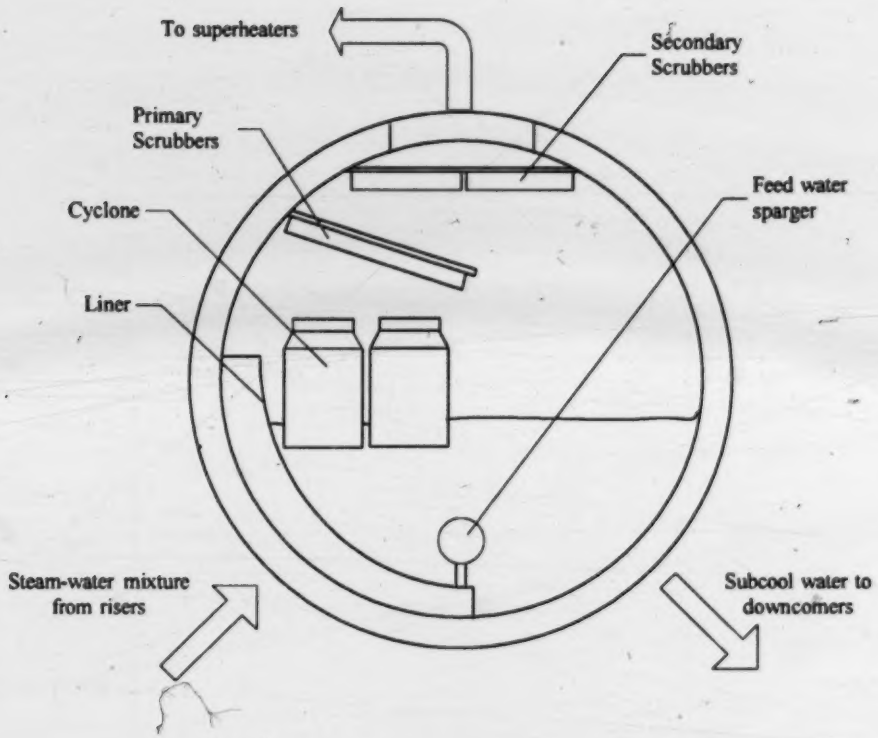

Figure 2.3: Schematic diagram of the steam drum structure.

The 0.203 m OD feedwater pipe is located near the bottom in the steam drum. Total of one hundred and ninety-five 0.0127 m holes are drilled at the top of the pipe. Because the temperature of the feedwater is significantly cooler than that of the recirculating boiler water, the mixture of the feedwater and the steam drum liquid still has temperature lower than saturation and it will stay at the bottom in the steam drum. Besides the heated downcomers supplying subcool water to the heated risers, there are two 0.406 m OD downcomers connected between the steam and mud drum outside the flue gas path.

2.2.5 Mud Drum

The mud drum has a similar apperance as the steam drum, except its dimension is comparatively smaller. Its length is 11.3 m and diameter is 1.22 m. The purpose of the mud drum is to:

1. Serve as a collecting chamber for foreign matter.
2. Serve as a distribution point for the steam generating tubes of the boiler bank and the water tubes in the furnace.

When the utility boiler is not in operation, the water in the mud drum is kept in the hot standby condition by using steam.

2.2.6 Economizer

The economizer is another item of heat exchanging equipment in the utility boiler. It functions to further recover the sensible heat of flue gas in order to increase the heat content of the feedwater. This step is important in boiler operation because the extent of the subcooling of water entering the downcomers will decrease. In other words, the hydraulic stability of the boiler bank will increase.

2.3 Steam Generation of the Utility Boiler

After understanding the functions of each section of the utility boiler, the explanation of how steam is generated can be undertaken. When the fire ball is formed in the furnace, the flue gas is continuously driven following the path shown in

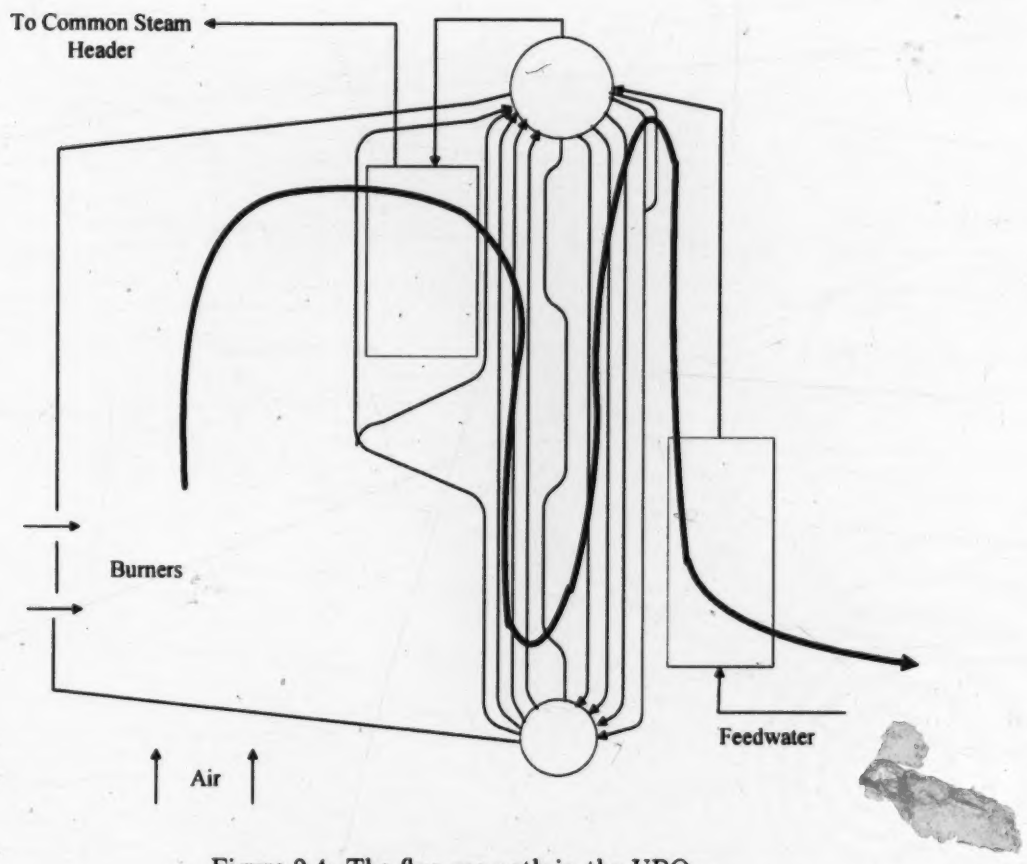

Figure 2.4: The flue gas path in the UBO.

Figure 2.4. The water tubes in the furnace receive radiant heat from the fire ball to produce steam, so the steam-water circulation must be maintained to protect other metal parts from temperature related failure.

The steam-water circulation is of natural-circulation type, meaning that no external force, such as a pump is used for assisting the movement of the fluid. The same kind of circulation occurs in the boiler bank as the flue gas passes the tubes in counterflow fashion. Because of the large heat transfer area in the boiler bank, the amount of steam generated is higher than that of the water tubes in the fur-

nace. The saturated steam generated from the water walls and the boiler bank goes to the steam drum, in which the water is mechanically separated from the steam. The high quality saturated steam is driven to the superheaters by the pressure difference between the steam drum and the common steam header. It passes through the primary superheater first, then the secondary superheater. An interstage attemperator is used to control the exit superheated steam temperature. The amount of steam generated is compensated by feeding feedwater back to the circulation circuit to maintain the operating water level in the steam drum at the designed operating conditions of the steam-water circuitry.

2.4 Conclusion

The utility boiler of Syncrude Canada Limited is designed to work at subcritical pressure and circulate steam-water mixture using natural circulation. The functions and structures of all components of the utility boiler, namely furnace, superheaters, steam drum, mud drum, convective boiler bank and economizer, are discussed and explained with the assistance of simplified schematic diagrams in this chapter. The furnace is a large-volume metal chamber which allows fuel-air mixture to combust and provide necessary heat to generate steam. The main functions of water walls inside the furnace and convective boiler bank are to maintain the temperature inside the boiler at which the metal parts will not be melted and to generate steam at the same time. Two superheaters, primary and secondary, connecting in series serve to superheat saturated steam from steam drum to steam

header. Steam drum and mud drum play important roles as collective and distributing nodes for steam and subcooled water respectively. Finally, economizer is needed to recover sensible heat from the expelled flue gas to maximize thermal efficiency.

Chapter 3

Two-Phase Flow and Heat Transfer

3.1 Introduction

For the last few decades, two-phase flow studies have received considerable attention because of its vast applications in industries such as nuclear reactors, steam power plants, and refrigeration systems. Its applications in steam power plant and nuclear reactor are most numerous. Using steam for driving turbogenerators is by far the most conventional method for electric power generation. Many methods and mechanisms have been developed to efficiently generate steam. One popular mechanism is to produce steam in an upward flowing channel using external heat source. Although the idea is as simple as boiling water, the complexity of the mechanism behind it did induce many researchers to develop many empirical correlations to characterize two-phase flow under different conditions. From an engineering perspective, the objective of the study of two-phase flow is to determine the heat transfer and pressure drop characteristics of a given flow. Therefore, this chapter will describe four two-phase flow regimes commonly categorized by

researchers. Then two analytical two-phase pressure drop models – homogeneous and separated flow models will be discussed. In order to successfully employ the analytical models, the void fraction has to be evaluated and its correlations are presented in following section. This will be followed by the description of flow boiling and two-phase heat transfer correlations.

3.2 Two-Phase Flow

Two-phase flow can be generally divided into two categories – adiabatic and diabatic flows. Adiabatic two-phase flow is a hydrodynamic problem which involves phase change by pressure, total flow rate, quality and fluid properties. Diabatic two-phase flow is a coupled thermohydrodynamic problem which involves phase change by heat transfer and hence a change of phase distribution and flow pattern; on the other hand, a change in phase distribution affects heat transfer characteristics. These observations suggest the complexity inherent in two-phase flow and the importance of knowing the flow pattern. The number of characteristic flow patterns and the names used for them changes from investigator to investigator. For example, Stultz and Kitto (1992) describe four diabatic vertical flow patterns. They are:

1. *Bubbly flow*, in which the discrete vapor phase is dispersed in a continuous liquid phase. Bubble size, and distribution are dependent on the flow rate, heat input rate and pressure. This flow pattern occurs at low void fractions.

2. *Slug flow*, in which relatively large liquid slugs appear in the flow as a result of the start of agglomeration of vapor bubbles. This flow occurs at moderate void fractions and low flow velocities. The flow pattern seems to occur at the transition between the bubbly and annular flows. This flow pattern does not appear at a high heat flux nor in a short flow channel.

3. *Annular flow*, in which a liquid layer is formed on the tube wall with a continuous steam core. Discontinuous liquid phase is present in the steam core as droplets, while discontinuous vapor phase appears as bubbles in the annulus. The presence of liquid phase in the core or vapor phase in the annulus is dependent upon the vapor velocities. This flow pattern occurs at high void fractions.

4. *Mist flow*, in which a continuous steam core carries entrained water droplets which slowly evaporate until a single-phase steam flow occurs. This is also referred to as dispersed flow.

3.3 Pressure Drop of Two-phase Flow

Pressure drop in two-phase flow is subject to the flow pattern as defined by its phase distribution as discussed in the preceeding section. The two-phase flow in a channel with heat addition is a variable density flow. If the pressure drop along the channel is relatively small compared with the absolute pressure, the flow is practically incompressible (Tong, 1965). The change in flow density is due to the

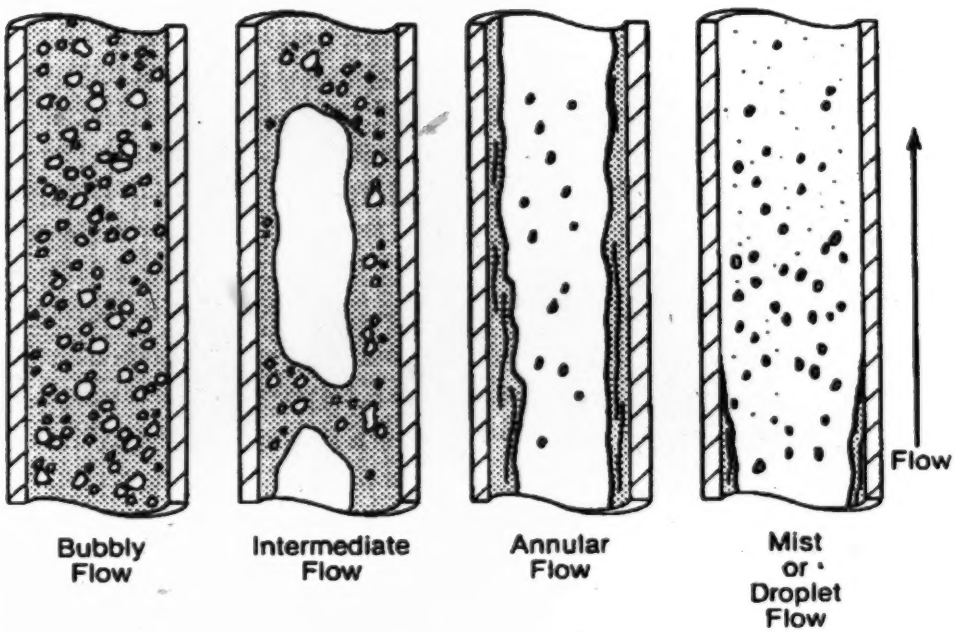

Figure 3.1: Flow pattern – co-current steam-water flow in a heated vertical tube.

phase change caused by heat to the channel. During the process of phase change, the void and velocity distributions are changed; and therefore, the momentum of the flow changes. The pressure drop of a vertical two-phase flow is composed of three components – frictional loss, accelerational change and gravitional force. The pressure drop for a two-phase flow can be written as

$$(\frac{dp}{dl})_{total} = (\frac{dp}{dl})_{friction} + (\frac{dp}{dl})_{acceleration} + (\frac{dp}{dl})_{gravitation} \tag{3.1}$$

Two analytical flow models based on Equation 3.1 have appeared in the literature for describing the two-phase flow pressure drop – the homogeneous and the separated flow models.

3.3.1 The Homogeneous Flow Model

The homogeneous model is the simpler approach for analyzing two-phase flows. The basic assumptions of a homogeneous model are

1. The velocity of vapor and liquid phase is equal.

2. Vapor and liquid phases are in thermodynamic equilibrium.

3. Single phase friction factor is applicable to the two-phase flow.

Using the homogeneous model, the steady state one dimensional momentum equation can be expressed as

$$-\frac{dp}{dl}_{total} = \frac{fG^2\bar{v}}{2D^2} + G^2\frac{d\bar{v}}{dl} + \bar{\rho}g\sin\theta \tag{3.2}$$

where the three terms on the right hand side represent the frictional, accelerational and gravitational pressure gradients repectively.

3.3.2 The Separated Flow Model

The separated flow model treats the flow as two separate streams; one of vapor and one of liquid, flowing at different velocities but in thermal equilibrium. The corresponding one dimensional momentum equation is

$$-\frac{dp}{dl}_{total} = \frac{fG^2\bar{v}}{2D^2} + G^2\frac{d}{dl}\left[\frac{x^2v_g}{\alpha} + \frac{(1-x)^2v_f}{1-\alpha}\right] + g\sin\theta\left[\alpha\rho_g + (1-\alpha)\rho_f\right] \tag{3.3}$$

where the three terms on the right hand side represent frictional, accelerational and gravitational pressure gradients respectively.

3.3.3 Frictional Pressure Drop

Two-phase frictional pressure drop is difficult to describe on theoretical basis. In most situations it is evaluated using empirical correlations developed from experimental data. Martinelli and Nelson (1948) suggested that the two-phase frictional pressure gradient can be calculated by relating the single-phase pressure gradient to a two-phase frictional multiplier. Thus, the two-phase friction multiplier is defined as the ratio of the two-phase frictional pressure gradient to the liquid-phase pressure gradient at the same total mass flow rate. This two-phase frictional factor will depend on steam quality and system pressure. According to this approach,

$$\Phi_{Lo}^2 = (dp/dl)_{TPF}/(dp/dl)_l \tag{3.4}$$

As shown in Figure 3.2, local Φ_{Lo}^2 was plotted versus local quality and pressure. Martinelli and Nelson applied extensive experimental data to correlate Φ_{Lo}^2 in terms of the following parameter for tubulent flows of vapor and liquid:

$$\chi_{tt} = (\frac{\mu_f}{\mu_g})^{0.1} (\frac{\rho_g}{\rho_f})^{0.5} (\frac{1-x}{x})^{0.9} \tag{3.5}$$

This is known as Lockhart-Martinelli parameter and it is a function of steam quality and system pressure. The shortcoming of the Martinelli-Nelson correlation is that it does not account for the effect of mass velocity on the two-phase frictional

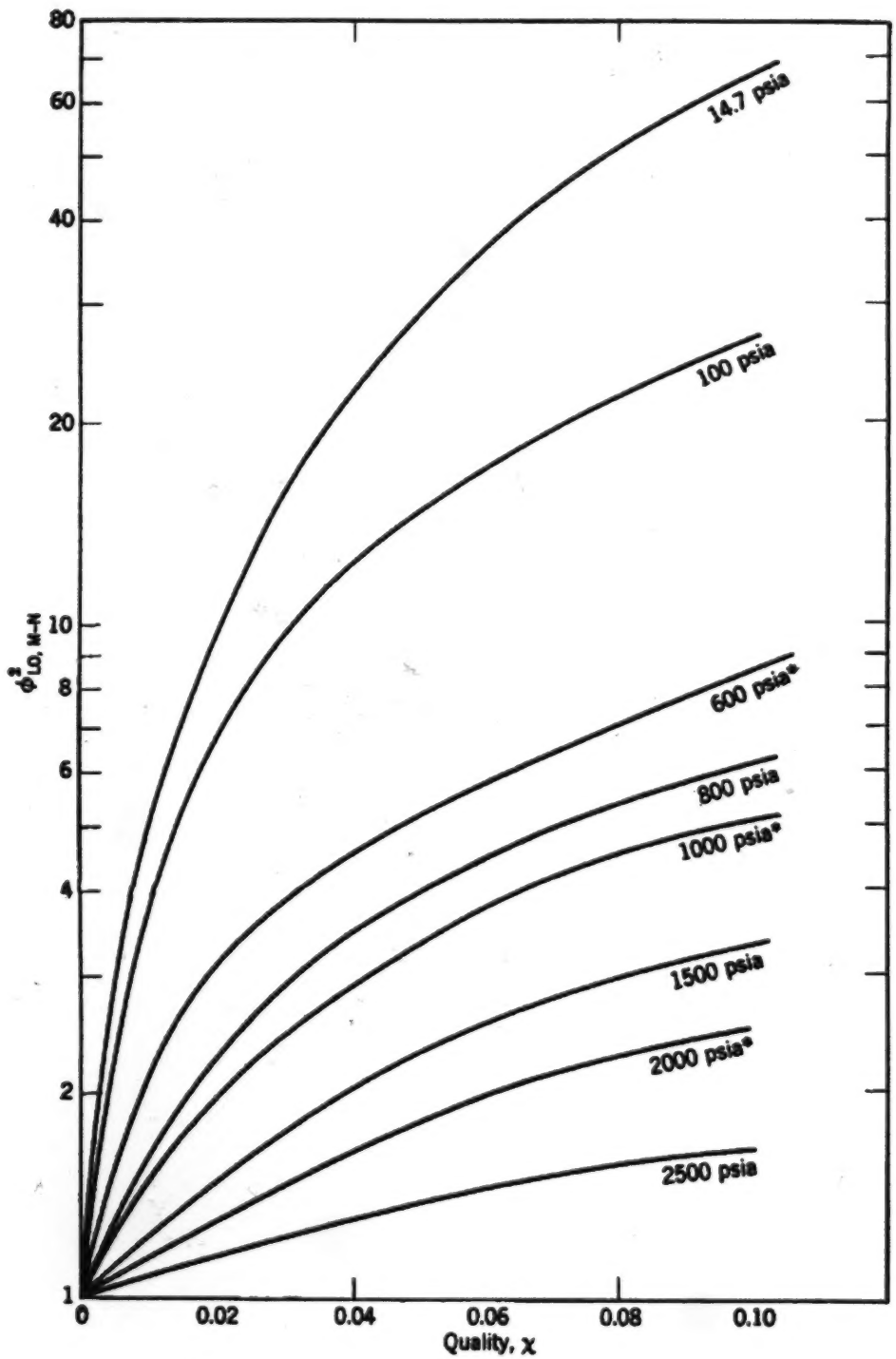

Figure 3.2: Martinelli-Nelson two-phase friction factor for low quality region.

pressure gradient which has been observed experimentally. Another correlation which is based on the Martinelli Nelson two-phase friction multiplier but accounts for the effect of mass flux is presented in (Shoukri, 1980),

$$\Phi_{Lo}^2 = q(G,P)\ \{1.2\ [\frac{\rho_f}{\rho_g}\ -\ 1]\ x^{0.824}\}\ +\ 1.0 \tag{3.6}$$

where

$$q(G,P) = \begin{cases} 1.36 + 0.00345P + 0.000136\ (G/10^6) - \\ 6.7 \times 10^{-6} P\ (G/10^6); & (G/10^6) < 0.7 \\ 1.26 - 0.00276P + 87.56\ (10^6/G) + \\ 1.419P\ (10^6/G); & (G/10^6) > 0.7 \end{cases}$$

where P is pressure, kPa, and G is mass flux, $kg/s\ m^2$.

While there are many investigators establishing empirical two-phase frictional correlations which involve the effect of flow patterns, mass velocity and even heat flux, the Martinelli-Nelson correlation is still the most widely used to evaluate two-phase frictional pressure gradient.

3.4 Two-phase Flow Void Correlation

In addition to obtaining knowledge of the flow pattern in two-phase flow, it is also crucial to understand quantitatively the relative amounts of each phase – the void fraction. Since one-dimensional flow is always assumed in pressurized water reactor, such as boilers, most quantities in the system are evaluated as the local

averages over the cross section of the flow channel. The void fraction is defined as the local vapor volume to the total flow volume at a cross section,

$$\alpha = \frac{A_g}{A_g + A_f} \tag{3.7}$$

Knowing the local void fraction one can calculate the local average density as

$$\rho_{local} = \alpha\, \rho_g + (1 - \alpha)\, \rho_f \tag{3.8}$$

The vapor volumetric flow ratio β is defined as the ratio of vapor volumetric flow to the total volumetric flow rate,

$$\beta = \frac{Q_g}{Q_g + Q_f} \tag{3.9}$$

A local quantity α and a flow quantity β can be related in an expression by a flow factor

$$C = \frac{\alpha}{\beta} \tag{3.10}$$

or

$$C = \frac{(1-\alpha)\, V_f + \alpha\, V_g}{V_g} \tag{3.11}$$

The flow factor can also be expressed as

$$C = \alpha + \frac{1-\alpha}{S} \tag{3.12}$$

Pressure MPa	C	Pressure MPa	C
0.489	0.790	7.86	0.808
0.979	0.783	10.8	0.827
1.96	0.783	13.7	0.850
2.94	0.785	17.7	0.904
3.92	0.788	19.6	0.938
5.88	0.796	20.6	0.975

Table 3.1: The flow factor at different pressure for steam-water data.

where S is the slip ratio defined as the ratio of the velocity of vapor to the velocity of liquid.

$$S = \frac{V_g}{V_f} \tag{3.13}$$

Some investigators, such as Kholodovski, Bankoff and Hughmark (Butterworth & Hewitt, 1978) developed correlations using the flow factor to estimate the slip ratio. Table 3.1 shows the values of flow factor at different pressure for steam-water data by Kholodovski (Butterworth & Hewitt, 1978).

For homogeneous flow model, since the velocities of vapor and liquid are the same, the slip ratio is equal to unity, and it can be expressed as

$$S = \frac{x}{1-x}\,\frac{1-\alpha}{\alpha}\,\frac{\rho_f}{\rho_g} = 1 \tag{3.14}$$

For separated flow model, there are many two-phase void correlations which take into account the effects of quality, pressure and mass velocity. The following two correlations, respectively, from Armand (Ginoux, 1978) and Collier (Ginoux, 1978)

are widely used:

$$\alpha = \frac{(0.833 + 0.167x)\, x\, v_g}{(1-x)\, v_f + x\, v_g} \quad \text{Armand} \tag{3.15}$$

$$\alpha = 1 - \frac{(1-x)}{\sqrt{\phi_{Lo}^2}} \quad \text{Collier} \tag{3.16}$$

The Collier void fraction correlation is based on Martinelli-Nelson two-phase friction multiplier.

3.5 Flow Boiling

Flow boiling or forced convective boiling describes the presence of heat transfer to the fluid which is flowing due to natural circulation or forced circulation by pump. The heat transfer is distinctive because of the variable-density flow nature of the working fluid. In addition, the nature of heat transfer in two-phase flow is dependent on the flow pattern or, in macroscopic view, the local void fraction and quality. To explain the various regimes of heat transfer in flow boiling the upward flow of a liquid in a vertical channel with heated wall is considered. The flow patterns of the imposed situation are postulated to develop as shown in Figure 3.3. At point A, the water enters the tube as subcooled liquid and convective heat transfer cools the tube. The point of incipience of boiling occurs at point B which is characterized by bubbly flow and known as subcooled boiling. The water temperature continues to rise until the bulk fluid reaches saturation temperature. Then another flow boiling phenomena, nucleate boiling, starts between point C

and D. At this location, the steam-water mixture progresses through a series of flow patterns: bubbly flow, slug flow and annular flow. The transition from one flow regime to another results from the complex interaction of the surface tension, pressure drop, steam-water densities and momentum effects coupled with surface boiling behavior. In the annular flow region, a point is reached where the liquid film becomes so thin that the nucleation in the film is suppressed, point F. Heat transfer occurs through conduction and convection across the liquid film with surface evaporation at the steam-water interface. For this annular flow regime, not all the liquid is on the heated wall. Dispersed liquid droplets are entrained in the steam core. This heat transfer mechanism is called convective boiling. Finally, point G is reached where the tube surface is no longer wet and is so called dry out or critical heat flux (CHF) occurs. This situation is typically associated with a temperature rise at tube wall. The magnitude of the temperature and the location depend upon various parameters, such as mass flux, heat flux and steam quality. Beyond point H, single phase heat transfer occurs as all liquid is evaporated.

3.6 Heat Transfer Correlation

As referred from Figure 3.3, at point A, single phase heat transfer occurs and Dittus-Boelter heat transfer correlation can be used.

$$\frac{D_e h}{k} = 0.023 \left(\frac{G D_e}{\mu}\right)^{0.8} \left(\frac{\mu C_p}{k}\right)^{0.4} \tag{3.17}$$

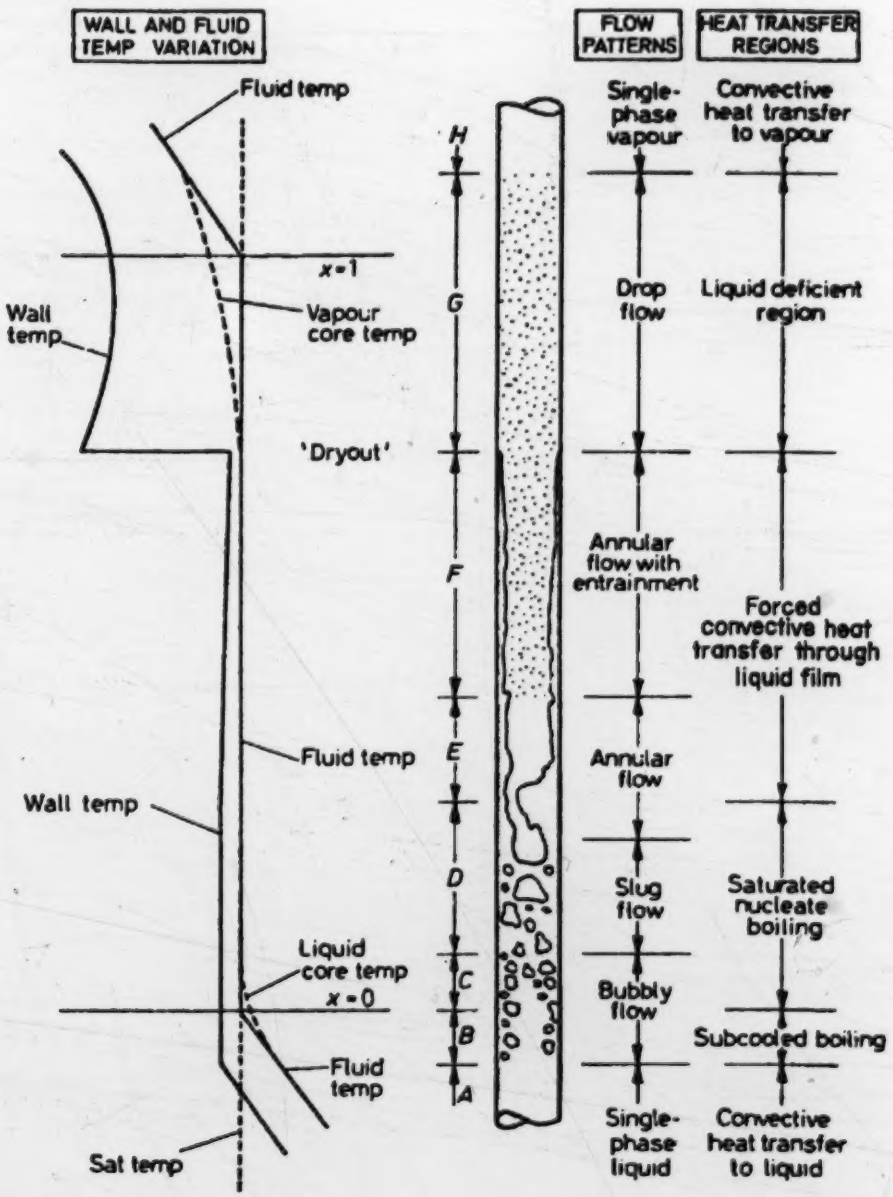

Figure 3.3: Flow boiling in a vertical heated tube.

where

D_e = hydraulic diameter.

h = heat transfer coefficient.

ρ = fluid density.

G = mass flux.

μ = dynamic viscosity of fluid.

C_p = heat capacity of fluid.

k = thermal conductivity of fluid.

As the bulk fluid temperature rises close to the saturation temperature, if the temperature difference between tube wall and the bulk fluid is greater than 5 ^oC, incipient boiling will take place. Bergles and Rohsenow have developed a heat transfer correlation for incipience of boiling by solving graphically the bubble growth equation to give

$$\frac{Q}{A} = 88.5812\,(\frac{P}{K})^{1.156}\,(T_w - T_s)^{(2.3/(\frac{P}{K})^{0.0234})} \tag{3.18}$$

where

$\frac{Q}{A}$ = boiling incipient heat flux, W/m^2.

P = pressure, kPa.

T_w = wall temperature, ^oC.

T_s = saturation temperature, ^oC.

K = conversion factor, 6.894757.

After the incipience of boiling, subcooled boiling occurs. At subcooled boiling the tube wall's temperature is at superheat, and a thin layer of bubbles is generated on the wall. However, the bulk fluid is still subcooled. Hence, one of the characteristics for subcooled boiling is the quality is less than 5 %. The correlation by Thom *et al* (Bergles *et al.*, 1981), is recommended due to its better agreement with the experimental data.

$$h = 1.40224\ (\frac{Q}{A})^{0.5}\ \exp[P/(8.68739 \times 10^3)] \tag{3.19}$$

where

$\frac{Q}{A}$ = heat flux,W/m^2.

T_w = wall temperature,^oC.

T_s = saturation temperature,^oC.

P = pressure,kPa.

For fully developed nucleate boiling, Chen's equation is recommended. Chen (Bergles *et al.*, 1981) applies Forster and Zuber's microconvective heat transfer relation for boiling and Dittus-Boelter macroconvective heat transfer relation for

forced convection. Therefore, Chen' correlation becomes

$$h = h_{mic} + h_{mac}$$

or

$$h = S(0.00122)\,\frac{k_l^{0.79} C_{pl}^{0.45} \rho_l^{0.49} \Delta T^{0.24} \Delta P^{0.25}}{\sigma^{0.5} \mu_l^{0.29} H_{fg}^{0.24} \rho_g^{0.24}} + F(0.023)(R_e)_l^{0.8}(P_r)_l^{0.4}\frac{k_l}{D_e} \quad (3.20)$$

where

k_l = thermal conductivity of liquid, W/m^2K.

C_{pl} = specific heat of liquid, J/kgK.

ρ_l = density of liquid, kg/m^3.

ρ_g = density of vapor, kg/m^3.

ΔT = temperature difference between tube wall and saturation, K.

ΔP = saturated vapor pressure difference according to ΔT, P_a.

σ = surface tension, N/m

μ_l = dynamic viscosity of liquid, Ns/m^2.

H_{fg} = latent heat of evaporation, J/kg.

D_e = equvalent diameter, m.

R_e = Reynolds number.

P_r = Prandtl number.

The parameter S in Equation 3.20 is a suppression factor defined as the ratio of the mean superheat seen by the growing bubble to the wall superheat. It is expressed as

$$S = \frac{1}{1 + 2.53 \times 10^{-6}\ Re_l^{1.17}} \tag{3.21}$$

Another parameter F in the equation is expressed as a funciton of the Martinelli parameter, χ_{tt}.

$$F = \begin{cases} 1 & \text{for } 1/\chi_{tt} \leq 0.1 \\ 2.35\ (1/\chi_{tt} + 0.213)^{0.736} & \text{for } 1/\chi_{tt} > 0.1 \end{cases}$$

As stated in (Butterworth & Hewitt, 1978), Chen's two-phase heat transfer correlation has the best agreement with experimental data. Therefore, Chen's correlation is by far the most recommended two-phase heat transfer correlation in literature. However, the application of Chen's correlation is rather complicated. Another two-phase heat transfer correlation by Pujol and Stenning (1968) gives a much simpler expression yet an adequate description for nucleate boiling.

$$h = h_{Lo}\ 4.0\ (\frac{1}{\chi_{tt}})^{0.37} \tag{3.22}$$

where

h = two-phase heat transfer coefficient, W/m^2K.

h_{Lo} = single phase heat transfer coefficient, W/m^2K.

χ_{tt} = Lockhart-Martinelli parameter.

Both of the above mentioned nucleate boiling correlations cover the quality ranging from 0 to 0.7. That means the correlations are able to account for the annular flow heat transfer. For quality higher than 0.7 other annular flow or film boiling heat transfer correlations are required. In fact there are many investigators establishing heat transfer correlations for this region because of the interest in the boiling crisis occurred at the transition from annular flow to mist flow. Because this is not the scope of this thesis, the correlations will not be presented and details can be found in (Butterworth & Hewitt, 1978), (Tong, 1965) and (Bergles *et al.*, 1981).

3.7 Conclusion

Two categories of two-phase flow can be identified: they are adiabatic and diabatic flows. The definition of different two-phase flow regimes is based mostly on experimental observations. Four flow regimes namely bubbly, slug, annular and mist flow are commonly recognized. Pressure drop for two-phase flow is greatly affected and characterized by flow patterns. Two flow models are usually employed to evaluate the local pressure drop – homogeneous and separated models. The homogeneous flow model assumes the velocity of vapor and liquid phase is equal, the vapor and liquid phases are in thermodynamic equilibrium and single phase friction factor is sufficient to the two-phase flow. On the other hand, the separated flow model treats the flow as two separated streams, allowing the velocity of vapor and liquid phases to be different but still assuming the two phases to be in thermal

equilibrium, and a two-phase friction factor is used. There are various two-phase friction factor correlations by investigators; however, the one from Martinelli and Nelson is most widely used and referenced. Depending upon the flow models selected, the local void fraction can be evaluated from slip ratio correlations which are dependent mostly on pressure and quality. An example of upward liquid flow in a vertical channel is applied to explain various heat transfer transitions one could expect for a typical flow boiling or forced convective boiling. Recommended heat transfer correlations for different flow patterns from literatures are stated and discussed.

Chapter 4

Steam Generation Model Development

4.1 Introduction

The purpose of a steam-water circuitry in a boiler is two-fold:

1. To generate saturated steam from the subcooled inlet water at the specified pressure and temperature.

2. To act as coolant to keep the metal components from temperature-related failure.

From design perspective, the above two purposes are interrelated because sufficient steam generation or steam-water circulation prevents excessive metal temperature or temperature differentials that can cause failure due to overheating and over-stressing. Thus, a circulation method, which can properly perform the mentioned purposes in association with other operating conditions, such as heat input, firing rate, and system pressure, is of major concern in boiler design.

A variety of circulation methods have been developed to circulate water and steam through the boiler system. These methods are usually classified by the means used to control the circulation through the evaporator tubes or risers. In general, they are broadly classified as "recirculating" or "once-through" types. For this particular UBO of SCL, the operating pressure is subcritical [$< 22.1 MPa$] and the circulating method is natural-circulation, a sub-category of recirculating types. Because of the complex nature of natural circulation, involving transitions of single-phase to two-phase flow mechanism and heat transfer, a steady-state model, comparatively simpler than dynamic model, is often adopted to study the boiler performance in association with other boiler components.

This chapter will show the development of the steady-state natural-circulation model suggested by Kakaç *et.al.* (Kakaç, 1991) and the transient natural-circulation model modified from the steady-state model. Then, the validation of both models will be discussed.

4.2 Natural Circulation

Natural circulation has been used for subcritical pressure drum-type boilers. It is initiated when the mean density difference between downcomers and risers produces sufficient pumping head to overcome the hydraulic resistances, such as friction, exit and entrance loss in the circuit. The flow rate in the circuit is governed by the heat input (fuel firing rate) and adjusted at design stage by appropriately sizing the number and diameter of all tubes of the steam-water circuit. From

the sizing of all tubes of the circuit, an important boiler design parameter, the circulation ratio, is set. The circulation ratio, defined as the ratio by weight of the water fed to the heated risers to the steam generated, determines whether the boiler is at design operating conditions. The inverse of the ratio actually gives the steam quality generated.

In steady-state, the balance of pressure drop in the downcomers and risers can be expressed as:

$$(z\ \bar{\rho}_d - \int_0^z \rho(z)\ dz)\ g = (\ \Delta P_{friction} + \Delta P_{acceleration} + \Delta P_{local}\ ) \qquad (4.1)$$

where

z = total vertical elevation, m

dz = incremental vertical elevations, m

$\rho(z)$ = heated tube local fluid density, kg/m^3

$\bar{\rho}_d$ = average downcomer fluid density, kg/m^3

g = acceleration of gravity, m/s^2

ΔP = circuitry pressure loss due to friction, fluid acceleration and local loss, Pa

Although the natural-circulation flow is determined by the heat input, the flow will not unrestrictedly increase in accordance with the increasing heat. A maximum flow will be reached and the flow will decline, if higher heat inputs are sustained,

because of larger pressure losses in the heated tubes due to higher steam quality throughout, without corresponding increases in pressure differential. Therefore, natural-circulation boilers are usually designed to operate in the region where increased heat corresponds to an increase in flow for all possible operating conditions. When operating in this mode, the circulation system tends to be self adjusting for various situations in heat absorption.

4.3 The Steady-State Natural-Circulation Model

The steady-state natural-circulation steam generation model suggested by Kakaç *et.al.* (Kakaç, 1991) is used. The impetus for developing the steady-state natural-circulation model is to simplify the establishment of a conventional fluid mechanic model mostly described by Navier-Stoke equations. For a steady flow, the natural-circulation is governed by the following equation:

$$\rho_1 gh - \Delta P_d = \sum \rho_i h_i g + \Delta P_r + \Delta P_{se} \tag{4.2}$$

where ρ_i and ρ_1 are the average densities of the water or the steam-water mixture in the risers and water in the downcomers; ΔP_d, ΔP_r, and ΔP_{se} are the hydraulic resistances of the downcomers, risers, and cyclones in the steam drum. Equation 4.2 is actually in the same form as Equation 4.1.

The left-hand side of Equation 4.2 represents the total pressure difference of the downcomers, Y_d, and the right-hand side terms express the total pressure difference of the risers, Y_r. Then the operating point of the circulation loop at

steady flow is

$$Y_d = Y_r \tag{4.3}$$

In Equation 4.2, Y_d and Y_r both depend on the local mass flow rate W, or the inlet water velocity of the risers v_o. Therefore, the total circulation rate is obtained when, for multi-loop circuit, all of the local mass flows satisfy the pressure drop balance requirements of the Equation 4.2, as applied to each loop. The determination of the individual pressure drop terms in Equation 4.2 will be shown in the following sections.

4.3.1 Calculation of the Hydraulic Resistance of the Downcomers

Since the fluid flow in the downcomers is single-phase water, ΔP_d can be determined by the following equation:

$$\Delta P_d = (\lambda \frac{L}{d} + \sum \xi_M) \frac{V^2}{2} \rho \tag{4.4}$$

where λ and ξ_M are the frictional coefficient and minor loss coefficients, L and d are the length and inner diameter of the tube section, and V is the inlet water velocity in the downcomers.

$$\lambda = \frac{1}{4\,[\,\log(\,3.7\frac{D}{\Delta}\,)\,]} \tag{4.5}$$

where Δ is the roughness of tube wall: for carbon steel and low alloy steel $\Delta = 0.06$. The determinations of the minor loss coefficients, ξ_M, can be found in (Kakaç,

1991).

4.3.2 Determination of the Density of the Steam-Water Mixture

The two-phase mixture density can be expressed as follows:

$$\rho_m = \alpha\rho_g + (1 - \alpha) \rho_l \tag{4.6}$$

where ρ_g and ρ_l are the saturation densities of steam and water; α is the local void fraction defined as

$$\alpha = \frac{1}{1 + S (\frac{1-\beta}{\beta})} \tag{4.7}$$

where S is the slip ratio which can be calculated as follows:

$$S = 1 + \frac{0.4 + \beta^2}{V_o^{0.5}} (1 - \frac{P}{22.1}) \tag{4.8}$$

where P is the absolute pressure, and β is the flow volumetric quality.

$$\beta = \frac{1}{1 + (\frac{1}{x} - 1)\frac{\rho_g}{\rho_l}} \tag{4.9}$$

where x is the steam mass quality of the two-phase mixture.

4.3.3 Calculation of the Hydraulic Resistance of the Risers

For a boiler with nonsteaming economizers, the state of water entering the risers is subcooled. When the subcooled water enters the risers, it has to be heated

to the boiling point. The amount of heat required to bring the subcooled water to saturation liquid state can be determined by the following:

$$Q_{ec} = W * (h_f - h_{dc}) \tag{4.10}$$

where Q_{ec} is the amount of heat required for bringing the subcooled water to saturation liquid state; W is the total mass flow; and h_f and h_{dc} are the saturation liquid enthalpy and the subcooled water enthalpy from the downcomers, respectively. The height occupied by the subcooled water can then be determined by the ratio of heat absorption between the economizer section and the entire tubes, and it can be expressed as:

$$H_{ec} = \frac{Q_{ec} * H}{Q} \tag{4.11}$$

where H_{ec} and H are the height of the economizer section and the entire riser; and Q is the total heat absorption from the risers. For convective generation bank, the total heat absorption is calculated as:

$$Q = W_{fg}\, C_{pfg}(T_{fi} - T_{fo}) \tag{4.12}$$

where W_{fg} is the mass flow of the flue gas; C_{pfg} is the heat capacity of the flue gas; and T_{fi} and T_{fo} are the inlet and exit flue gas temperature, respectively. For

individual water walls, it is calculated as:

$$Q = Q_{ww} A_w \tag{4.13}$$

where Q_{ww} is the heat flux inside the furnace and A_w is the projected heat transfer area. The heat flux inside the furnace can be calculated as:

$$Q_{ww} = \frac{H_{ww}}{A_T} \tag{4.14}$$

where H_{ww} is the radiant heat from combustion and A_T is the total projected heat transfer area. The steam generated can be determined by the following:

$$W_s = \frac{(Q - Q_{ec})}{h_{fg}} \tag{4.15}$$

where W_s is the steam generation rate; h_{fg} is the heat of evaporation. Then, the exit steam quality is equal to

$$x = \frac{W_s}{W} \tag{4.16}$$

It will be used later to calculate two-phase frictional corrective factor and steam volume quality.

The hydraulic resistance of the evaporating portion of the risers, ΔP_{ev}, is

$$P_{ev} = \left(\sum \xi_M + \Phi_{Lo}^2 \lambda \frac{L_{ev}}{d} \right) \frac{V_o^2}{2} \rho \left[1 + \frac{x_e}{2} \left(\frac{\rho_l}{\rho_g} - 1 \right) \right] + \xi_{ex} \frac{V_o^2}{2} \rho \left[1 + x_e \left(\frac{\rho_l}{\rho_g} - 1 \right) \right] \tag{4.17}$$

where ξ_M is the coefficient of minor losses for the steam-water mixture; L_{ev} is the length of the evaporating portion of the riser; x_e is the exit steam quality; ξ_{ex} is the loss coefficient of the tube exit; and Φ^2_{Lo} is the two-phase frictional corrective coefficient. $\Phi^2_{Lo} = 1.0$ when $\rho V = 1000 kg/m^3$. For other cases, Φ^2_{Lo} can be obtained from the following equations:

when $\rho V < 1000 kg/m^2 s$

$$\Phi^2_{Lo} = 1 + \frac{\bar{x}\,(1-\bar{x})\,(\frac{1000}{\rho V} - 1)\,\frac{\rho_l}{\rho_g}}{1 + \bar{x}\,(\frac{\rho_l}{\rho_g} - 1)} \tag{4.18}$$

when $\rho V > 1000 kg/m^2 s$

$$\Phi^2_{Lo} = 1 + \frac{\bar{x}\,(1-\bar{x})\,(\frac{1000}{\rho V} - 1)\,\frac{\rho_l}{\rho_g}}{1 + (1-\bar{x})\,(\frac{\rho_l}{\rho_g} - 1)} \tag{4.19}$$

Then, the total hydraulic resistance of the risers is

$$\Delta P_r = \Delta P_{uh1} + \Delta P_{ec} + \Delta P_{ev} + \Delta P_{uh2} \tag{4.20}$$

where ΔP_{uh1} and ΔP_{uh2} are the unheated section of the risers; ΔP_{ec} and ΔP_{ev} are the economizer and evaporating sections of the risers, respectively. The hydraulic resistances of the unheated sections of the risers are calculated using Equations 4.4 or 4.17 depending on the fluid's state in the unheated sections.

4.3.4 Calculation of the Hydraulic Resistance of the Steam-Water Separator

The evaluation of the hydraulic resistance of the steam-water separator is similar to that of evaluating other hydraulic resistances and its expression is:

$$\Delta P_{se} = K\frac{V_{se}^2}{2}\rho_m \tag{4.21}$$

where ΔP_{se} is the hydraulic resistance of the steam-water separator; K is the design loss constant; V_{se} is the velocity of the steam-water mixture flow in the separator; and ρ_m is the steam-water mixture density. There is one unknown in Equation 4.21, which is K. Since this is a design parameter of the separator for this particular utility boiler, it is obtained by trial and error until the desired operating condition is obtained. The steam-water mixture density can be evaluated using the average exit steam quality from all risers sections.

4.4 Numerical Approach for Solving the Steady-State Model

The circulation calculation as suggested by Kackaç involves a graphical solution which is outlined below. For a simple circuit (all risers have similar geometrical characteristics), a range of inlet velocities is selected and the corresponding local mass flow rates can be calculated using

$$W = \rho v_o A \tag{4.22}$$

Then, curves for $Y_d = f(W)$ and $Y_r = f(W)$ can be established and the intersection of the two curves determines the operating point or the total circulation rate of the circuit. For multi-loop circuit, several Y_r curves are obtained and the operating point is determined differently. A new total Y_r curve is established by adding up the mass flow rate of each loop Yr curve at a fixed pressure drop. The intersection of the new Y_r and Y_d curves is the operating point of the circulation circuit. Figure 4.1 and 4.2 show the circulation characteristic curves of a simple and complex circuits respectively.

Obviously, graphical method is not able to give rigorous numerical values. Therefore, development of numerical schemes to solve Equation 4.2 is necessary. First, in order to quickly check the results of Equation 4.2, bisection algorithm was employed. Although this method is slow, it certainly calculates the answer correctly. In addition, other numerical schemes, such as secant, Newton and regular falsi have been investigated to improve the speed of the simulations. However, they all fail to solve the equation due to poor region of attraction. Hence the bisection method is employed to solve the equation and its implementaion is shown in Figure 4.3. The general idea of the bisection method is to find a pressure drop at which the corresponding circulation rate satisfies Equation 4.2. Several parameters, such as the feedwater temperature, the flue gas mass flow, the heat input to the furnace wall, the entrance and exit flue gas temperature of the boiler bank, and the dimensions of all tubes, are set before implementing the scheme. In additions, two initial values, Y_1 and Y_2, which are the upper and lower bound pressure drop, are selected. The upper bound value can be the static pressure drop

of the downcomers and the lower bound value can be any reasonable value larger than zero. The range of the bound is bisected and a new pressure drop, Y, is used to calculate the local mass flow at different risers sections and the downcomers. The risers of the utility boiler are divided into six sections, namely the boiler bank, three side walls, the rear wall and the front wall. The six local mass flow rates are calculated according to the pressure drop, Y. The strategy for solving the local mass flow, which also employs bisection numerical method, is shown in Figure 4.4. Similarly, a range of circulation velocities is selected and bisected. The bisected value is then used to calculate the local pressure drop at individual riser sections. If the difference between the local pressure drop at a corresponding mass flow and the bisected pressure drop, Y is less than a tolerance, the local circulation mass flow is obtained. Otherwise, if the local pressure drop is larger than the bisected one, the circulation velocity is set to be the new upper bound value, which will be used to bisect a new velocity with the old lower bound velocity. A reverse procedure is used when the local pressure drop is less than the bisected one. Total circulation rate, obtained by summing all local mass flow, is compared with the corresponding flow in downcomers. If the difference is smaller than a tolerance, the operating circulation flow is obtained. However, if the condition does not match, a new pressure drop is established. If the total flow rate of the risers is higher than that of the downcomers, the upper bound is set to be the previous bisected pressure drop value and a new pressure drop value is obtained by bisecting the new upper and the old lower bound values. The vice versa conditions are set if the total flow rate of the risers is lower than that of the downcomers. Once the

total circulation rate is obtained, it is compared with the previous result. If the difference between the two values is small, operating circulation rate is obtained. If not, the total circulation rate is used to establish a new enthalpy of the subcooled water entering the risers and another run is implemented.

4.5 Results and Discussions of the Steady-State Model

The simulated results of the steady-state model, which were evaluated at 94.5 kg/s steam generation load, are shown in Table 4.1. There are two sets of operating conditions from the study reports of Syncrude Canada Limited to test the model and their parameters are shown in Table 4.2. The radiant heat to the water walls is evaluated by combustion calculation as suggested by Kakaç *et.al.* (Kakaç, 1991). The details of the calculations can be found in Chiu(Chiu, 1996). The simulated steam generation rate for Case 1 and 2 is 94.0 and 91.0 kg/s, respectively. The discrepancy between the designed and simulated steam load for Case 1 and 2 is 0.5% and 3.7%, respectively. The circulation ratio discrepancy for both cases is 0.7%. One point that must be emphasized is that the circulation ratio is a parameter set at design stage according to the operating pressure and steam load of the designed boiler. The selection of this parameter is to provide a guide line to size the number and diameter of tubes. At different operating conditions this parameter may vary slightly from the designed value. Therefore, the percentage discrepancy of the simulated circulation ratio is acceptable. In addition, the agreement of the simulated circulation ratio reflects the correct loss

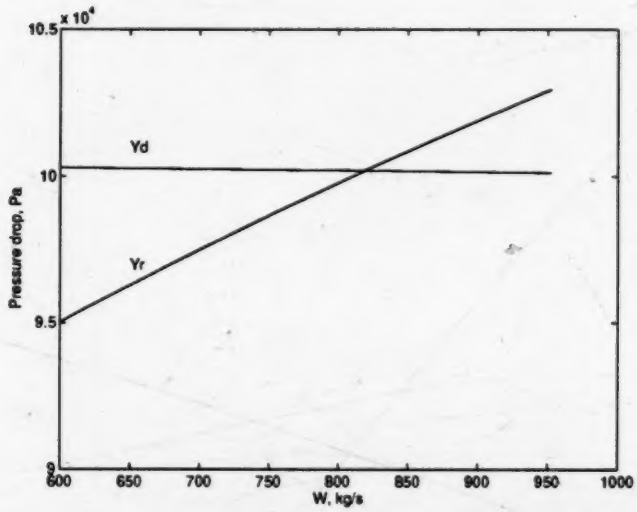

Figure 4.1: Circulation characteristic curves of a simple circuit.

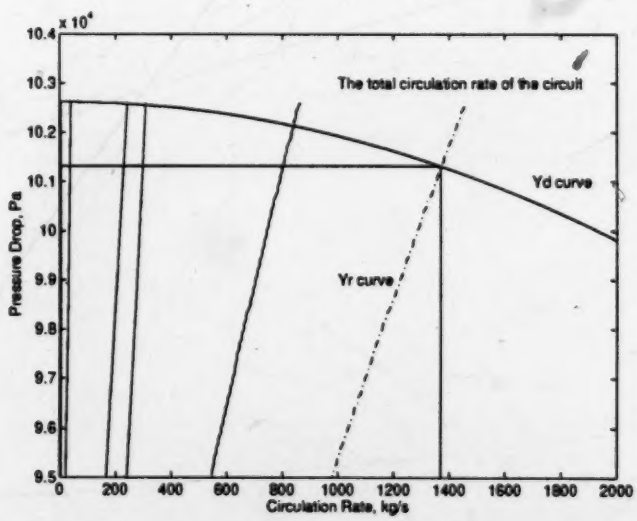

Figure 4.2: Circulation characteristic curves of a complex circuit.

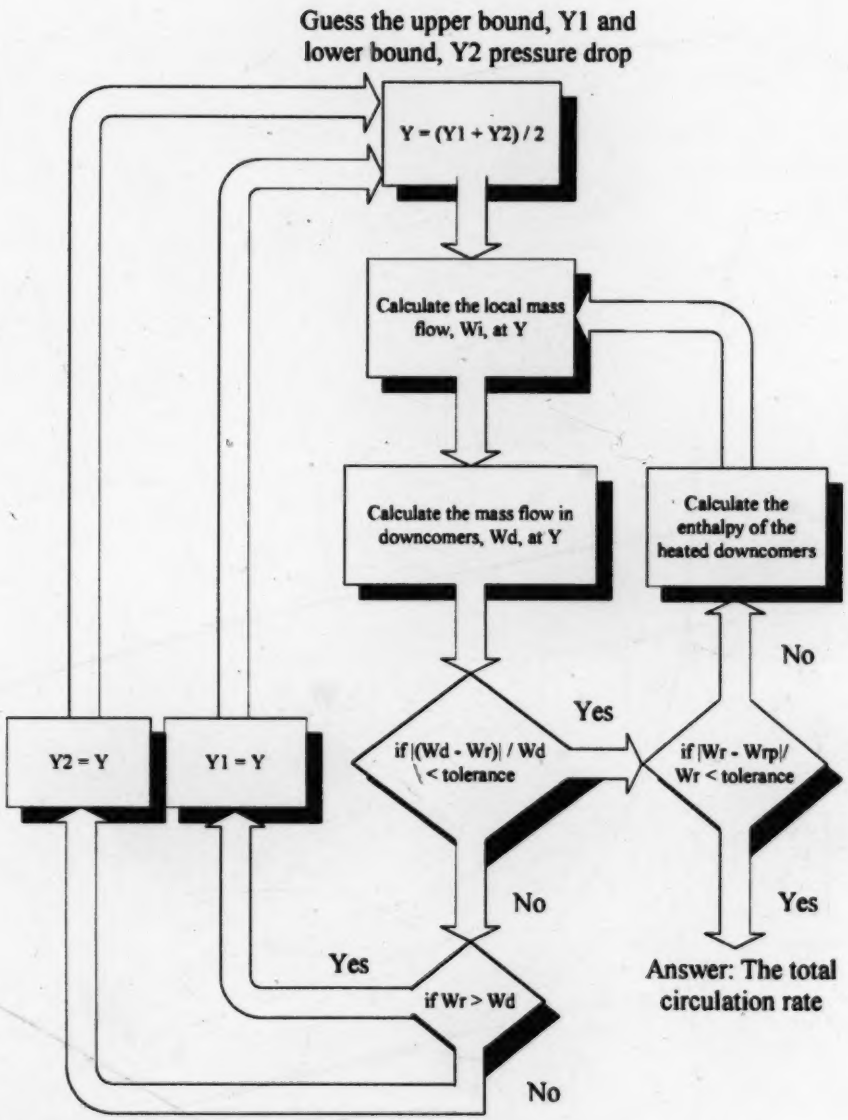

Figure 4.3: The flow chart of calculating the total circulation rate using bisection method.

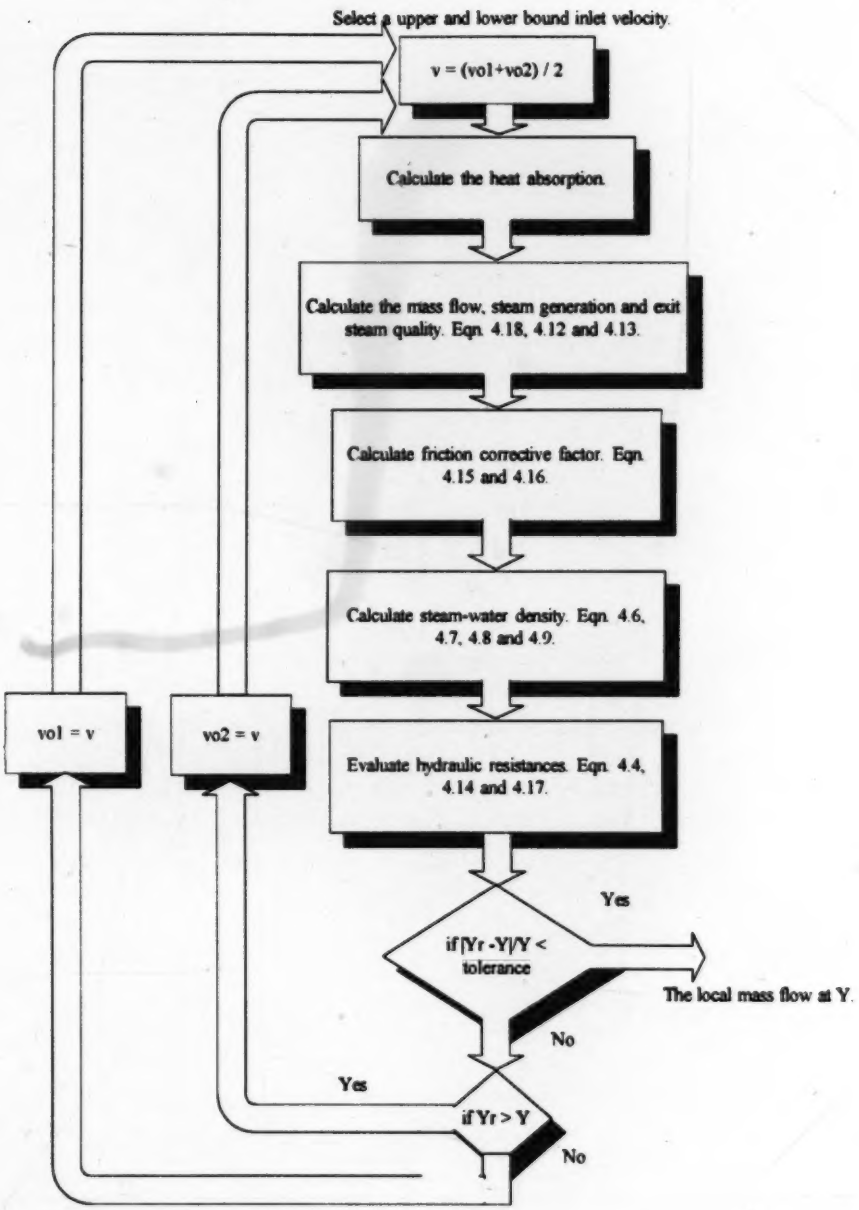

Figure 4.4: The flow chart of calculating the local mass flow using bisection method.

coefficients used in evaluating pressure-drop terms in Equation 4.2.

The simulated results of the individual steam generation and circulation rate of each risers section are also shown in Table 4.1. It is found that the circulation ratio of individual section is not equal to 13.5, whereas the total circulation ratio is in agreement with the design value. However, the results can be justified according to their geometric arrangement. The three side walls are connected to the mud drum and steam drum through distributed headers which add significant hydraulic resistances to the circuit and this implies that the circulation rate would be restricted or probably less than others for the same flow areas. On the other hand, both rear and front walls are directly connected to the mud drum and the steam drum which indicates that the hydraulic resistances of these two sections would be less than those having distributed headers for the same flow areas. From the above considerations, one could deduce that the three side walls would have lower circulation rate than that of the front and rear water walls. This observation is shown in the simulated results. In addition, it is important to ensure that the circulation ratio at each individual section is not less than or equal to unity under normal operating conditions because it indicates whether the circulation circuit has undergone high quality steam generation which might lead to boiling crisis, such as sudden increase in tube wall temperature. Since there are no data available for local circulation rate, the simulated results cannot be completely validated.

	Case 1		Case 2	
Item	Steam Flow	Total Mass Flow	Steam Flow	Total Mass Flow
Units	kg/s		kg/s	
Boiler Bank	26.3	565.9	30.7	592.5
Front Side Wall	8.5	24.7	7.7	29.4
Middle Side Wall	8.9	38.0	8.1	39.6
Rear Side Wall	9.2	58.6	8.3	57.4
Rear Wall	11.8	224.4	10.5	189.1
Front Wall	29.2	366.3	25.7	333.6
Total	94.0	1277.8	91.0	1241.6

Table 4.1: Steam and circulation flow at individual circuitry of the steady-state model.

Item	Case 1	Case 2
Heat to the Water Walls (W)	1.18e8	1.10e8
Fuel Consumption Rate (kg/s)	6.3	6.1
Flue Gas Entering Boiler Bank (^oC)	882.2	932.2
Flue Gas Leaving Boiler Bank (^oC)	392.2	333.9
Feedwater Temperature to Steam Drum (^oC)	212.2	183.9
Steam Drum Pressure (MPa)	7.2	7.2

Table 4.2: Parameters used to simulate the steady-state model at peak load conditions.

Item	Design	Case 1	Case 2
Steam Flow	94.5	95.5	93.9
Total Circulation Flow	1275.8	1277.8	1241.6
Circulation Ration	13.5	13.6	13.6

Table 4.3: Simulation results of the steady-state model at peak load conditions.

4.6 The Transient Natural-Circulation Model

The failure of the steady-state natural-circulation model to calculate the results efficiently prompts a new direction to solve the problem, which is the transient natural- ciculation model. The derivation of the transient natural-circulation model is based on Equation 4.2, balancing the pressure drop between downcomers and risers plus the dynamic acceleration term. The transient momentum equations describing the fluid in the downcomers and risers are as follows, respectively:

$$-\rho_d h_d \frac{dv_d}{dt} = P_{md} - P_{sd} - \rho_d h_d g + \Delta P_d \tag{4.23}$$

$$\rho_i h_i \frac{dv_i}{dt} = P_{md} - P_{sd} - \rho_i h_i g - \sum \Delta P_{ri} \tag{4.24}$$

where the subscript i in Equation 4.24 denotes individual riser section. Other variables can be referred to Section 4.3.

Combining Equations 4.23 and 4.24 the derivative of the local mass flow with respect to time can be obtained as

$$\frac{dW_i}{dt} = \frac{A_i}{h_i} \left[\rho_d h_d g - \rho_i h_i g - \Delta P_d - \sum \Delta P_{ri} - \frac{h_d}{A_d} \frac{dW_d}{dt} \right] \tag{4.25}$$

where A_i and A_d are the total cross sectional area of a riser section and downcomers; ρ_i and ρ_d are the average densities in the risers and downcomers; h_i and h_d are the height of the risers and downcomers; and $\frac{dW_i}{dt}$ and $\frac{dW_d}{dt}$ are the derivative of local and total mass flow with respect to time of the risers and downcomers, respectively. The hydraulic resistances, ΔP_d and $\sum \Delta P_{ri}$, are determined using

the same equations mentioned in Section 4.3.

4.7 Numerical Approach for Solving the Transient Model

Matlab/Simulink is employed to simulate the transient circulation model and its block diagrams are shown in Appendix A. The structure of the Simulink block diagrams for this transient model is hierarchical. It consists of three layers of block diagrams and each layer is hierarchically linked. The top layer shows the input parameters to the model and allows the output parameters to be saved at workspace or displayed using graphical device in Simulink. The second layer is the expanded form of the block called "Risers". The input parameters to the block "Risers" are distributed to six different blocks in the second layer. The six blocks are linked to the third layer which contains the Matlab script files from which the steam generation rate and derivative of mass circulation rate with respect to time are calculated. These two results are linked back to and shown in the top layer for ease of display and organization. Although this model is for independent simulation for the steam generation section, it will be incorporated with the rest of the boiler model which includes the furnace, superheaters, steam drums and economizer from the works of Chiu (Chiu, 1996).

Since the steam-generation model is only part of the boiler model, parameters such as heat transfer rate to water walls, H_{ww}, flue gas flow rate, M_{fg}, temperature difference across the generation bank, ΔT, feedwater temperature to steam drum, T_{fw}, and fuel consumption rate, m_f, are required. Most of the pa-

rameters are obtained from data specification sheet provided by SCL. Others, such as heat transfer rate to water walls and flue gas flow rate are obtained from the combustion simulation of the furnace by Chiu (Chiu, 1996).

With a set of initial conditions, the six Equations 4.25 of the corresponding riser sections are integrated using Gear numerical scheme and the sum of the local mass flow will then be the total circulation flow in the circuit. Among the numerical integration schemes available in Simulink, such as Runge-Kutta, Euler, Adam and Gear, the Gear method is selected because of its stability to deal with stiff differential equations. The advantage of Gear method is its capability to adjust the step size to accomodate stiff system. The methods for evaluating the hydraulic resistances and densities in Equation 4.25, and the steam generation rate are the same as explained in steady-state model. The total circulation rate is then numerically differentiated with respect to time and fedback as the value of $\frac{dW_d}{dt}$ is fedback for the calculations of the following step.

4.8 Results and Discussions of the Transient Model

Because of the limited availability of data, an extensive validation of this independent transient model is not possible. In fact, no data on transient circulation flows for the boilers being modeled are available; therefore, the validation of this independent model is limited to steady state comparison only. At this stage, one of the main reasons for the development of the transient model is achieved. The speed of simulations has improved significantly compared to that of the steady-state model. The iterative calculations required for steady-state solution have

	Case 1		Case 2	
Item	Steam Flow	Total Mass Flow	Steam Flow	Total Mass Flow
Units	kg/s		kg/s	
Boiler Bank	25.4	623.3	28.4	650.5
Front Side Wall	7.9	40.4	7.5	40.4
Middle Side Wall	8.5	43.5	8.0	43.8
Rear Side Wall	8.9	64.2	8.4	63.6
Rear Wall	9.7	136.9	9.2	126.6
Front Wall	30.0	322.3	28.0	314.6
Total	90.3	1230.7	89.5	1239.5

Table 4.4: Steam and circulation flow at individual circuitry of the transient model.

Item	Design	Case 1	Case 2
Steam Flow	94.5	95.9	95.7
Total Circulation Flow	1275.8	1230.7	1239.5
Circulation Ration	13.5	13.6	13.8

Table 4.5: Simulation results of the transient model at peak load conditions.

been spread out over time, achieving both dynamics and algorithmic efficiency. The same cases from Table 4.2 for testing the steady-state model is used by this transient model. The results are shown in Table 4.4 and 4.5. The discrepancy between the designed steam generation rate and the simulated results is 4.4% and 5.3% for Case 1 and 2, respectively. The circulation ratio is 13.6 and 13.8 for Case 1 and 2, respectively. As explained in previous section, the circulation ratio is a value set at design stage for sizing tubes. The discrepancy between the designed and the simulated value is 0.7% and 2.2% for Case 1 and 2, respectively. The agreement of the simulated circulation ratio reflects salutary operation of all risers sections at designed operating conditions.

In addition, this transient model is incorporated with the rest of the boiler components into an interconnected system and the simulated performance of the

boiler is examined by Chiu (Chiu, 1996). For testing the operations of the boiler, control schemes have to be incoporated for regulating the firing rate and the feed-water flow rate. The simulation was set up for running the whole boiler for 14000 seconds. A step increase of 10% of the nominal load, $94.5kg/s$, was added at 2000 s. Afterwards, two step decreases of the steam load demand of the same magnitude as step increase were added at 5000 s and 8000 s. Finally, the steam demand was returned to nominal value at 11000 s, allowing the steam generation to settle at steady state again.

Figure 4.5 and 4.6 show the steam load demand or the input to the boiler. The overall performance of the circulation circuit is satisfactory and stable in the system including the other boiler components. The circulation ratio and the steam quality shown in Figure 4.19 and 4.20 further provide a solid support for the salutary operations of the circulation circuit. With the step up of steam demand the firing rate will increase to meet the demand and likewise the steam quality. The opposite responses are observed for the step down situation. Once again, the circulation ratio for other operating conditions is not exactly equal to 13.5 because the inverse of the circulation ratio is the steam quality generated. In other words, operating the boiler at other conditions than the designed one should not generate the same steam quality. From Figure 4.7 to 4.18 the steam generation and circulation rate of individual risers section are plotted. One particular observation is made for the three side walls. As the steam demand is increased from $94.5kg/s$ to $103.9kg/s$, the local circulation rate of each side wall decreases while other circuits' circulation increases. This is one important characteristic of natural circulation

that the circulation rate will not unrestrictedly increase as the heat input increases as mentioned in Section 4.2. Therefore, one could predict that if the steam demand is higher than $103.9 kg/s$, the excess heat may cause a boiling crisis, such as tube melting, because of a lack of circulating water in certain risers to maintain the tube metal temperature. Otherwise, all risers sections perform well at and below nominal operating conditions as simulated.

4.9 Conclusion

Natural circulation for steam generation is widely adopted for subcritical pressure operating boilers. The circulation flow is initiated when the mean density difference between the downcomers and risers produces sufficient pumping head to overcome the hydraulic resistances along the circulation path. The steady-state natural-circulation model from Kackaç is used to study the steady-state characteristics of the steam generation circuits. In addition, it also serves as a measure stick or guideline for the development of the transient circulation model which is validated independently using data from SCL's reports. The results of the validation for the independent transient model are in agreement with the specification data. With two specified heat inputs to water walls and generation bank at designed steam generation, $94.5 kg/s$, the steam generation rate is 4.4% and 5.3% off the designed value. In addition, the simulated circulation ratio of 13.6 and 13.8 reflects the proper operations of the model.

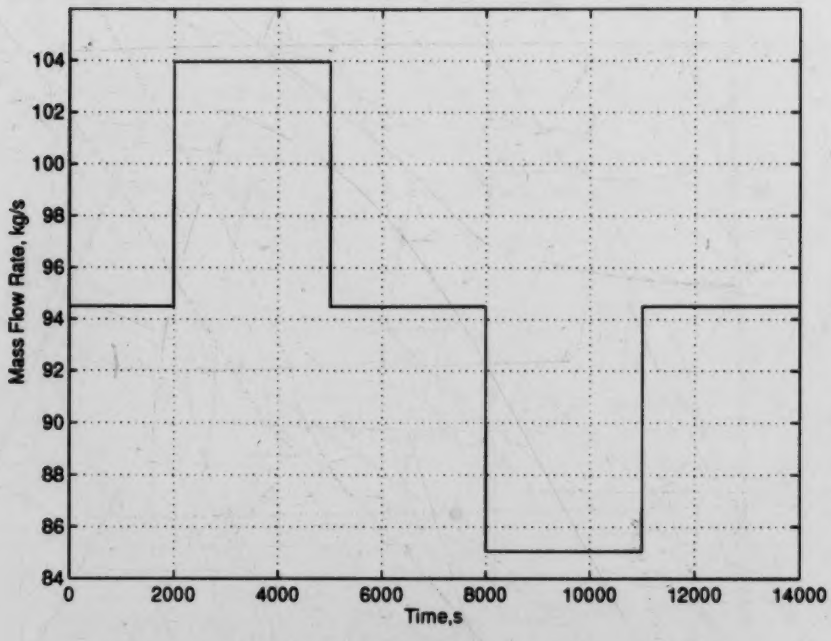

Figure 4.5: The steam demand from the common header.

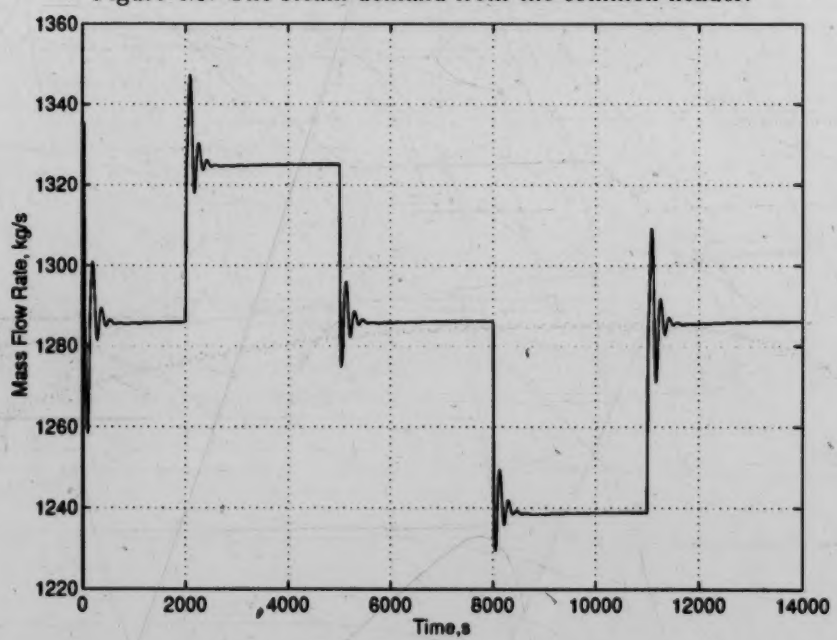

Figure 4.6: The total circulation rate of the steam generation circuit.

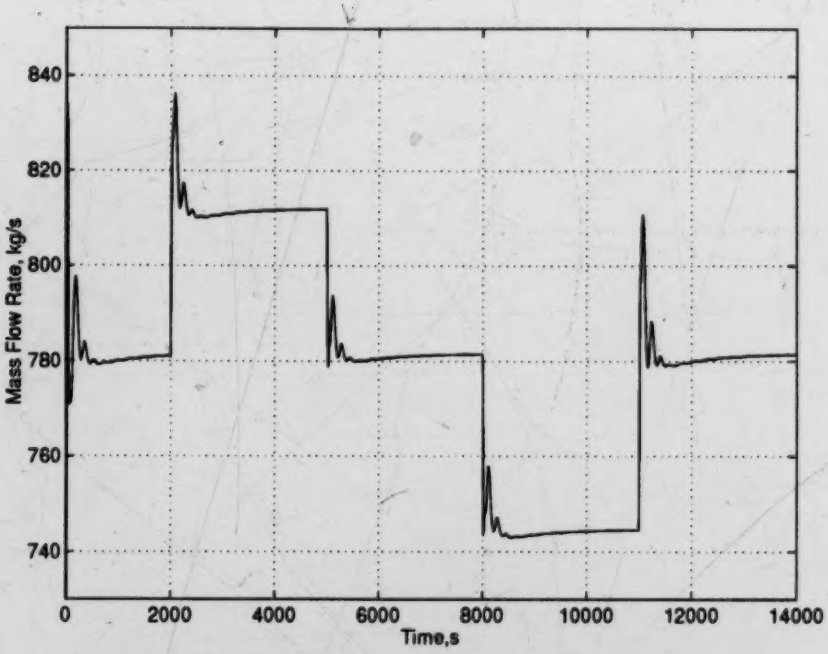

Figure 4.7: The circulation rate of the generation bank.

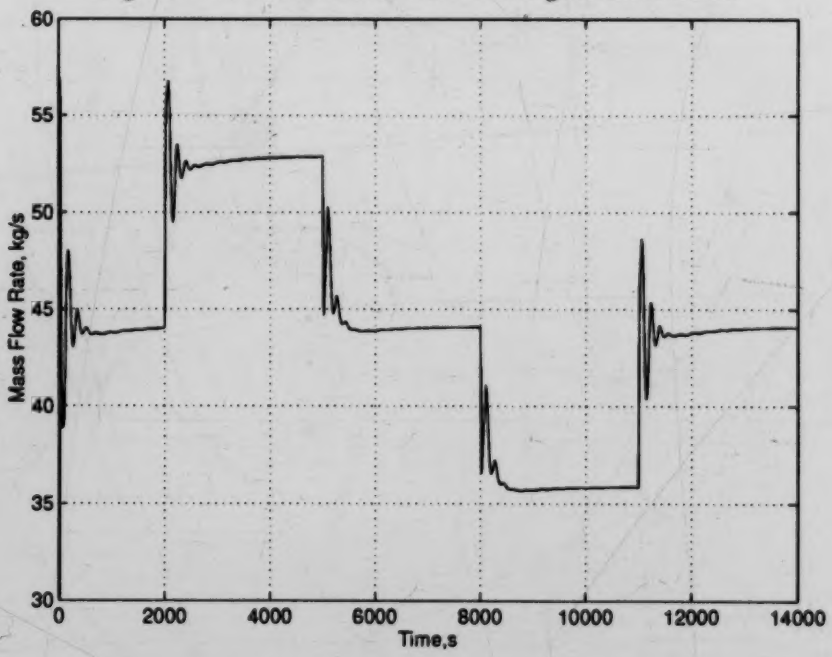

Figure 4.8: The steam generation rate of the generation bank.

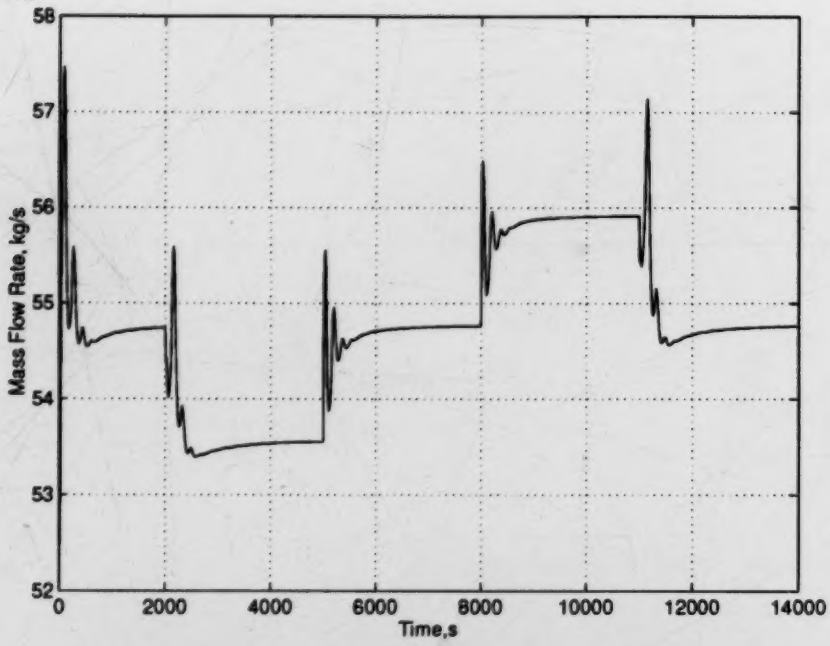

Figure 4.9: The circulation rate of the front side walls.

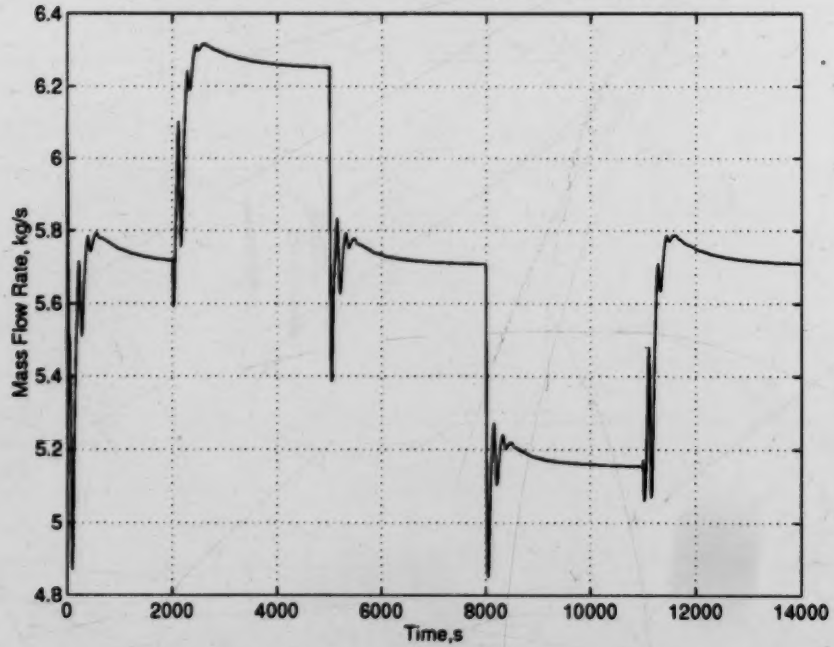

Figure 4.10: The steam generation rate of the front side walls.

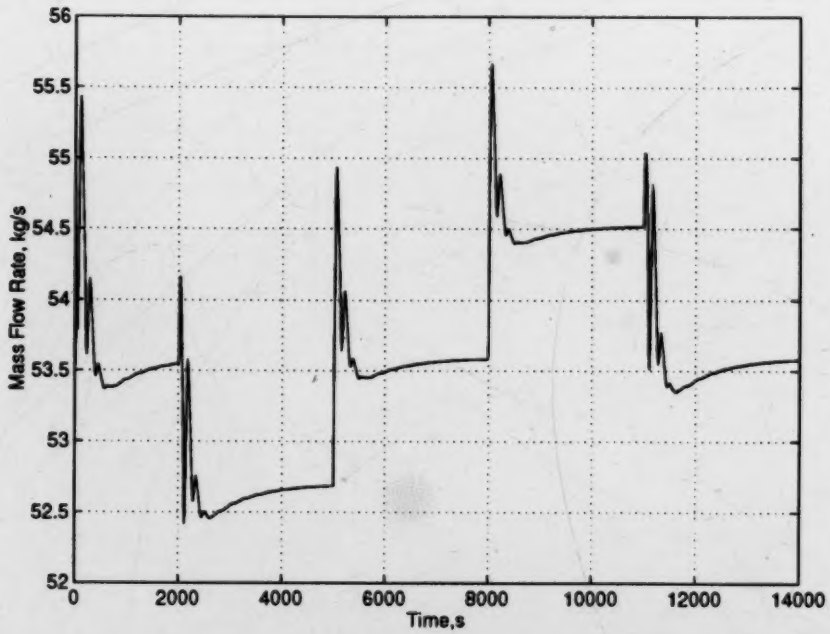

Figure 4.11: The circulation rate of the middle side walls.

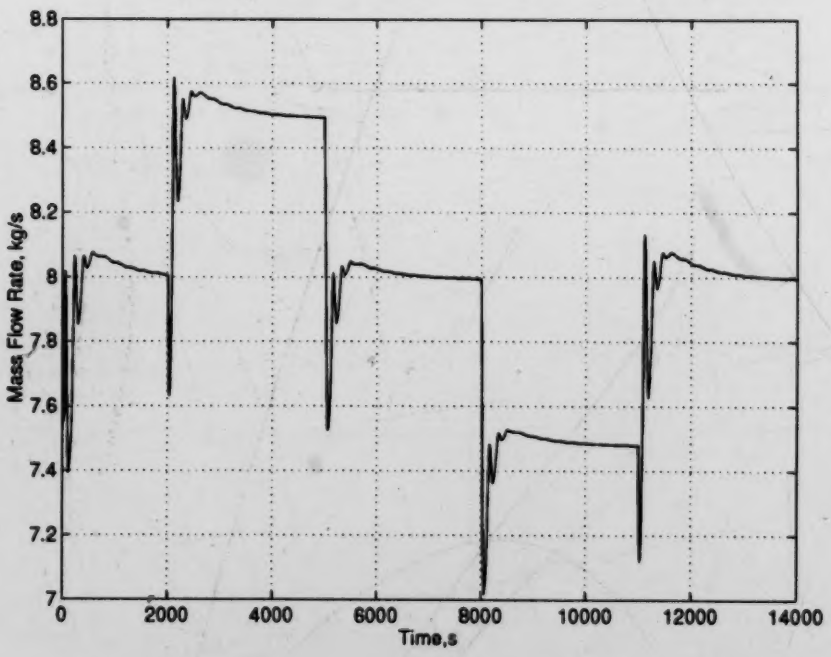

Figure 4.12: The steam generation rate of the middle side walls.

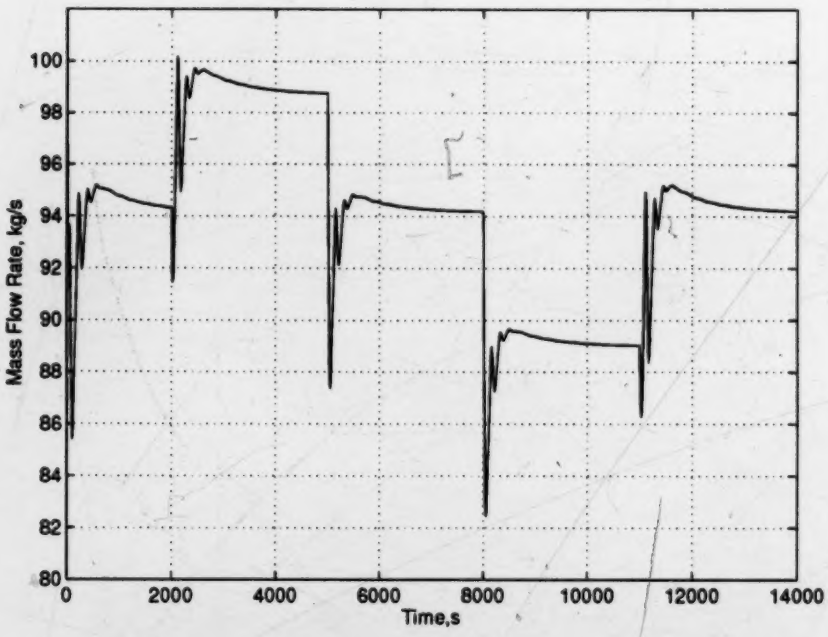

Figure 4.13: The circulation rate of the rear side walls.

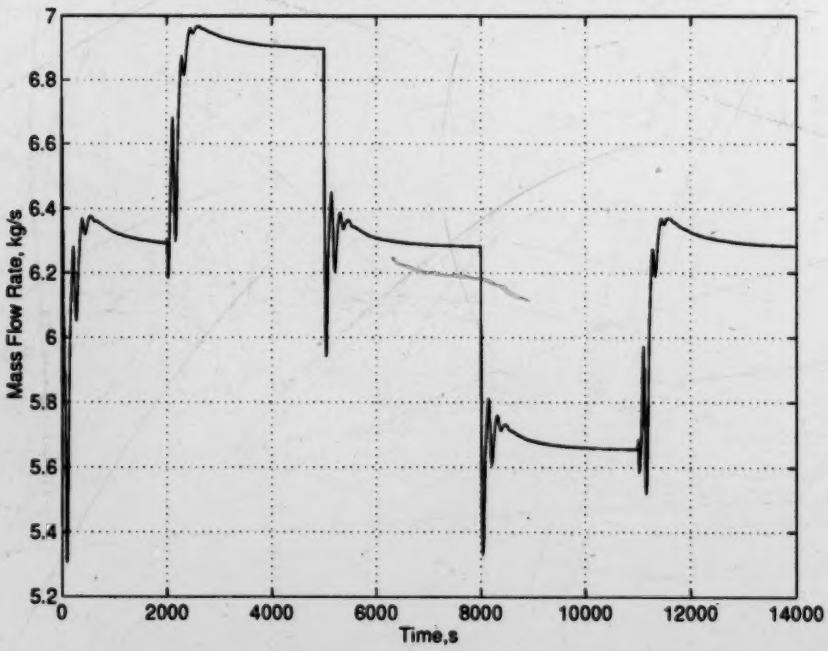

Figure 4.14: The steam generation rate of the rear side walls.

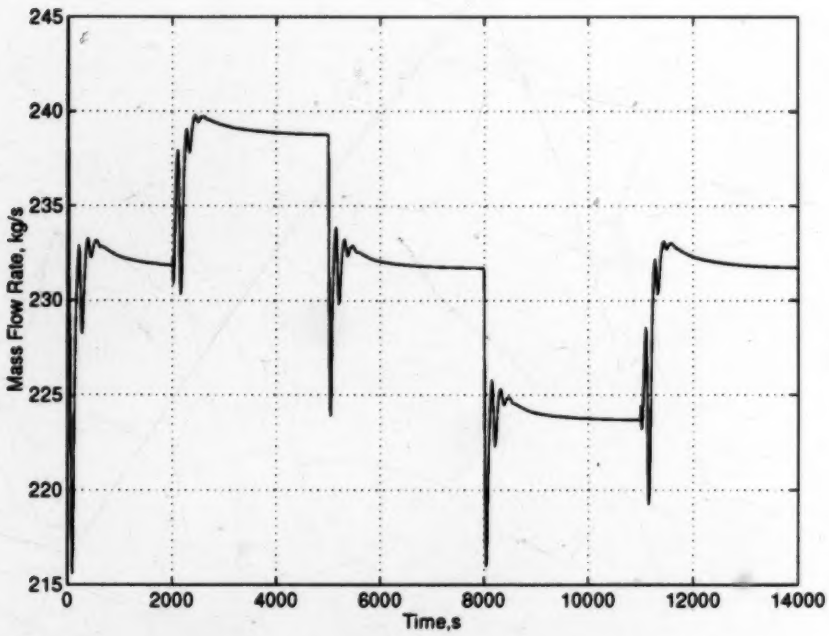

Figure 4.15: The circulation rate of the front wall.

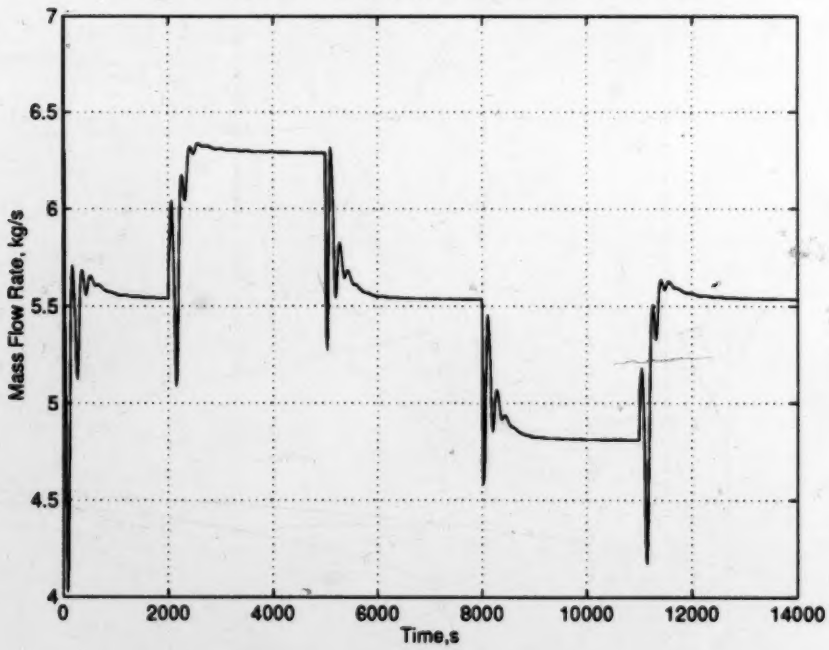

Figure 4.16: The steam generation rate of the front wall.

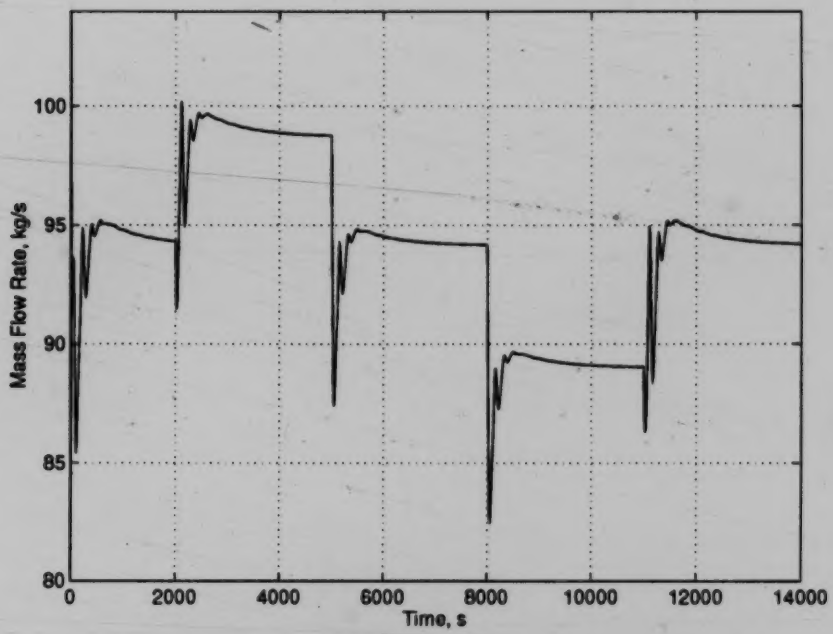

Figure 4.17: The circulation rate of the rear wall.

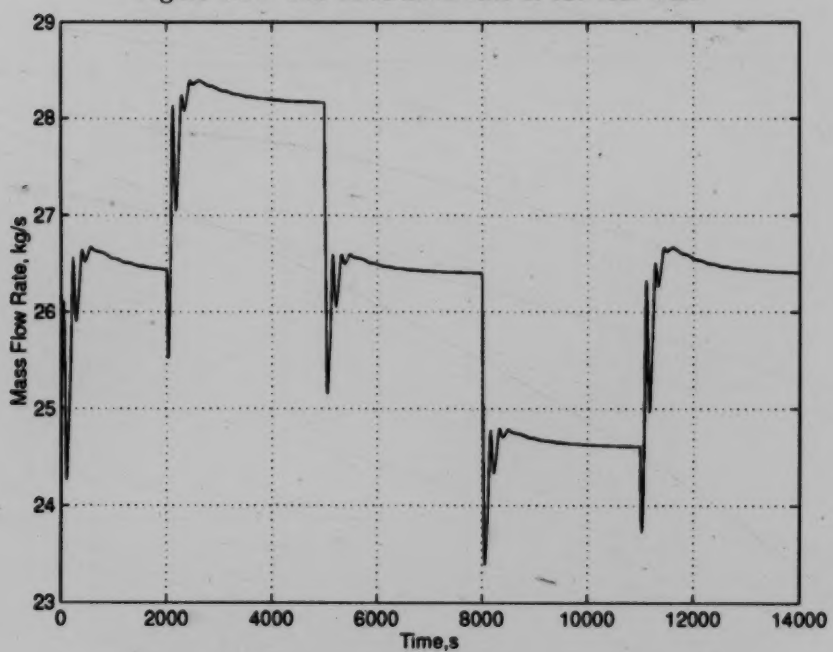

Figure 4.18: The steam generation rate of the rear wall.

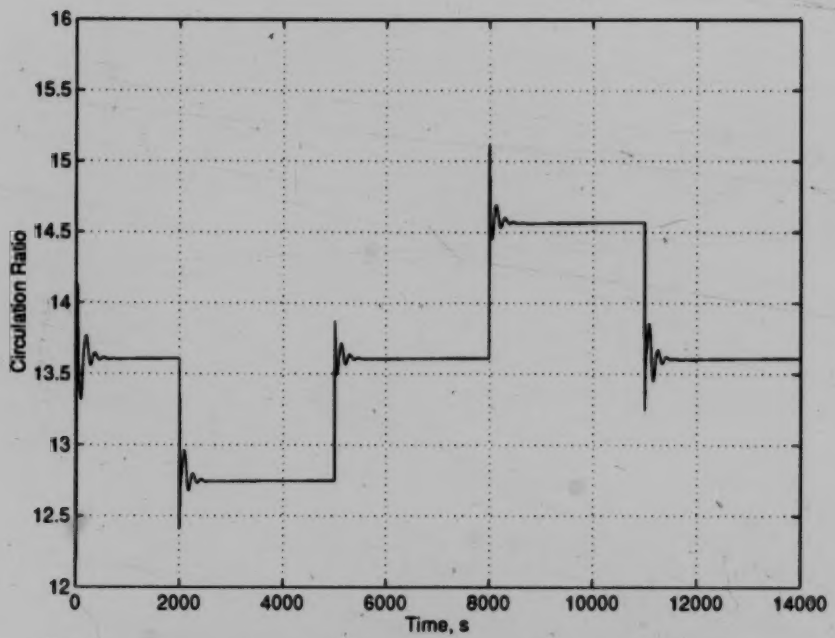

Figure 4.19: The circulation ratio of the overall circuit.

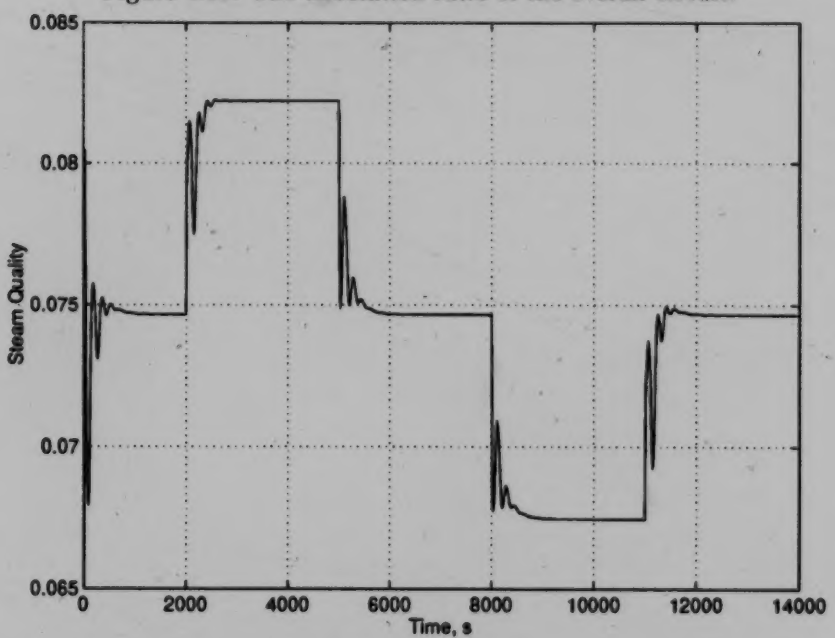

Figure 4.20: The steam quailty generated from the circulation circuit.

The transient circulation model is incorporated with the remaining submodels developed by Chiu(Chiu, 1996) and the simulated performance of the boiler is examined. The whole circuit is capable of generating steam in accordance with the demanded steam load; however, the local circulation rate of the three side walls would not be maintained because, at that amount of heat input, the increase of pressure losses in the water walls do not correspond to the increase in pressure differential. Therefore, the utility boiler should not be operated at the steam load larger than the designed value, $94.5 kg/s$, or attention has to be paid. s

Chapter 5

The Hydraulic Flow Network Model

5.1 Introduction

A detailed natural-circulation model can be developed to further study the transient phenomena of the circuit. The simulation requires numerical integration of equations which account for the mass, energy and momentum of the working fluid. Implicit finite difference simulation is one of the approaches to do the work. However, because of the physical geometry of the circulation circuit, extensive discretization and programming are needed. The hydraulic network approach is employed to study the transient circulation. In addition, the implicit numerical integration method by Porsching *et.al.* (Porsching *et al.*, 1971) is recommended because of its advantage in treating complex hydraulic flow networks. This chapter will explain the hydraulic network approach using the generation bank section as an example to study the transient behavior of the natural circulation circuit. The development of the hydraulic network model will also be shown.

5.2 Basic Principles

The basic geometric ingredients of a hydraulic network are nodes and links as illustrated in Figure 5.1. There are two kinds of links, namely, non-critical and critical. Figure 5.1 shows an example of a noncritical link k with node i as initial node and node j as terminal node. This assignment determines the direction of positive flow from node i to node j. Physically, a noncritical link corresponds to a flowpath in which the flow is governed by a one-dimensional momentum balance equation of the form:

$$\dot{W}_k = f_k(t, P_i, P_j, W_k) \tag{5.1}$$

where W_k is the flowrate in the link; P_i and P_j are the pressures at the initial and terminal nodes of the link respectively; and t is time. The function f_k is generally nonlinear in its four arguments.

Critical link is geometrically similar to noncritical link except it does not have a terminal node. Figure 5.2 shows an example of a critical link k with node i as initial node.

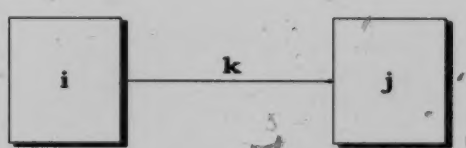

Figure 5.1: A noncritical link.

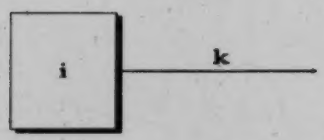

Figure 5.2: A critical link.

The flow in a critical link is determined by an algebraic function

$$W_k = g_k(P_i) \tag{5.2}$$

Thus, the flow depends only on the pressure at the initial node of the link. This happens when leakage takes place at the end of the link or the link flow is independent of its terminal node conditions, for example simulation of a choked flow condition.

A node in a network can be associated with a finite number of noncritical and critical links which may either initiate from or terminate at the node. Thus, a node i is associated with two index sets, T_i and I_i. The set T_i is the set of links for which i is the terminal node and I_i is the set of links for which i is the initial node.

Conditions of the node are governed by the mass and energy conservation equations which are coupled to the momentum equation in association with the equation of state of the form

$$P_i = \pi(U_i, M_i) \tag{5.3}$$

where U_i and M_i are the internal energy and mass of the fluid in node i. The energy and mass equations are as follow:

$$\dot{U}_i = \sum_{\nu \in T_i} H_\nu W_\nu - \sum_{\nu \in I_i} H_\nu^* W_\nu - \sum_{\nu \in I_{ci}} H_\nu^* g_\nu(P) + Q_i \tag{5.4}$$

$$\dot{M}_i = \sum_{\nu \in T_i} W_\nu - \sum_{\nu \in I_i} W_\nu - \sum_{\nu \in I_{ci}} g_\nu(P) \tag{5.5}$$

In these equations, $\dot{U}_i$ and $\dot{M}_i$ denote the change in internal energy and mass of the fluid in node i with respect to time, Q_i is a time-dependent heat source, H_ν and H_ν^* are prescribed time-dependent enthalpies, and W_ν is prescribed time-dependent mass flow. The expression $g_\nu(P)$ denotes the function describing the critical flow.

5.3 The Implicit Integration Method for the Hydrodynamic Network System

Let $y = col[\ W_1, \ldots, W_K, U_1, \ldots, U_N, M_1, \ldots, M_N\ ]$ and $F = col[\ F_1, \ldots, F_{K+2N}\ ]$, where the components F_i are the right-hand sides of Equations 5.1, 5.4 and 5.5. The K and N are the number of links and nodes respectively. Then these equations can be written in vector form as

$$\dot{y} = F(t, y) \tag{5.6}$$

The approximate solution $y^{t+\Delta t}$ may be computed by the formula

$$[\ I - \Delta t\ J(t^n, y^n)\ ]\ \Delta y^{n+1} = \Delta t\ F(t^n, y^n) \tag{5.7}$$

where $\Delta y^{n+1} = y^{n+1} - y^n$; $J(t^n, y^n)$ is the Jacobian matrix of the transformation of $F(t^n, y^n)$; I is the identity matrix; Δt is the time step; and n is time. The determination of y^{n+1} amounts for the determination of the increment Δy^{n+1}.

Let a system contain N nodes and K links with energy and mass balance equations of the form of Equations 5.4 and 5.5 for each node. For each i, there are $K+i$ energy equations and $K+n+i$ mass equations of the form of Equation 5.7. Linearization of Equations 5.4 and 5.5 results in:

$$\begin{aligned}
&\Delta U_i^{n+1} - \Delta t \sum_{T_i} H_\nu \Delta W_\nu^{n+1} + \Delta t \sum_{I_i} H_\nu^* \Delta W_\nu^{n+1} \\
&+\Delta t \{ \sum_{I_{ei}} H_\nu^* (\frac{\partial g}{\partial P_i}) (\frac{\partial P_i}{\partial U_i}) \Delta U_i^{n+1} + \sum_{I_{ei}} H_\nu^* (\frac{\partial g}{\partial P_i}) (\frac{\partial P_i}{\partial M_i}) \Delta M_i^{n+1} \} \\
&-\Delta t \frac{\partial Q_i}{\partial W} = \Delta t \, F_{K+i}(t^n, y^n)
\end{aligned} \tag{5.8}$$

and,

$$\begin{aligned}
&\Delta M_i^{n+1} - \Delta t \sum_{T_i} \Delta W_\nu^{n+1} + \Delta t \sum_{I_i} \Delta W_\nu^{n+1} \\
&+\Delta t \{ \sum_{I_{ei}} (\frac{\partial g}{\partial P_i}) (\frac{\partial P_i}{\partial U_i}) \Delta U_i^{n+1} + \sum_{I_{ei}} (\frac{\partial g}{\partial P_i}) (\frac{\partial P_i}{\partial M_i}) \Delta M_i^{n+1} \} \\
&= \Delta t \, F_{K+i}(t^n, y^n)
\end{aligned} \tag{5.9}$$

Solving Equations 5.8 and 5.9 for ΔU_i^{n+1} and ΔM_i^{n+1}, it is found that

$$\Delta U_i^{n+1} = \Delta t \, [\gamma_{1i} + \sum_{\nu \in T_i} (\alpha_{1i} + \beta_{1i} H_\nu) \Delta W_\nu^{n+1}$$

$$- \sum_{\substack{\nu \in I_i \\ \nu \le K}} (\alpha_{1i} + \beta_{1i} H_\nu^*)\, \Delta W_\nu^{n+1} \,] \tag{5.10}$$

$$\Delta M_i^{n+1} = \Delta t \;\Big[\, \gamma_{2i} + \sum_{\nu \in T_i} (\alpha_{2i} + \beta_{2i} H_\nu)\, \Delta W_\nu^{n+1} - \sum_{\substack{\nu \in I_i \\ \nu \le K}} (\alpha_{2i} + \beta_{2i} H_\nu^*)\, \Delta W_\nu^{n+1} \,] \tag{5.11}$$

where

$$\alpha_{1i} = -\frac{\Delta t}{D_i} \frac{\partial P_i}{\partial M_i} \sum_{\substack{\nu \in I_i \\ \nu > K}} H_\nu^* \frac{\partial g_\nu}{\partial P_i}$$

$$\beta_{1i} = \Big(1 + \Delta t \frac{\partial P_i}{\partial M_i} \sum_{\substack{\nu \in I_i \\ \nu > K}} \frac{\partial g_\nu}{\partial P_i} \Big) / D_i$$

$$\gamma_{1i} = \beta_{1i}\, F_{K+i}(t^n, y^n) + \alpha_{1i}\, F_{K+N+i}(t^n, y^n)$$

$$\alpha_{2i} = \Big(1 + \Delta t \frac{\partial P_i}{\partial U_i} \sum_{\substack{\nu \in I_i \\ \nu > K}} H_\nu^* \frac{\partial g_\nu}{\partial P_i} \Big) / D_i$$

$$\beta_{2i} = -\frac{\Delta t}{D_i} \frac{\partial P_i}{\partial U_i} \sum_{\substack{\nu \in I_i \\ \nu > K}} \frac{\partial g_\nu}{\partial P_i}$$

$$\gamma_{2i} = \alpha_{2i}\, F_{K+N+i}(t^n, y^n) + \beta_{2i}\, F_{K+i}(t^n, y^n)$$

$$D_i = \Big(1 + \Delta t \frac{\partial P_i}{\partial M_i} \sum_{\substack{\nu \in I_i \\ \nu > K}} \frac{\partial g_\nu}{\partial P_i} \Big) \Big(1 + \Delta t \frac{\partial P_i}{\partial U_i} \sum_{\substack{\nu \in I_i \\ \nu > K}} H_\nu^* \frac{\partial g_\nu}{\partial P_i} \Big) - \Delta t^2 \Big(\frac{\partial P_i}{\partial U_i} \sum_{\substack{\nu \in I_i \\ \nu > K}} \frac{\partial g_\nu}{\partial P_i} \Big) \Big(\frac{\partial P_i}{\partial M_i} \sum_{\substack{\nu \in I_i \\ \nu > K}} H_\nu^* \frac{\partial g_\nu}{\partial P_i} \Big)$$

Then the K momentum equations of the form in Equation 5.16 becomes

$$\Big(1 - \Delta t \frac{\partial f_k}{\partial W_k} \Big) \Delta W_k^{n+1} - \Delta t \Big[\frac{\partial f_k}{\partial U_i} \Delta U_i^{n+1} + \frac{\partial f_k}{\partial U_j} \Delta U_j^{n+1} + \frac{\partial f_k}{\partial M_i} \Delta M_j^{n+1} + \frac{\partial f_k}{\partial M_j} \Delta M_j^{n+1} \Big] = \Delta t\, F_k(t^n, y^n) \tag{5.12}$$

Upon eliminating the ΔU_i^{n+1}, ΔU_j^{n+1}, ΔM_i^{n+1} and ΔM_j^{n+1} using Equations 5.10 and 5.11 from Equation 5.12, there results a reduced system of K equations consisting of only the unknown flowrate increments. The system is written in vector form as

$$A\ \Delta W^{n+1} = Z \tag{5.13}$$

where

$$\begin{aligned} A &= [a_{k\nu}] \\ \Delta W^{n+1} &= col[\ \Delta W_1^{n+1}, \ldots, \Delta W_K^{n+1}\ ] \\ Z &= col[\ z_1, \ldots, z_K\ ] \end{aligned}$$

The elements in the column vector Z are described by

$$z_k = \Delta t\ F_k(t^n, y^n) + \Delta t^2\ [\ \frac{\partial f_k}{\partial U_i}\ \gamma_{1i} + \frac{\partial f_k}{\partial U_j}\ \gamma_{1j} + \frac{\partial f_k}{\partial M_i}\ \gamma_{2i} + \frac{\partial f_k}{\partial M_j}\ \gamma_{2j}\ ] \tag{5.14}$$

and A is a K × K matrix and its elements $a_{k\nu}$ are given by

$$\begin{aligned} a_{kk} &= 1 - \Delta t\ \frac{\partial f_k}{\partial W_k} - \Delta t^2\ [\ \frac{\partial f_k}{\partial U_j}\ (\alpha_{1j} + \beta_{1j} H_k)\ +\ \frac{\partial f_k}{\partial M_j}\ (\alpha_{2j}\ + \beta_{2j} H_k) \\ &\quad - \frac{\partial f_k}{\partial U_i}\ (\alpha_{1i} + \beta_{1i} H_k^*) - \frac{\partial f_k}{\partial M_i}\ (\alpha_{2i}\ +\ \beta_{2i} H_k^*)\ ]; \end{aligned} \tag{5.15}$$

and if $\nu \neq k$,

$$
a_{k\nu} = \begin{cases}
-\Delta t^2 \ \left[\frac{\partial f_k}{\partial U_i} (\alpha_{1i} + \beta_{1i} H_\nu) + \frac{\partial f_k}{\partial M_i} (\alpha_{2i} + \beta_{2i} H_\nu) \right] \\
\qquad\qquad \text{if } \nu \in T_i,\ \nu \notin I_j, \\
\Delta t^2 \ \left[\frac{\partial f_k}{\partial U_i} (\alpha_{1i} + \beta_{1i} H_\nu^*) + \frac{\partial f_k}{\partial M_i} (\alpha_{2i} + \beta_{2i} H_\nu^*) \right] \\
\qquad\qquad \text{if } \nu \in I_i,\ \nu \notin T_j, \\
-\Delta t^2 \ \left[\frac{\partial f_k}{\partial U_j} (\alpha_{1j} + \beta_{1j} H_\nu) + \frac{\partial f_k}{\partial M_j} (\alpha_{2j} + \beta_{2j} H_\nu) \right] \\
\qquad\qquad \text{if } \nu \in T_j,\ \nu \notin I_i, \\
\Delta t^2 \ \left[\frac{\partial f_k}{\partial U_j} (\alpha_{1j} + \beta_{1j} H_\nu^*) + \frac{\partial f_k}{\partial M_j} (\alpha_{2j} + \beta_{2j} H_\nu^*) \right] \\
\qquad\qquad \text{if } \nu \in I_j,\ \nu \notin T_i, \\
-\Delta t^2 \ \left[\frac{\partial f_k}{\partial U_i} (\alpha_{1i} + \beta_{1i} H_\nu) + \frac{\partial f_k}{\partial M_i} (\alpha_{2i} + \beta_{2i} H_\nu) \right. \\
\qquad \left. - \frac{\partial f_k}{\partial U_j} (\alpha_{1j} + \beta_{1j} H_\nu^*) - \frac{\partial f_k}{\partial M_j} (\alpha_{2j} + \beta_{2j} H_\nu^*) \right] \\
\qquad\qquad \text{if } \nu \in I_j,\ \nu \in T_i, \\
-\Delta t^2 \ \left[\frac{\partial f_k}{\partial U_j} (\alpha_{1j} + \beta_{1j} H_\nu) + \frac{\partial f_k}{\partial M_j} (\alpha_{2j} + \beta_{2j} H_\nu) \right. \\
\qquad \left. - \frac{\partial f_k}{\partial U_i} (\alpha_{1i} + \beta_{1i} H_\nu^*) - \frac{\partial f_k}{\partial M_i} (\alpha_{2i} + \beta_{2i} H_\nu^*) \right] \\
\qquad\qquad \text{if } \nu \in I_i,\ \nu \in T_j, \\
\qquad 0 \text{ otherwise.}
\end{cases}
$$

Depending upon the geometric arrangement of a hydraulic network, the A matrix can be of different structure. For the network shown in Figure 5.3, the A matrix would have the structure shown in Figure 5.4. The character x denotes the only possible nonzero elements of A.

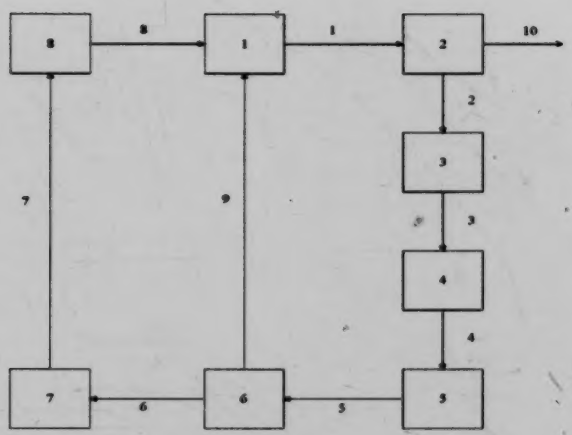

Figure 5.3: An 8-node network with 1 critical link.

$$\begin{bmatrix}
x & x & 0 & 0 & 0 & 0 & 0 & x & x \\
x & x & x & 0 & 0 & 0 & 0 & 0 & 0 \\
0 & x & x & x & 0 & 0 & 0 & 0 & 0 \\
0 & 0 & x & x & x & 0 & 0 & 0 & 0 \\
0 & 0 & 0 & x & x & x & 0 & 0 & x \\
0 & 0 & 0 & 0 & x & x & x & 0 & x \\
0 & 0 & 0 & 0 & 0 & x & x & x & 0 \\
x & 0 & 0 & 0 & 0 & 0 & x & x & x \\
x & 0 & 0 & 0 & x & x & 0 & x & x
\end{bmatrix}$$

Figure 5.4: The structure of the A matrix corresponding to the example network.

5.4 Derivation of the Hydraulic Network's Formulations

In the previous section, the derivation of the implicit integration method was explained. However, the detailed descriptions of the formulations mentioned have not been accomplished. This section will show the derivation of the formulations required for the development of the hydraulic network model.

The momentum balance equation that appeared in form of Equation 5.1 is

$$\dot{W}_k = \frac{A_k}{L_k}\left\{ P_i - P_j - [\,(\,\frac{f_k L_k}{D_k} + K_k\,)\;\phi_k^2\;\;\Omega_k\,]\;\frac{|W_k|W_k}{2\rho_f A_k^2} \pm E_k\;\rho_i\;g + \frac{W_k^2}{A_k^2}\,(\,v_i' - v_j'\,)\right\} \tag{5.16}$$

where A_k, L_k and D_k are the area, length, and diameter of a link k; P_i and P_j are the pressure at node i and j; f_k, K_k, ϕ_k^2, and Ω_k are the friction factor, fitting loss, Martinelli-Nelson two-phase flow multiplier and two-phase flow dependent multiplier; ρ is the local average, saturation liquid and saturation density; W_k is the mass flow in the link k; E_k is the elevation change; v_i' and v_j' are the specific volume of node i and j respectively.

The friction factor, f_k, can be calculated iteratively using Colebrook equation

$$\frac{1}{\sqrt{f_k}} = -0.86856\;\ln[\,\frac{1}{3.7}\frac{\epsilon}{D_k} + \frac{2.51}{R_e\sqrt{f_k}}\,] \tag{5.17}$$

where $\frac{\epsilon}{D_k}$ is the relative roughness inside the tube, and R_e is the Reynold number. However, the iterative evaluation of f_k at each time step is too time consuming

and a simpler form which requires no iteration in f_k is used

$$f_k = 0.0052 + \frac{1.1}{R_e^{-0.65}} \tag{5.18}$$

The detailed evaluation of the numerical values in Equation 5.18 can be found in (de Nevers, 1991). The single phase friction loss is corrected by the two-phase flow multiplier, ϕ_k^2, which is given in Chapter 2. The effective specific volume for slip model of each node is calculated as follow:

$$v' = \frac{x^2}{\alpha\rho_g} + \frac{(1-x)^2}{(1-\alpha)\rho_f} \tag{5.19}$$

where x is mass quality, α is local void fraction, and ρ_g and ρ_f are the vapor and liquid saturation densities.

The momentum equation is differentiated with respect to mass flow, $\left(\frac{\partial F_k}{\partial W_k}\right)_{U,M}$, internal energy, $\left(\frac{\partial F_k}{\partial U}\right)_{W,M}$, and nodal mass, $\left(\frac{\partial F_k}{\partial M}\right)_{W,U}$, as appearing in Equation 5.14 and 5.15. The formulations of each derivative are as follows:

$$\begin{aligned}\left(\frac{\partial F_k}{\partial W_k}\right)_{U,M} = \frac{A_k}{L_k}\Bigg\{ &-\left(\frac{f_k L_k}{D_k}\right)\frac{\partial \phi_k^2}{\partial W_k}\frac{|W_k|W_k}{2\rho_f A_k^2} - \left(\frac{f_k L_k}{D_k}\right)\frac{|W_k|\phi_k^2}{\rho_l A_k^2} \\ &-\frac{\partial f_k}{\partial W_k}\frac{L_k\phi_k^2}{D_k}\frac{|W_k|W_k}{2\rho_l A_k^2} + \frac{2Wk}{A_k^2}\left(v_i' - v_j'\right)\Bigg\}\end{aligned} \tag{5.20}$$

where

$$\frac{\partial \phi_k^2}{\partial W_k} = \frac{1}{A_k}\left\{\frac{\partial q}{\partial G}\left[\,1.2\left(\frac{\rho_f}{\rho_g} - 1\right)x^{0.824}\right\}\right. \tag{5.21}$$

$$\frac{\partial f_k}{\partial W_k} = -0.715 \frac{D_k}{\mu_k A_k} \left(\frac{W_k D_k}{\mu_k A_k}\right)^{-1.65} \tag{5.22}$$

Equation 5.21 is based on Equation 3.6 in Chapter 3. The partial derivative term, $\frac{\partial q}{\partial G}$, can be obtained as

$$\frac{\partial q}{\partial G} = \begin{cases} 1.36 \times 10^{-10} - 6.7 \times 10^{-12} P; & (G/10^6) < 0.7 \\ -87.56\ (10^6/G^2) - 1.419P\ (10^6/G^2); & (G/10^6) > 0.7 \end{cases}$$

and

$$\left(\frac{\partial F_k}{\partial U_i}\right)_{W,M} = \frac{\partial F_k}{\partial P_i} \frac{\partial P_i}{\partial U_i} \tag{5.23}$$

$$\left(\frac{\partial F_k}{\partial U_j}\right)_{W,M} = \frac{\partial F_k}{\partial P_j} \frac{\partial P_j}{\partial U_j} \tag{5.24}$$

$$\left(\frac{\partial F_k}{\partial M_i}\right)_{W,U} = \frac{\partial F_k}{\partial P_i} \frac{\partial P_i}{\partial M_i} \tag{5.25}$$

$$\left(\frac{\partial F_k}{\partial M_j}\right)_{W,U} = \frac{\partial F_k}{\partial P_j} \frac{\partial P_j}{\partial M_j} \tag{5.26}$$

where

$$\left(\frac{\partial F_k}{\partial P_i}\right)_{W,M} = \frac{A_k}{L_k} \left\{1 - \left[\left(\frac{f_k L_k}{D_k} + K_k\right) \frac{\partial \phi_k^2}{\partial P_i}\right] \frac{|W_k| W_k}{2\rho_f A_k^2} + \frac{W_k^2}{A_k^2} \frac{\partial v_i'}{\partial P_i}\right\}$$

$$\left(\frac{\partial F_k}{\partial P_j}\right)_{W,U} = \frac{A_k}{L_k} \left\{-1 + \frac{W_k^2}{A_k^2} \frac{\partial v_j'}{\partial P_j}\right\} \tag{5.27}$$

For single phase, $\left(\frac{\partial P}{\partial U}\right)_{W,M}$ and $\left(\frac{\partial P}{\partial M}\right)_{W,U}$ can be expressed as $\frac{1}{M}\left(\frac{\partial P}{\partial u}\right)_\rho$ and $\frac{1}{V}\left(\frac{\partial P}{\partial \rho}\right)_u$, respectively. The evaluation of the two partial derivatives require to use Helmholtz function and partial derivative transformation relationships. The

former partial derivative can be experessed as:

$$\frac{1}{M}\left(\frac{\partial P}{\partial \hat{u}}\right)_{\rho} = \frac{1}{M}\left\{\left(\frac{\partial P}{\partial \hat{u}}\right)_{T} + \left(\frac{\partial P}{\partial T}\right)_{\hat{u}}\left(\frac{\partial T}{\partial \hat{u}}\right)_{\rho}\right\} \tag{5.28}$$

It can then be expanded as the following:

$$\frac{1}{M}\left(\frac{\partial P}{\partial \hat{u}}\right)_{\rho} = \frac{1}{M}\left\{\left(\frac{\partial P}{\partial \rho}\right)_{T}\left(\frac{\partial \rho}{\partial \hat{u}}\right)_{T} + \left(\frac{\partial P}{\partial \rho}\right)_{\hat{u}}\left(\frac{\partial \rho}{\partial T}\right)_{\hat{u}}\left(\frac{\partial T}{\partial \hat{u}}\right)_{\rho}\right\} \tag{5.29}$$

and the latter can be expressed as the following:

$$\frac{1}{V}\left(\frac{\partial P}{\partial \rho}\right)_{\hat{u}} = \frac{1}{V}\left\{\left(\frac{\partial P}{\partial \rho}\right)_{T} + \left(\frac{\partial P}{\partial T}\right)_{\rho}\left(\frac{\partial T}{\partial \rho}\right)_{\hat{u}}\right\} \tag{5.30}$$

and the term $\left(\frac{\partial T}{\partial \rho}\right)_{\hat{u}}$ can be evaluated using triple product rule:

$$\left(\frac{\partial T}{\partial \rho}\right)_{\hat{u}}\left(\frac{\partial \hat{u}}{\partial T}\right)_{\rho}\left(\frac{\partial \rho}{\partial \hat{u}}\right)_{T} = -1 \tag{5.31}$$

or

$$\left(\frac{\partial T}{\partial \rho}\right)_{\hat{u}} = \frac{-\left(\frac{\partial \hat{u}}{\partial \rho}\right)_{T}}{\left(\frac{\partial \hat{u}}{\partial T}\right)_{\rho}} \tag{5.32}$$

With the expanded form of Equations 5.28 and 5.30, Helmholtz function can be utilized to evaluate the partial derivatives appeared in the above expressions. Helmholtz function, expressed as a function of density and temperature, is commonly adopted to construct steam table due to its accuracy and simplicity in estimating pressure, enthalpy, internal energy and entropy. Its expression is as

follows:

$$\psi = \psi_o(T) + RT\ [\ \ln\rho\ +\ \rho Q(\rho,\tau)\ ] \tag{5.33}$$

where

$$\psi_o = \sum_{i=1}^{6} \frac{C_i}{\tau^{i-1}} + C_7 \ln T + C_8 \ln \frac{T}{\tau} \tag{5.34}$$

and

$$Q = (\tau - \tau_c) \sum_{j=1}^{7} (\tau - \tau_{oj})^{j-2}\ [\ \sum_{i=1}^{8} A_{ij}(\rho - \rho_{oj})^{i-1} + e^{-E\rho} \sum_{i=9}^{10} A_{ij}\rho^{i-9}\ ] \tag{5.35}$$

The coefficients of the function can be found in (Keenan *et al.*, 1969). The basic relations for determining values of pressure and specific internal energy are as follows:

$$P = \rho^2 \left(\frac{\partial\psi}{\partial\rho}\right)_\tau \tag{5.36}$$

or

$$P = \rho RT \left[1 + \rho Q + \rho^2 \left(\frac{\partial Q}{\partial\rho}\right)_\tau\right] \tag{5.37}$$

$$\hat{u} = \left[\frac{\partial(\psi\tau)}{\partial\tau}\right]_\rho \tag{5.38}$$

or

$$\hat{u} = RT\rho\tau \left(\frac{\partial Q}{\partial\tau}\right)_\rho + \frac{d\psi_o\tau}{d\tau} \tag{5.39}$$

where

$$\left(\frac{\partial Q}{\partial\rho}\right)_\tau = \quad (\tau - \tau_c) \sum_{j=1}^{7} (\tau - \tau_{oj})^{j-2} \left[\sum_{i=2}^{8} A_{ij}(i-1)(\rho - \rho_o j)^{j-2}\right.$$

$$- \quad Ee^{-E\rho}\sum_{i=9}^{10} A_{ij}\rho^{i-9} + e^{-E\rho}A_{10j}\Bigg] \tag{5.40}$$

$$\left(\frac{\partial Q}{\partial \tau}\right)_\rho = \sum_{j=1}^{7}(\tau-\tau_{aj})^{j-1}\left[\sum_{i=1}^{8} A_{ij}(\rho-\rho_{aj})^{i-1} + e^{-E\rho}\sum_{i=9}^{10} A_{ij}\rho^{i-9}\right]$$
$$+ \quad (\tau-\tau_c)\sum_{j=1}^{7}(j-2)(\tau-\tau_{aj})^{j-3}\left[\sum_{i=1}^{8} A_{ij}(\rho-\rho_{aj})^{i-1}\right.$$
$$+ \quad \left. e^{-E\rho}\sum_{i=9}^{10} A_{ij}\rho^{i-9}\right] \tag{5.41}$$

$$\frac{d\psi_o\tau}{d\tau} = \psi_o + \tau\frac{d\psi_o}{d\tau} \tag{5.42}$$

where

$$\frac{d\psi_o}{d\tau} = \sum_{i=2}^{6} C_i\left(\frac{1-i}{\tau^i}\right) - (C_7 + 2C_8)\frac{1}{\tau} \tag{5.43}$$

Therefore, by differentiating the expressions of pressure and specific internal energy with respect to appropriate thermodynamic properties, all terms in Equations 5.29 and 5.30 can be evaluated and their expressions are as follows:

$$\left(\frac{\partial P}{\partial \rho}\right)_T = RT\left[1 + \rho Q + \rho^2\left(\frac{\partial Q}{\partial \rho}\right)_\tau\right]$$
$$+ \quad \rho RT\left[Q + \rho\left(\frac{\partial Q}{\partial \rho}\right)_T + 2\rho\left(\frac{\partial Q}{\partial \rho}\right)_\tau\right.$$
$$+ \quad \left.\rho^2\frac{\partial}{\partial \rho}\left\{\left(\frac{\partial Q}{\partial \rho}\right)_\tau\right\}_T\right] \tag{5.44}$$

$$\left(\frac{\partial \dot{u}}{\partial \rho}\right)_T = RT\tau\left(\frac{\partial Q}{\partial \tau}\right)_\rho + RT\rho\tau\frac{\partial}{\partial \rho}\left[\left(\frac{\partial Q}{\partial \tau}\right)_\rho\right]_T \tag{5.45}$$

$$\left(\frac{\partial \hat{u}}{\partial T}\right)_\rho = \frac{\partial}{\partial T}\left\{\frac{\partial \psi_o \tau}{\partial \tau}\right\}_\rho + 1000 R\rho \frac{\partial}{\partial T}\left\{\left(\frac{\partial Q}{\partial \tau}\right)_\rho\right\}_\rho \tag{5.46}$$

where

$$\begin{aligned}\frac{\partial}{\partial \rho}\left[\left(\frac{\partial Q}{\partial \tau}\right)_\rho\right]_T = & \sum_{j=1}^{7}(j-2)(\tau-\tau_{aj})^{j-2}\left[\sum_{i=2}^{8}A_{ij}(i-1)(\rho-\rho_{aj})^{i-2}\right. \\ & - \left. Ee^{-E\rho}\sum_{i=9}^{10}A_{ij}\rho^{i-9} + e^{-E\rho}A_{10j}\right] \\ & + (\tau-\tau_c)\sum_{j=1}^{7}(j-2)(\tau-\tau_{aj})^{j-3}\left[\sum_{i=2}^{8}A_{ij}(i-1)\,(\rho-\rho_{aj})^{i-2}\right. \\ & - \left. Ee^{-E\rho}\sum_{i=9}^{10}A_{ij}\rho^{i-9} + e^{-E\rho}A_{10j}\right] \end{aligned} \tag{5.47}$$

$$\begin{aligned}\frac{\partial}{\partial T}\left\{\left(\frac{\partial Q}{\partial \tau}\right)_\rho\right\}_\rho = & \sum_{j=1}^{7}(j-2)(\tau-\tau_{aj})^{j-3}\left(\frac{-1000}{T^2}\right)\left[\sum_{i=1}^{8}A_{ij}\,(\rho-\rho_{aj})^{i-1}\right. \\ & + \left. e^{-E\rho}\sum_{i=9}^{10}A_{ij}\rho^{i-9}\right] + \left(\frac{-1000}{T^2}\right)\sum_{i=1}^{7}(j-2)(\tau-\tau_{aj})^{j-3} \\ & \left[\sum_{i=1}^{8}A_{ij}(\rho-\rho_{aj})^{i-1} + e^{-E\rho}\sum_{i=9}^{10}A_{ij}\rho^{i-9}\right] \\ & + (\tau-\tau_c)\sum_{i=1}^{7}(j-2)(j-3)(\tau-\tau_{aj})^{j-4}\left(\frac{-1000}{T^2}\right) \\ & \left[\sum_{i=1}^{8}A_{ij}(\rho-\rho_{aj})^{i-1} + e^{-E\rho}\sum_{i=9}^{10}A_{ij}\rho^{i-9}\right] \end{aligned} \tag{5.48}$$

For two-phase region, Helmholtz function cannot be used for evaluating the partial derivatives because it is derived to obtain thermodynamic properties at single-phase regions and on saturation line only. Therefore, small perturbation at a specific pressure with respect to specific internal energy or density is used to evaluate $\frac{1}{M}\left(\frac{\partial P}{\partial \hat{u}}\right)_\rho$ and $\frac{1}{V}\left(\frac{\partial P}{\partial \rho}\right)_{\hat{u}}$.

5.5 Determination of Pressure and Temperature at Nodes

The change of mass flow, ΔW^{n+1}, is obtained by Equation 5.13; and thus, mass flow is calculated as follow:

$$W^{n+1} = \Delta W^{n+1} + W^n \tag{5.49}$$

Then, ΔU^{n+1} and ΔM^{n+1} can be evaluated using Equation 5.10 and 5.11, respectively. Similarly, the internal energy and nodal mass are determined in the same manner as mass flow:

$$U^{n+1} = \Delta U^{n+1} + U^n \tag{5.50}$$

$$M^{n+1} = \Delta M^{n+1} + M^n \tag{5.51}$$

Once the internal energy and nodal mass are obtained, the density and specific internal energy can be determined as follows:

$$\rho = \frac{M}{V} \tag{5.52}$$

$$\hat{u} = \frac{U}{M} \tag{5.53}$$

These two intensive thermodynamic properties, ρ and $\hat{u}$, are used to determine the pressure and temperature of each node. The strategy for determining the pressure and temperature are based on Figure 5.5 and 5.6 and are stated as follows:

For saturation liquid,

$$\rho > \rho_{critical} \text{ and } \hat{u} = \hat{u}_{satf}(\rho)$$

The pressure is:

$$P = P_{satf}(\rho) \text{ or } P = P_{satf}(\hat{u})$$

For saturation vapor,

$$\rho < \rho_{critical} \text{ and } \hat{u} = \hat{u}_{satf}(\rho)$$

The pressure is:

$$P = P_{satg}(\rho) \text{ or } P = P_{satg}(\hat{u})$$

For subcooled liquid,

$$\rho > \rho_{critical} \text{ and } \hat{u} > \hat{u}_{satf}(\rho)$$

The pressure is:

$$P = P_{satf}(\rho) + \left(\frac{\partial P}{\partial \hat{u}}\right)_{\rho} [\hat{u} - \hat{u}_{satf}(\rho)]$$

For superheated steam,

$$\rho < \rho_{critical} \text{ and } \hat{u} > \hat{u}_{satf}(\rho)$$

The pressure is:

$$P = P_{satg}(\rho) + \left(\frac{\partial P}{\partial \hat{u}}\right)_{\rho} [\hat{u} - \hat{u}_{satg}(\rho)]$$

For two-phase equilibrium mixture,

$$\rho > \rho_{critical} \text{ and } \hat{u} < \hat{u}_{satf}(\rho)$$

$$\rho < \rho_{critical} \text{ and } \hat{u} < \hat{u}_{satf}(\rho)$$

The pressure is found by iterative procedure to satisfy the following equaitons:

$$\rho = (1-\alpha)\rho_f(P) + \alpha\rho_g(P)$$

$$\frac{x}{1-x}\frac{1-\alpha}{\alpha}\frac{\rho_f}{\rho_g} = 1$$

$$\hat{u} = (1-x)\hat{u}_f(P) + x\hat{u}_g(P)$$

5.6 Node-link Representation of the Hydraulic Network Model

The generation bank used for this hydraulic network model consists of 874 tubes of risers and 933 tubes of downcomers. Its schematic diagram is shown in Figure 5.7. One representative dimension of all risers and downcomers is used to simplify the overall structure of the network model. In fact, it is ideal to divide the downcomers and risers into rows according to their geometric arrangement; for example, those have similar bending angle and length should be grouped. Figure 5.8 shows the node-link representation of Figure 5.7. The steam drum is divided into two nodes; one is the liquid zone denoted as 0 and the other is the vapor and liquid

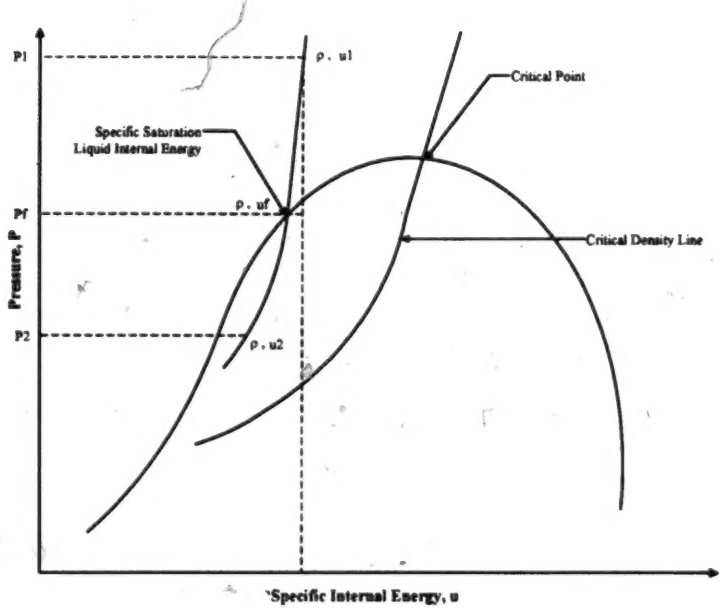

Figure 5.5: The pressure-specific internal energy diagram.

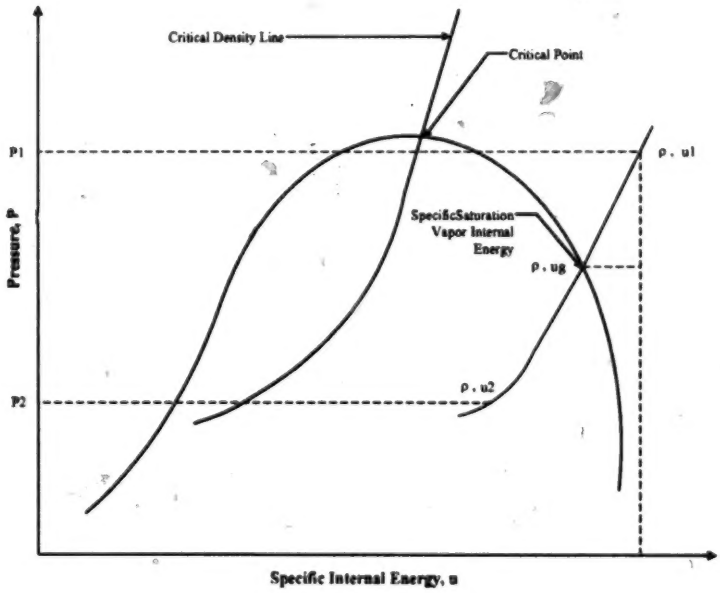

Figure 5.6: The pressure-specific internal energy diagram.

Number	Link		Node
	Length m	Diameter m^2	Volume m^3
0	0.27	0.056	14.1
1	5.87	0.056	1.24
2	5.97	0.056	25.6
3	0.37	0.056	1.67
4	0.38	0.056	12.6
5	3.11	0.056	1.63
6	5.45	0.056	11.7
7	3.11	0.056	11.7
8	0.38	0.056	1.63
9	-	-	32.2

Table 5.1: Measurements of the length and diameter of the links and the volume of the nodes.

zone denoted as 9. The number of nodes depends upon how detailed the operating information, such as pressure, steam quality and temperature is required. In this case, the heated downcomers and risers are divided into three and four nodes, respectively. The mud drum is the fifth node denoted as 4 in the diagram. With ten nodes there are nine links denoted from 0 to 8. The length and area of each link and the volume of each node are shown in Table 5.1. The volume of each node of downcomers and risers is calculated by multiplying the number of tubes to the volume of a single node. This will facilitate the calculations of heat transfer and circulation rate in the circuit.

5.7 Heat Transfer Model for the Hydraulic Network Model

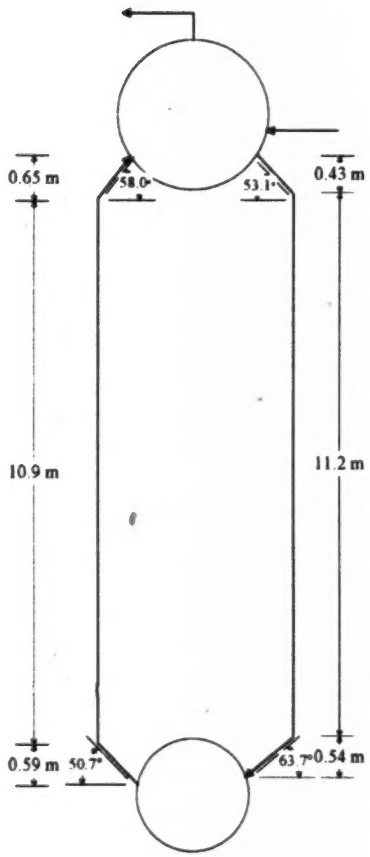

Figure 5.7: The schemetic diagram of the generation bank section.

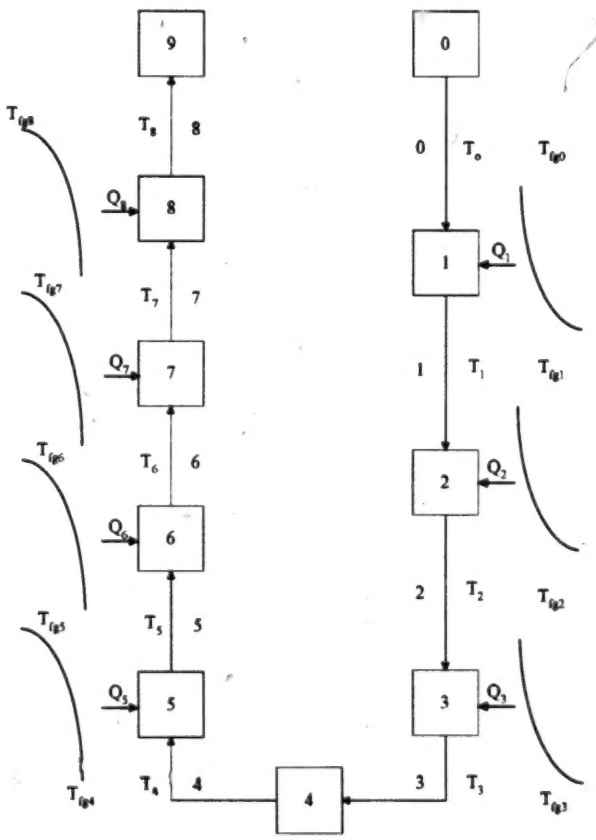

Figure 5.8: The node-link representation of the generation bank.

The heat transfer model for the generation bank section adopts the log-mean temperature difference (LMTD) modelling technique for a counter-flow heat exchanger. The generation bank of the utility boiler is actually an immense counter-flow heat exchanger. Therefore, each node of the hydraulic network model is treated as a counter-flow heat exchanger which has its local overall heat transfer coefficient and temperature profile. Figure 5.8 shows the distributions of the heat transfer model. The heat transfer from flue gas to water can be expressed as:

$$\frac{dT_w}{dt} = \frac{1}{M_w C_{pw}} (W_{fg} C_{pfg} (T_{fi} - T_{fo}) - h_i A (T_w - T_b)) \tag{5.54}$$

where

T_w = tube wall temperature, K.

T_{fi} = inlet flue gas temperature, K.

T_{fo} = exit flue gas temperature, K.

T_b = bulk temperature of water or steam-water mixture, K.

C_{pw} = specific heat capacity of the tubes, $\frac{kJ}{kgK}$.

C_{pfg} = specific heat capacity of the flue gas, $\frac{kJ}{kgK}$.

M_w = mass of the tubes, kg.

h_i = convective heat transfer coefficient of water or steam-water mixture, $\frac{W}{m^2 K}$.

A = heat transfer area, m^2.

W_{fg} = mass flow of flue gas, $\frac{kg}{s}$.

One assumption for Equation 5.54 is the neglect of lag due to conductive heat transfer across the tube wall, which can be justified by the thin wall thickness. Therefore, an average tube wall temperature is calculated. The local convective heat transfer coefficient, h_i, is evaluated depending upon the state of water inside the tubes and the temperature difference between tube wall and bulk fluid. The strategy for evaluating h_i is showm in Figure 5.9 which is based on the forced convective boiling heat transfer discussions in Chapter 3.

The determination of the exit flue gas temperature of each node uses LMTD methods and its equations are as follows:

$$T_{fo} = T_{fi} - \eta \, (T_{fi} - T_{wi}) \tag{5.55}$$

where

T_{fo} = exit flue gas temperature, K.

T_{fi} = inlet flue gas temperature, K.

T_{wi} = inlet water or steam-water mixture temperature, K.

η = efficiency of the heat exchanger.

The efficiency of the heat exchanger, η, can be evaluated as follow:

$$\eta = \frac{1 - e^{-\gamma}}{1 - \frac{W_{fg} C_{pfg}}{W_{wi} C_{pwi}} e^{-\gamma}} \tag{5.56}$$

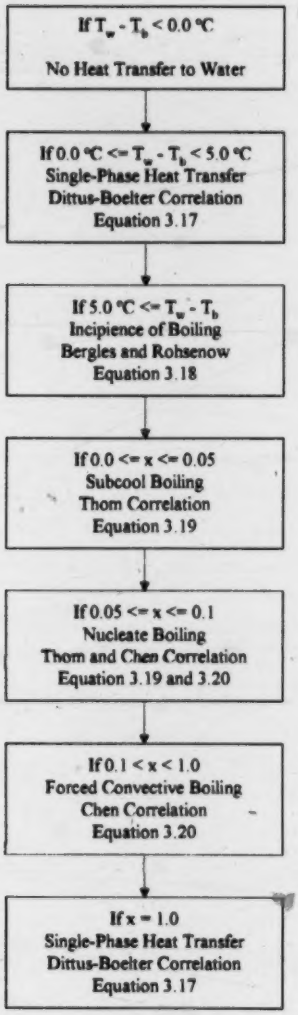

Figure 5.9: The flow diagram for determining the heat transfer coefficient.

where

W_{wi} = mass flow of water or steam-water mixture, $\frac{kg}{s}$.

C_{pwi} = specific heat capacity of water or steam-water mixture, $\frac{kJ}{kgK}$.

$$\gamma = U_o A \left(\frac{1}{W_{fg} C p_{fg}} - \frac{1}{W_{wi} C p_{wi}} \right)$$

where

U_o = the local overall heat transfer coefficient, $\frac{W}{m^2 K}$.

A = heat transfer areas, m^2.

The local overall heat transfer coefficient, U_o, is evaluated referring to the outer surface heat transfer area, and its expression is:

$$\frac{1}{U_o} = \frac{r_i}{r_o h_{fg}} + \frac{r_i}{k} \log_e \frac{r_i}{r_o} + \frac{1}{h_i} \tag{5.57}$$

where

r_i = inner radius of a tube, m.

r_o = outer radius of a tube, m.

h_{fg} = heat transfer coefficient of the flue gas, $\frac{W}{m^2 K}$.

5.7.1 The Implicit Integration Method for the Heat Transfer Model.

Using the same implicit integration scheme explained in previous section, a system of heat transfer equations can be established to calculate the heat transferred from flue gas to water at each node. Let $y = col[\ T_{w1}, \ldots, T_{wN}\ ]$ and $F = col[\ F_1, \ldots, F_N\ ]$ where F is the right hand side of Equation 5.54. These equations can be written in vector form as:

$$\dot{y} = F(t, y) \tag{5.58}$$

The approximate solution may be calculated by the following formula:

$$[\ I - \Delta t\ J(t^n, y^n)\ ]\ \Delta y^{n+1} = \Delta t\ F(t^n, y^n) \tag{5.59}$$

where $\Delta y^{n+1} = y^{n+1} - y^n$; $J(t^n, y^n)$ is the Jacobian matrix of the transformation of $F(t^n, y^n)$; I is the identity matrix; Δt is the time step; and n is time. The determination of y^{n+1} follows from the determination of the increment Δy^{n+1}.

The term $[\ I - \Delta t\ J(t^n, y^n)\ ]$ is a diagonal matrix denoted as B of terms $1 + \frac{\Delta t A_i h_i}{C_{pw}}$, where A_i is the inner heat transfer area, and h_i is the local convective heat transfer coefficient of the water or steam-water mixture. Then, the tube wall temperature can be calculated as:

$$\Delta T_w^{n+1} = B^{-1} \Delta t\ F(t^n, y^n) \tag{5.60}$$

5.8 The Programming Structure of the Hydraulic Flow Network

The hydraulic flow network model adopts MATLAB as the operating platform. Being interfaced with MATLAB, all algorithms are written using C language. The flow diagram of the program is shown in Figure 5.10. A set of initial conditions is selected before implementing the program. The parameters of the initial conditions are used by "Update.c" to evaluate the A matrix and z_k of Equation 5.13 from which the ΔW^{n+1} can be determined. The ΔW^{n+1} is then used by "Calrhou.m" to evaluate the mass flow, W_k^{n+1}, nodal density, ρ^{n+1}, and specific internal energy, $\hat{u}^{n+1}$, for the next step. The tube wall temperature for the next step is calculated using parameters at present step by "CaldTw.c". The state of each node, the pressure and temperature, is determined by "CalPT.c" using density, ρ^{n+1}, specific internal energy, $\hat{u}^{n+1}$, pressure, P^n, temperature, T^n, and state indicator, tbp^n. Note that the pressure and temperature calculated from "CalPT.c" are for next step. The new pressure, P^{n+1}, density, ρ^{n+1}, and state indicator, tbp^{n+1}, are used to evaluate the quality, x^{n+1}, of each node. With the next-step parameters, such as P^{n+1}, T^{n+1}, W_k^{n+1}, x^{n+1}, tbp^{n+1} the local convective heat transfer coefficient, h_i^{n+1}, can be determined by "Sethi.c" according to the conditions set in Figure 5.9. The final step here is to evaluate the flue gas temperature using T^{n+1}, W_k^{n+1}, x^{n+1}, tbp^{n+1}, W_{fg}^{n+1}, h_i^{n+1} and T_f^n. W_{fg} and T_f are the mass flow of flue gas and the flue gas temperature at different locations, respectively. All the next-step parameters are then fed back to "Update.c" for continuing the calculations mentioned above

until steady state or specified time span is reached.

The following section will explain the structure of each algorithm from previous paragraph.

Update.c

The flow diagram of "Update.c" is shown in Figure 5.11. The specific volume, quality, viscosity, specific enthalpy, void fraction, $\frac{\partial P}{\partial M}$ and $\frac{\partial P}{\partial U}$ are first evaluated for each node using pressure, temperature, mass flow, nodal volume, nodal mass, density, heat input, specific internal energy and state indicator at present step. These parameters will then be used to evaluate the energy and mass balance of each node; the single-phase friction factor, the two-phase correctional multiplier, $\frac{\partial f}{\partial W_k}$, $\frac{\partial \phi_k^2}{\partial W_k}$, the momentum balance and its derivative with respect to mass flow, $\frac{\partial f_k}{\partial W_k}$ of each link. With information of each node and link evaluated, the A matrix and the column vector z_k can be filled and passed to MATLAB at which the ΔW_k^{n+1} will be evaluated using built-in Gaussian elimination algorithm.

Calrhou.m

This MATLAB script file functions to manipulate the incremental mass flow, ΔW_k^{n+1}, and specific enthalpy to evaluate the incremental internal energy, ΔU^{n+1}, and nodal mass, ΔM^{n+1} of Equation 5.8 and 5.9, respectively. Then, the internal energy and nodal mass; density and specific internal energy can be evaluated using Equation 5.50, 5.51, 5.52 and 5.53, respectively. The density and specific internal energy will be passed to MATLAB workspace and used by the following subroutines.

CaldTw.c

The flow diagram of "CaldTw.c" is shown in Figure 5.12. This algorithm is to evaluate the incremental tube wall temperature using the method discussed in Section 5.7.1. The B matrix and the column vector containing the right side of Equation 5.54 are passed to MATLAB at which the incremental tube wall temperature, ΔT_w^{n+1}, will be evaluated using Gaussian elimination algorithm.

Calx.c

This short algorithm is to determine the steam quality of each node using pressure, density and state indicator at next-step. The flow diagram is shown in Figure 5.13.

CalPT.c

This algorithm is to evaluate the state of each node, pressure and temperature, using two intensive thermodynamic properties, density and specific internal energy. The pressure and temperature from pervious step will serve as an initial guess to Newton numerical scheme to evaluate the state at single and two-phase regions. The strategy mentioned in Section 5.5 will be used to determine the pressure, temperature, and state indicator which will be passed to MATLAB workspace to be used by the following algorithms. The flow diagram is shown in Figure 5.14.

Sethi.c

This algorithm is to determine the local convective heat transfer coefficient for each node using pressure, temperature, mass flow rate, steam quality and state

indicator of next step. The strategy for determining the use of different heat transfer correlations depends on the temperature difference between the tube wall and the bulk fluid. The flow diagram of the "Sethi.c" is shown in Figure 5.15.

CalTf.c

This algorithm is to evaluate the flue gas temperature at specific location along the risers and downcomers. The technique used to achieve this is explained in Section 5.7. The flow diagram is shown in Figure 5.16. The specific heat capacity and the overall heat transfer coefficient are first evaluated, then the γ and η of Equation 5.56 can be determined. The exit flue gas temperature of each node can now be evaluated using Equation 5.55.

At this stage, the first set of input parameters to "Update.c" has been evaluated to be the parameters for the next step. This new set of parameters is now fed back to the begining of the program for the continuation of the loop. The program can be terminated when steady-state or a specific time span is reached.

5.9 Simulation Setup for the Hydraulic Network Model

Referring to Figure 5.8 node 0 and 9 serve as the boundary of the circulation circuit. The pressure at node 0 and 9 is set at 7.2 MPa and the enthalpy entering the downcomers is set at 1237.1kJ/kg which corresponds to the subcooled water state at 7.2 MPa. The energy and mass balance of the two nodes are assumed to be constant. A set of initial conditions is selected for each node and link and it is shown in Table 5.2. The volume of each node and the length and diameter of

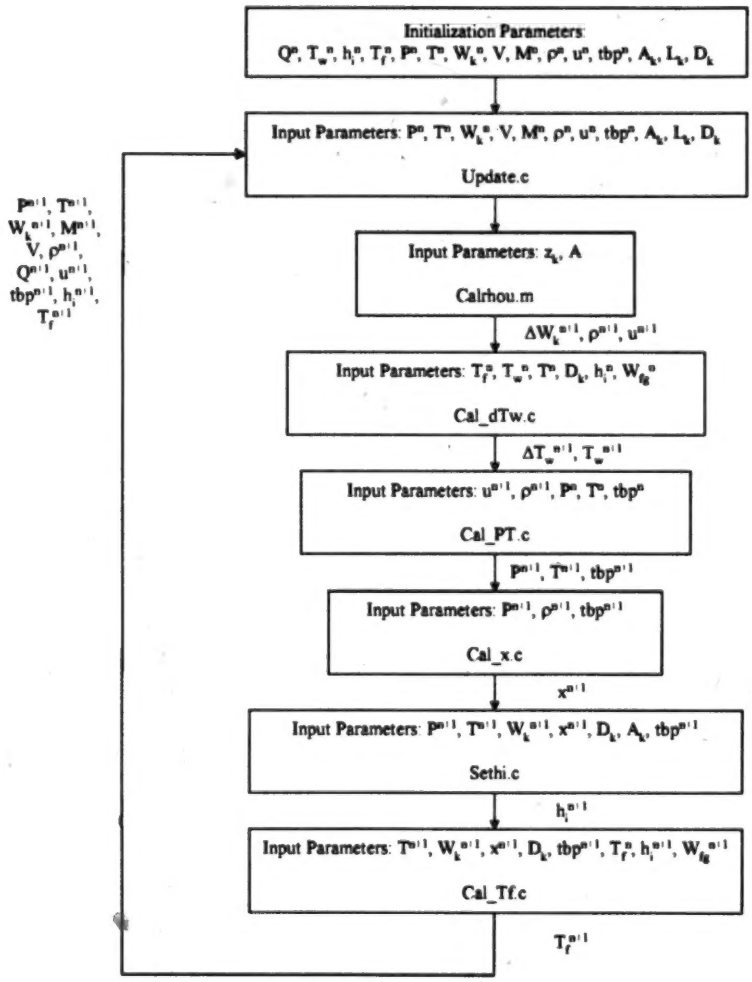
Initialization Parameters
Q^n, T_w^n, h_i^n, T_f^n, P^n, T^n, W_k^n, V, M^n, ρ^n, u^n, tbp^n, A_k, L_k, D_k
Input Parameters: P^n, T^n, W_k^n, V, M^n, ρ^n, u^n, tbp^n, A_k, L_k, D_k
Update.c
P^{n+1}, T^{n+1}, W_k^{n+1}, M^{n+1}, V, ρ^{n+1}, Q^{n+1}, u^{n+1}, tbp^{n+1}, h_i^{n+1}, T_f^{n+1}
Input Parameters: z_k, A
Calrhou.m
ΔW_k^{n+1}, ρ^{n+1}, u^{n+1}
Input Parameters: T_f^n, T_w^n, T^n, D_k, h_i^n, W_{fg}^n
Cal_dTw.c
ΔT_w^{n+1}, T_w^{n+1}
Input Parameters: u^{n+1}, ρ^{n+1}, P^n, T^n, tbp^n
Cal_PT.c
P^{n+1}, T^{n+1}, tbp^{n+1}
Input Parameters: P^{n+1}, ρ^{n+1}, tbp^{n+1}
Cal_x.c
x^{n+1}
Input Parameters: P^{n+1}, T^{n+1}, W_k^{n+1}, x^{n+1}, D_k, A_k, tbp^{n+1}
Sethi.c
h_i^{n+1}
Input Parameters: T^{n+1}, W_k^{n+1}, x^{n+1}, D_k, tbp^{n+1}, T_f^n, h_i^{n+1}, W_{fg}^{n+1}
Cal_Tf.c
T_f^{n+1}

Figure 5.10: The flow diagram of the hydraulic flow network.

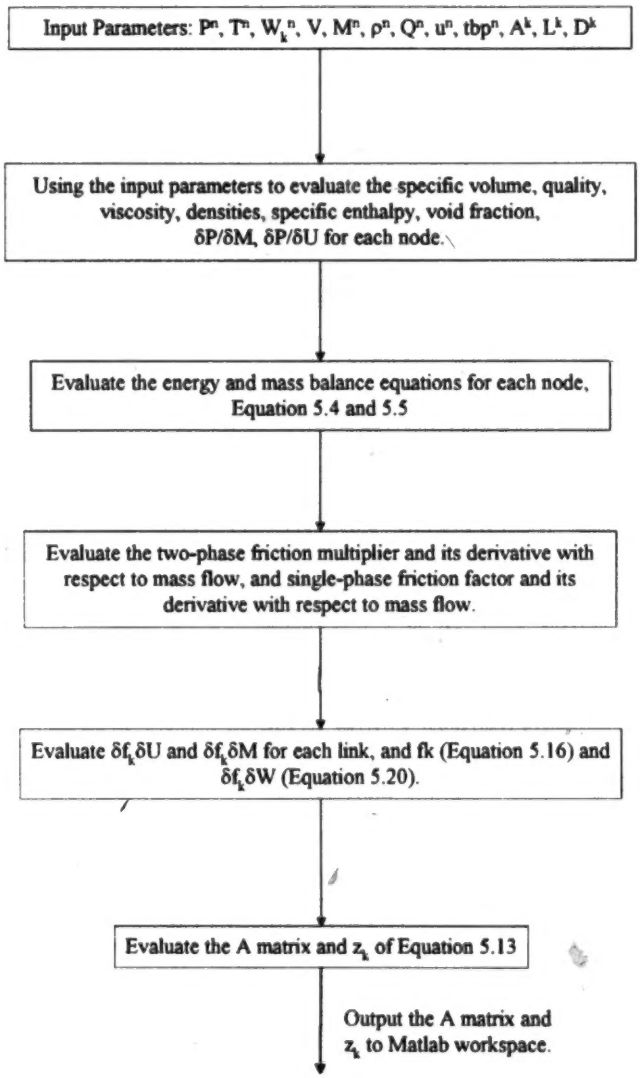
Input Parameters: P^n, T^n, W_k^n, V, M^n, ρ^n, Q^n, u^n, tbp^n, A^k, L^k, D^k
Using the input parameters to evaluate the specific volume, quality, viscosity, densities, specific enthalpy, void fraction, $\delta P/\delta M$, $\delta P/\delta U$ for each node.
Evaluate the energy and mass balance equations for each node, Equation 5.4 and 5.5
Evaluate the two-phase friction multiplier and its derivative with respect to mass flow, and single-phase friction factor and its derivative with respect to mass flow.
Evaluate $\delta f_k \delta U$ and $\delta f_k \delta M$ for each link, and fk (Equation 5.16) and $\delta f_k \delta W$ (Equation 5.20).
Evaluate the A matrix and z_k of Equation 5.13
Output the A matrix and z_k to Matlab workspace.

Figure 5.11: The flow diagram of the Update.c algorithm.

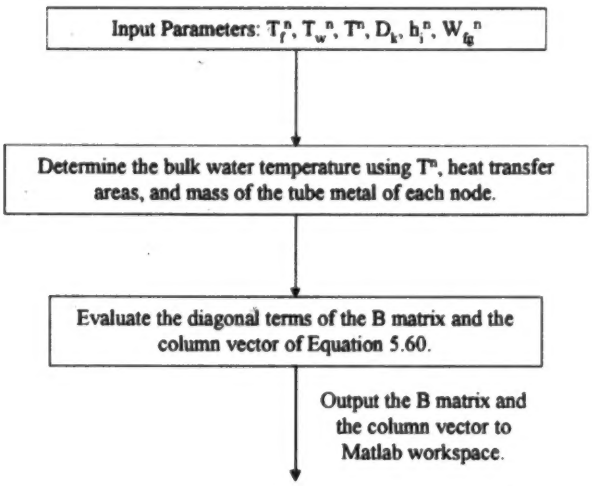
Input Parameters: T_f^n, T_w^n, T^n, D_k, h_i^n, W_{fg}^n
Determine the bulk water temperature using T^n, heat transfer areas, and mass of the tube metal of each node.
Evaluate the diagonal terms of the B matrix and the column vector of Equation 5.60.
Output the B matrix and the column vector to Matlab workspace.

Figure 5.12: The flow diagram of the CaldTw.c algorithm.

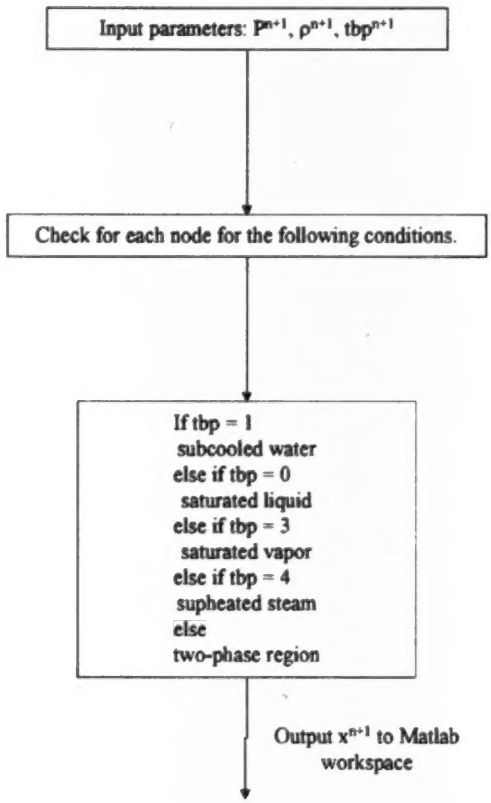

Figure 5.13: The flow diagram of the Calx.c algorithm.

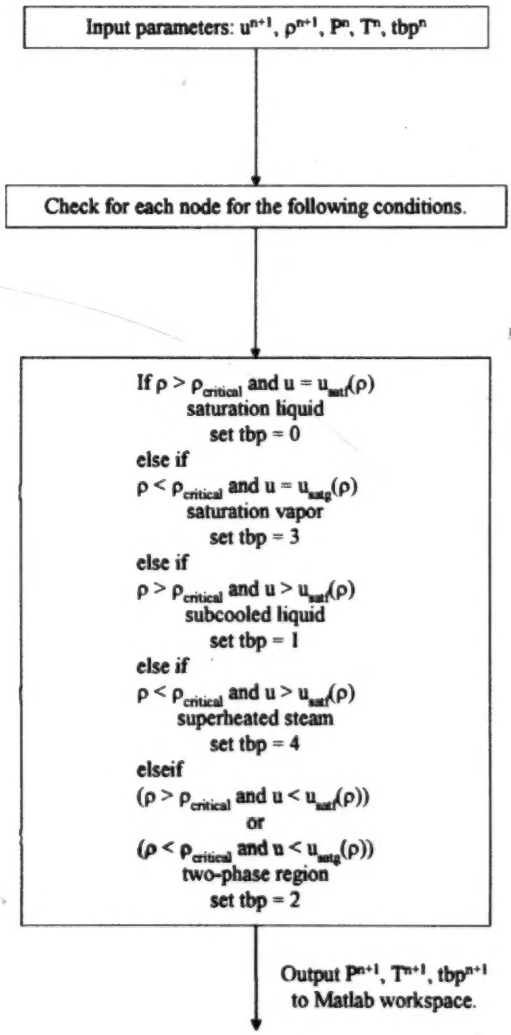

Figure 5.14: The flow diagram of the CalPT.c algorithm.

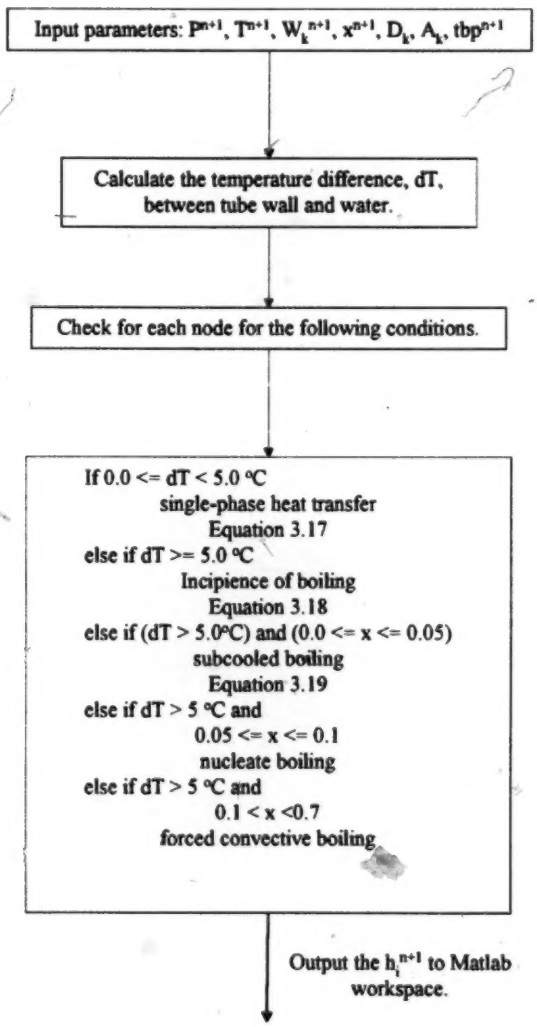

Figure 5.15: The flow diagram of the Sethi.c algorithm.

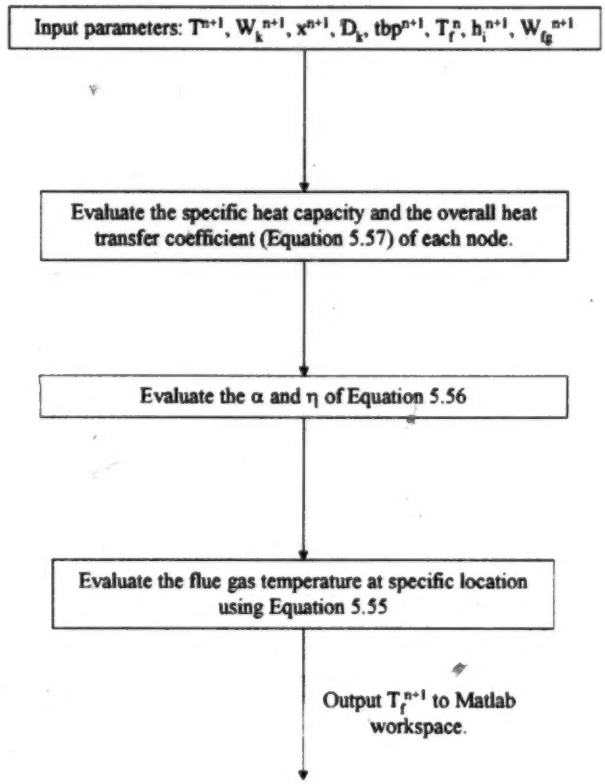
Input parameters: T^{n+1}, W_k^{n+1}, x^{n+1}, D_k, tbp^{n+1}, T_f^n, h_i^{n+1}, W_{fg}^{n+1}
Evaluate the specific heat capacity and the overall heat transfer coefficient (Equation 5.57) of each node.
Evaluate the α and η of Equation 5.56
Evaluate the flue gas temperature at specific location using Equation 5.55
Output T_f^{n+1} to Matlab workspace.

Figure 5.16: The flow diagram of the CalTf.c algorithm.

each link are shown in Table 5.1. The model can be simulated according to the programming structure explained in previous section.

5.10 Results and Discussions of the Hydraulic Network Model

The boundary conditions of the established generation bank model are the steam drum pressure and inlet subcooled water enthalpy. A step increase and decrease of 55 ^oC of the flue gas inlet temperature to the generation bank are implemented to examine the dynamic response of the circulation flow. In addition, the inlet water enthalpy is also subjected to a step increase and decrease of 9 ^oC of feed water to examine the effect of subcooling on the dynamic response of the circulation flow.

Steady-state is reached using the parameters in Table 5.2 before any step change is implemented. Figure 5.17 and 5.18 show a step increase and decrease of 55 ^oC of the inlet flue gas temperature to the generation bank at 10 s, respectively. Both figures show the dynamics of the circulation flow of each link as specified in Section 5.6. For the circulation flow response subjected to the step increase in heat input, it is expected the circulation flow rate will increase. At steady state, this is observed. However, the circulation flow rate at the inlet of the downcomers is actually decreasing 6.3 % from the steady state right after the heat input increases. The flow later increases and settles at a new steady state. The same transient phenomena are reported and explained in Çoq *et.al.*, (1983) and Lee *et.al.*, (1976). The flow boiling instability experiment done by Lee *et.al.*, (1976) shows the effect

Number	Node										Link
	P	T	Q	T_w	T_f	h_i	ρ	$\hat{u}$	tbp	M	W_k
	MPa	K	kW	K	K	J/Wm^2	kg/m^3	kJ/kg		kg	kg/s
0	7.2000	553.2	0.0	0.0	0.0	0.0	750.6	1227.5	1	10561.0	769.2
1	7.2016	553.0	494.1	554.6	624.1	3839.5	752.1	1226.1	1	929.3	769.2
2	7.2443	557.2	17244.0	557.5	627.4	3856.5	743.9	1248.3	1	1906.4	769.2
3	7.2872	557.6	1768.8	561.2	743.2	3858.3	743.1	1250.6	1	1241.2	769.2
4	7.2892	558.1	1912.5	561.5	755.1	3963.8	742.2	1253.0	1	9368.7	769.2
5	7.2870	558.6	2056.3	562.7	755.1	4069.4	741.2	1255.7	1	1207.4	769.2
6	7.2649	561.6	19680.0	563.2	768.9	7490.0	697.9	1274.0	2	8153.8	769.2
7	7.2275	561.3	31927.0	564.8	901.1	11309.0	489.2	1304.1	2	5714.4	769.2
8	7.2112	561.1	58741.0	565.2	1115.5	12424.0	461.9	1309.6	2	752.6	769.2
9	7.2000	560.9	0.0	0.0	1155.0	0.0	352.1	1344.3	2	10996.0	-

Table 5.2: The initial conditions of each node and link for the simulation.

of a step increase in heat input to the transient response at the constant circulation flow. The experiment shows that the inlet circulation mass flow reverses right after the heat input increases. The amplitudes of the flow reversal decreases with time and the flow finally settles at steady state again. Although this experiment is not of natural-circulation flow boiling type, it presents an important transient phenomena of flow boiling under which is subjected to heat variations. This flow reversal phenomena is also reported in Coq *et.al.*, (1983). This transient phenomena is explained by a sudden rise in pressure caused by a fast vaporization of the liquid in the heated section. This sudden increase in pressure in two-phase section is shown in Figure 5.19. Other transient phenomena, such as the flow response in two-phase section is not explained but the simulated response can be justified. From the simulation, the inlet mass flow decreases spontaneously after the heat input increases while the mass flow in two-phase sections goes to the opposite direction. The increased heat input causes the rise of steam quality, as shown in Figure 5.21, which increases the volume difference between two-phase and single-phase nodes and so as the flow. However, the sudden decrease in flow in downcomers imposes a significant drag on two-phase section of which the flow rate slightly decreases after the time required by the two-phase section to receive the signal of the drastic flow decrease. Afterwards mass flow in the circuit is self-adjusted to balance the pressure drop in the risers and downcomers and reaches a higher steady-state value induced by the increased heat input. An opposite situation to the step decrease in heat input is then expected. The circulation of water in downcomers increases 6.2 % from the steady state due to the decrease in pressure in two-phase section.

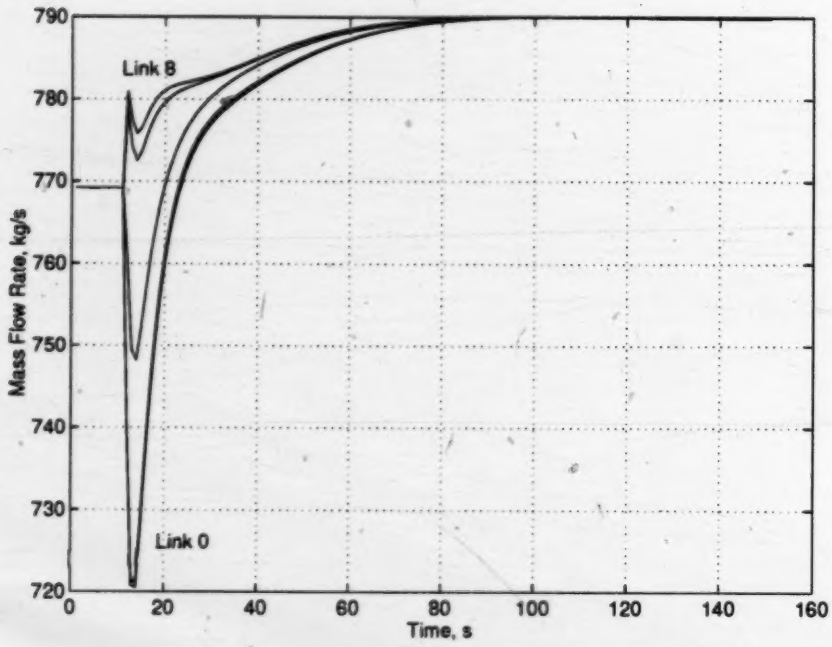

Figure 5.17: The circulation flow response to the step increase of the flue gas inlet temperature.

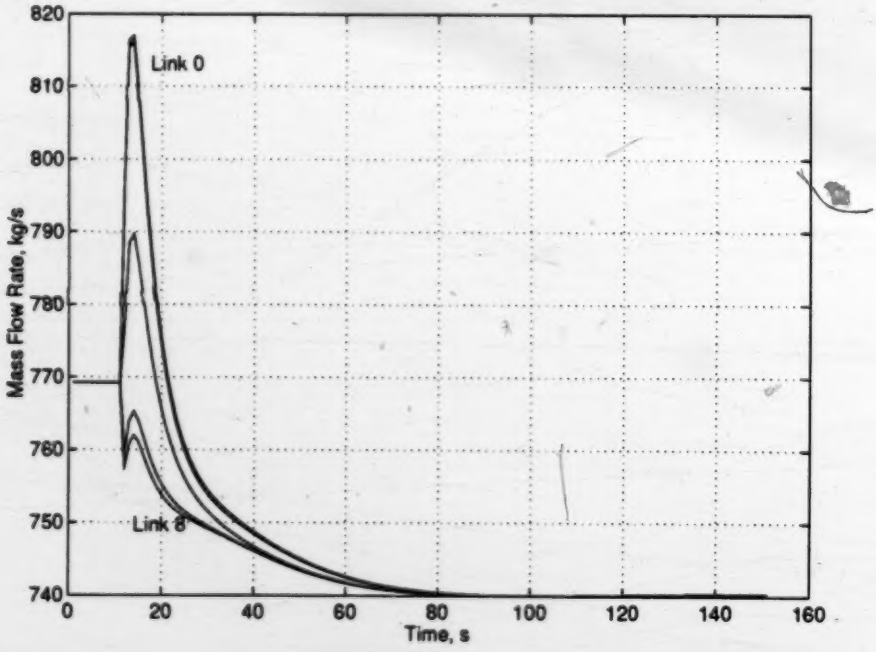

Figure 5.18: The circulation flow response to the step decrease of the flue gas inlet temperature.

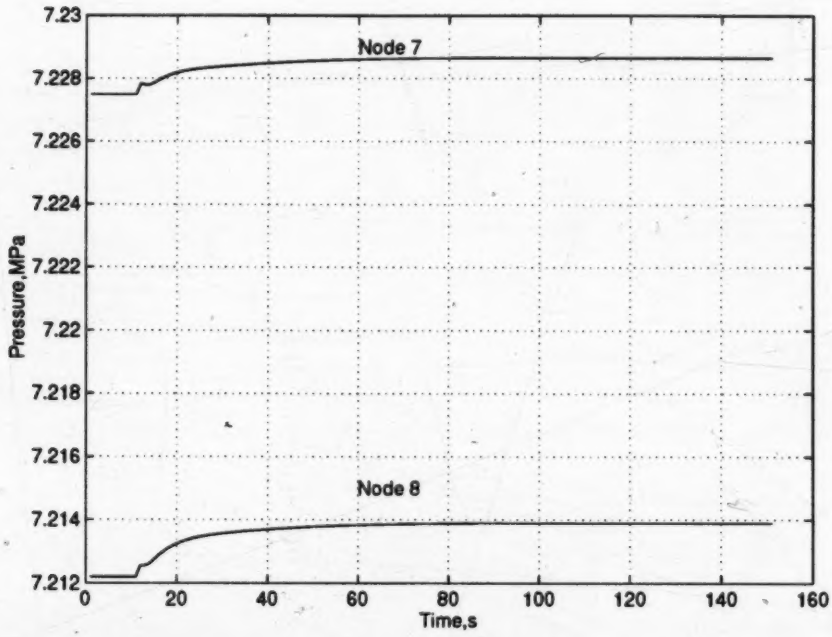

Figure 5.19: The pressure response at node 7 and 8 under a step increase of the inlet flue gas temperature.

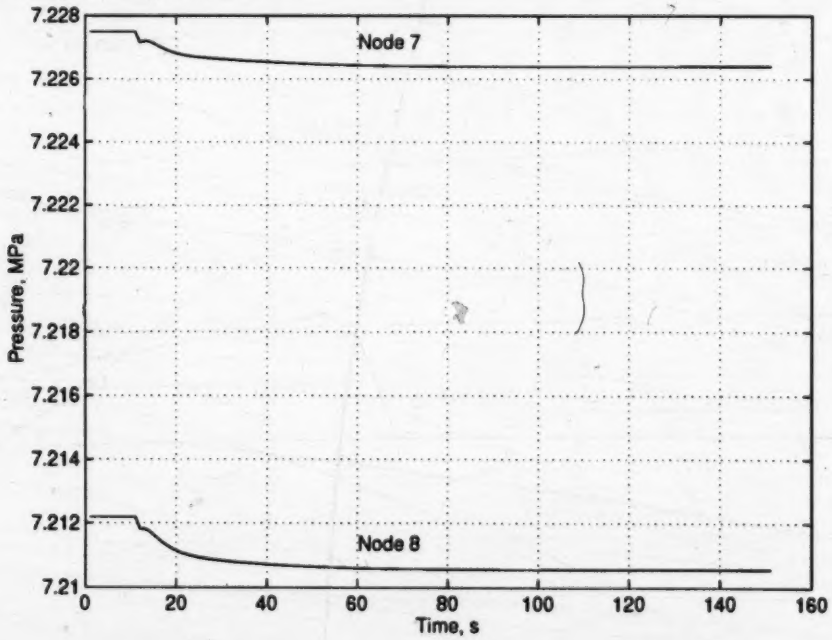

Figure 5.20: The pressure response at node 7 and 8 under a step decrease of the inlet flue gas temperature.

Figure 5.20 shows the decrease in pressure at two-phase section. Although the flow in two-phase section decreases owing to the decrease of acclerational force caused by the difference in specific volume, it is pushed by the upcoming circulating water as the hump shown in Figure 5.18. Then, the circulation at each link decreases and asymtotically approaches a lower steady-state value. As shown in Figure 5.17 and 5.18, the settling time for the circulation flow of the step heat decrease is the same as that of the step heat increase.

Similar to the step change of heat input, the step change of inlet water enthalpy at 10 s is implemented after the system reaches steady state. The transient responses of the circlation flow subjected to step changes in inlet water enthalpy are shown in Figure 5.23 and 5.24. As the inlet water enthalpy increases, the increased enthalpy will propagate through the circuit. While keeping heat input constant, the enthalpy in the circuit is expected to increase and so is the steam quality in two-phase section. The increase in vaporization of liquid causes an increase in pressure resulting in a slight decrease in mass flow in downcomers as the effect of step increase in heat input. The propagation process of the heat enthalpy to subsequent nodes is sluggish or overdamped. The farther the nodes from the inlet the more overdamping is observed. This is shown in Figure 5.25. However, the decrease in flow by the increased inlet enthalpy is not as severe as that by the increase in heat input. In addition, because of the overdamped response of the propagation of heat enthalpy, the decrease of mass flow in each link is in phase. The circulation flow later increases after approximately 20 s, and reaches at a higher steady-state value.

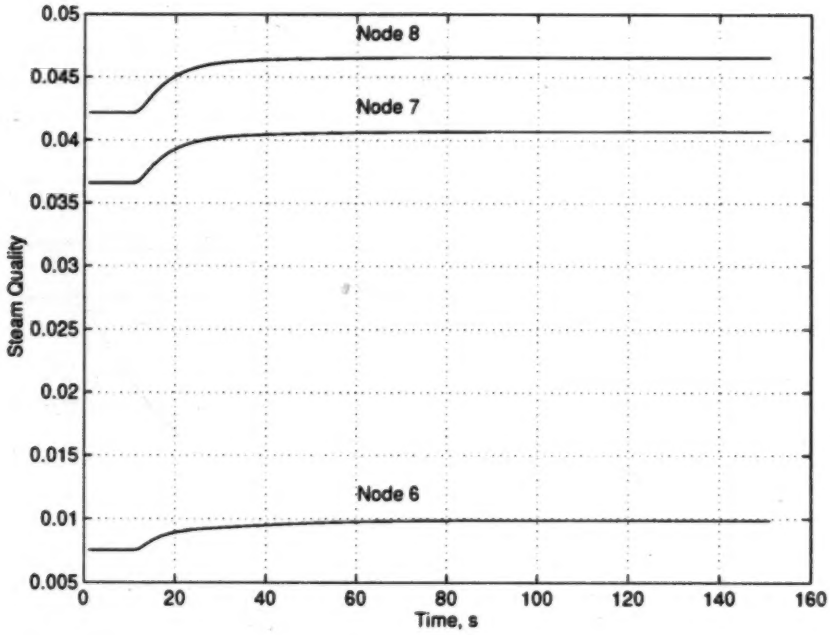

Figure 5.21: The steam quality response to the step increase of the flue gas inlet temperature.

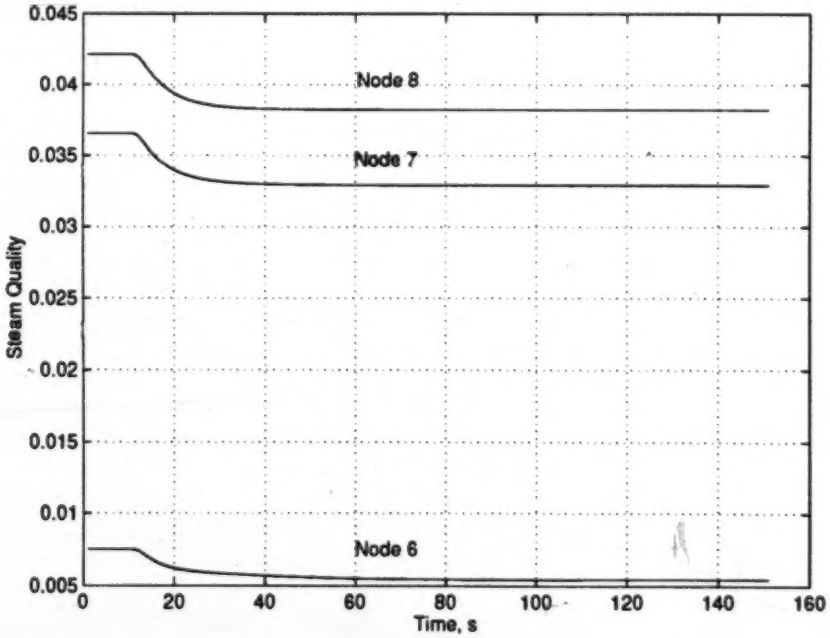

Figure 5.22: The steam quality response to the step decrease of the flue gas inlet temperature.

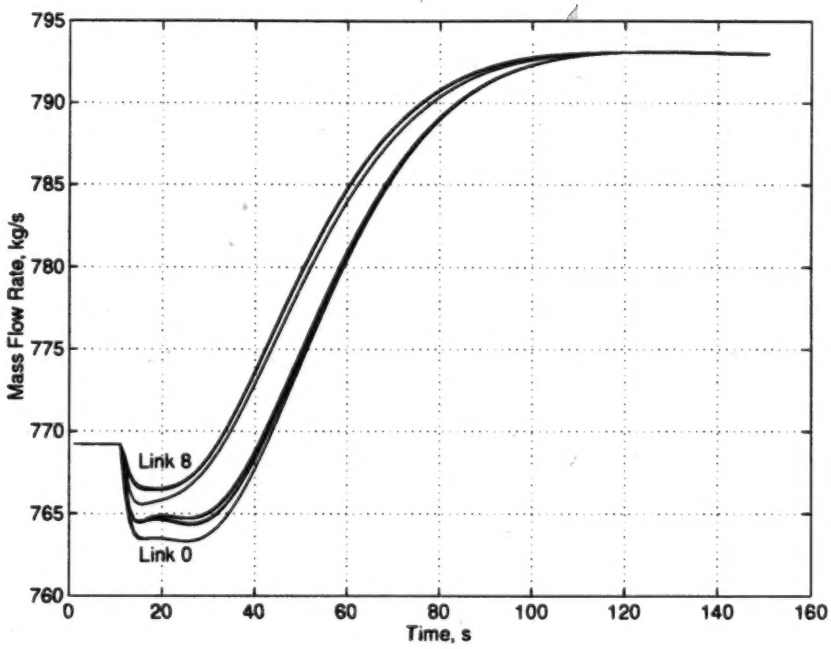

Figure 5.23: The circulation flow response to the step increase of inlet water enthalpy.

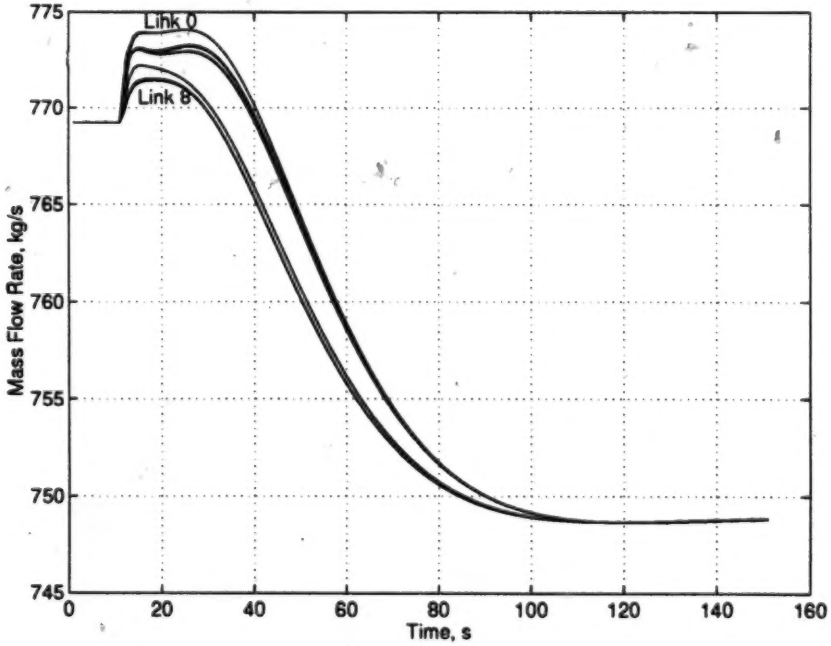

Figure 5.24: The circulation flow response to the step decrease of inlet water enthalpy.

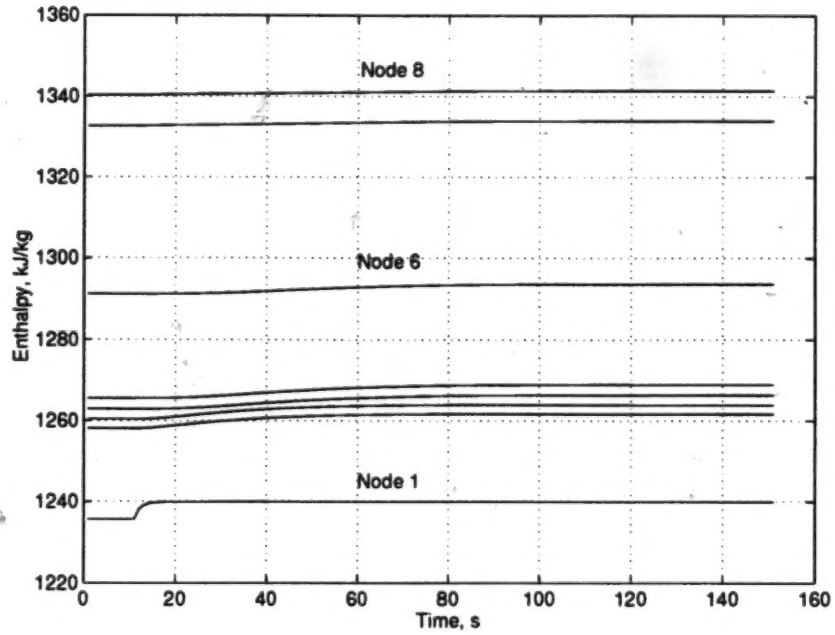

Figure 5.25: The response of heat enthalpy at each node under a step increase of inlet water enthalpy.

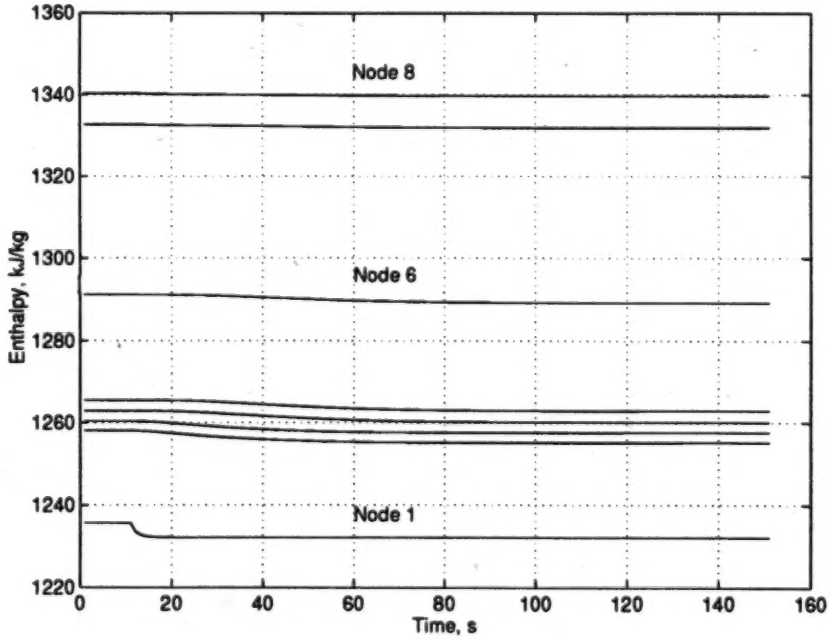

Figure 5.26: The response of heat enthalpy at each node under a step decrease of inlet water enthalpy.

The opposite situation occurs to the step decrease of inlet water enthalpy as shown in Figure 5.24. The enthalpy at each node is decreased due to the decreased inlet water enthalpy in an overdamped fashion as shown in Figure 5.26. The steam quality and pressure in two-phase section drops and the circulation flow slightly increases. After approximately 20 s, the circualtion flow recovers and settles at a lower steady-state value. As shown in Figure 5.23 and 5.24, the settling time for both cases is almost the same.

5.11 Conclusion

The hydraulic flow network concept and the numerical integration method from Porsching *et.al.* is adopted to simulate the circulation flow in the generation bank as model. The development of the model using the proposed method is explained in addition to the programming structure for the simulation. The simulation program adopts MATLAB as the operating platform and C code to maximize the performance. Step changes in inlet flue gas temperature and inlet water enthalpy are performed to examine the transient responses of the circulation circuit. The model is capable of showing important dynamics under the mentioned step changes which are validated using literature results. The circulation flow acts more vigorously to step changes in heat input. The circulation flow in downcomers decreases spontaneously at the increase of heat input. This inverse response also occurs at step decrease in heat input of which the settling time is approximately the same as that of the step heat increase. The step changes in inlet water enthalpy

have effects similar to those changes in heat input. The increased inlet water enthalpy causes a rise of enthalpy in each node. This in turn will slightly increase the pressure in two-phase section and a drop in circulation flow is observed. An opposite response is observed for the step decrease in inlet water enthalpy. The settling time for both cases under step changes in inlet water enthalpy is almost the same. This hydraulic flow network model is capable of predicting the inverse dynamics of the natural-circulation flow boiling. It is expected that a more elaborate transient analyses can be done, once this model is incorporated with the rest of the boiler components.

Chapter 6

Conclusions

This thesis has provided a detailed descriptions of the structures and functions of the utility boiler. This utility boiler is designed to generate steam at 94.5 kg/s using natural-circulation method and operating at subcritical pressure. The boiler includes a furnace, two superheaters, a steam drum, a mud drum, steam-generation circuit and an economizer. The natural-circulation circuit consists of the membrane side walls covering the furnace and the convective generation bank connected between steam drum and mud drum.

A theoretical background on two-phase flow and heat transfer is also provided. Two categories of two-phase flow - adiabatic and diabatic are identified in addition to two two-phase flow models - homogeneous and separated. Various two-phase friction multipliers and correlations for evaluating void fraction are shown. Heat transfer correlations for single phase and two phase are stated and discussed.

This thesis has successfully modeled the steam-generation circuit of the natural-circulation utility boiler. The modified transient circulation model from Kacaç *et.al* (Kakaç, 1991) steady-state natural-circulation model provides a satisfactory performance along with other boiler's components, such as furnace, super-

heaters, steam drum and economizer. This transient circulation model is able to generate the amount of steam which is in agreement with the nominal operating value. Different operating loads were also examined to study the responses of the circulation model. It is found that simulating the boiler model below nominal value reflects the salutary operation of the circulation circuit. That is, the circulation ratio is always larger than one. However, the circulation circuit of the front and middle side walls of furnace shows an adverse operating situation when the steam load is set at 103.9 kg/s. The water circulating rate decreases even though the steam generation rate increases due to the increased heat input. This is one of the characteristics of natural circulation. The larger pressure losses in heated risers induced by higher heat input do not correspond to increase in pressure differential; and therefore, the flow will decline. This suggests the utility boiler should not be operated at the steam load of 103.9 kg/s or higher.

The hydraulic flow network concept from Porsching *et.al.* (Porsching *et al.*, 1971) is adopted to investigate the feasibility for this approach to model the natural circulation. The convective generation bank is used as a model example. A heat transfer model using log-mean temperature difference theory is incorporated to simulate the heat input to the generation bank. The hydraulic flow network model is capable of predicting the inverse dynamics when the generation bank is under step heat changes and step inlet water enthalpy changes. The extent of the inverse dynamics response is more severe for step change in heat input than for step changes in inlet water enthalpy. This transient dynamic phenomenon is a crucial factor which contributes to the inverse dynamics observed from steam drum level

response in boiler operation.

6.1 Recommendations

Although the transient model modified from Kackaç *et. al.* (Kakaç, 1991) steady-state model is sufficient to show the agreement with data at steady state comparison, the actual dynamics of the circulation circuit during step changes in heat input and step changes in inlet water enthalpy caused by changes in feedwater flow rate has not been revealed. Therefore, if a more accurate model is required, this model has to be modified or other approaches may be used. The hydraulic flow network model is proved to be able to predict the important dynamics of the natural circulation - the inverse dynamics, but an extensive studies are needed to provide the overall dynamics of the boilers, especially the steam drum dynamics because control schemes are sensitive to the dynamics variations in steam drum. Therefore, the combination of this generation bank model using hydraulic flow network concept with the steam drum should be studied to further validate the method.

References

Abbott, M.M., & Vanness, H.C. (eds). 1976. *Thermodynamics.* Schaum's Outline Series. U.S.A: McGraw-Hill Book Company.

Bergles, A. E., Collier, J. G., Delhaye, J. M., Hewitt, G. F., & Mayinger, F. 1981. *Two-Phase Flow and Heat Transfer in the Power and Process Industries.* U.S.A.: Hemisphere Publishing Corporation.

Butterworth, D., & Hewitt, G.F. 1978. *Two-Phase Flow and Heat Transfer.* Oxford: Oxford University Press.

Cheres, E. 1990. Small and Medium Size Drum Boiler Models Suitable for Long Term Dynamic Response. *IEEE Transactions on Energy Conversion*, **5**(4), 686–692.

Chiu, A. 1996. *Dynamic Simulation of a Boiler System.* M. Sc. Thesis.

Coq, G. LE, Libmann, M., Raymond, P., Souchet, Y., & Sursock, J. P. 1983. The Triton Computer COde Finite Difference Methods for One-dimensional SIngle or Two-Fluid Flow Transient Computation. *Pages 495–512 of:* Plesset, Milton S., Zuber, Novak, & Catton, Ivan (eds), *Transient Two-Phase Flow.* Pasadena, California: Hemisphere Publishing Corporation.

de Nevers, Noel. 1991. *Fluid Mechanics for Chemical Engineers.* second edn. Toronto: McGraw-Hill, Inc.

Delhaye, J. M., Giot, M., & Riethmuller, M. L. (eds). 1981. *Thermohydraulics of Two-Phase Systems for Industrial Design Engineering.* Thermal and Fluids Engineering. U.S.A: Hemisphere Publishing Corporation.

Dollin F., *et.al.* 1970. *UK Steam Tables in SI Units 1970.* United Kingdom Committee on the Properties of Steam, London.

Eahhe, E., & Grigull, U. (eds). 1977. *Heat Transfer in Boiling.* U.S.A.: Hemisphere Publishing Corporation.

Felder, Richard M., & Rousseau, Ronald W. 1986. *Elementary Principles of Chemical Processes.* second edn. New York: John Wiley & Sons, Inc.

Gerald, Curtis F., & Wheatley, Patrick O. 1990. *Applied Numerical Analysis.* fourth edn. U.S.A.: Addison-Wesley Publishing Company.

Ginoux, Jean J. (ed). 1978. *Two-Phase Flows and Heat Transfer with Application to Nuclear Reactor Design Problems.* Thermal and Fluids Engineering. U.S.A.: Hemisphere Publishing Corporation.

Hansen, Arthur G. 1967. *Fluid Mechanics.* New York: John Wiley and Sons, Inc.

Incropera, Frank P., & Witt, David P. De. 1990. *Introduction to Heat Transfer.* second edn. Toronto: John Wiley & Sons, Inc.

Kakaç, Sadik (ed). 1991. *Boilers, Evaporators and Condensers.* New York: John Wiley & Sons, Inc.

Keenan, Josphen H., Keyes, Frederick G., Hill, Philip G., & Moore, Joan G. (eds). 1969. *Steam Tables.* New York: John Wiley & Sons, Inc.

Lee, Samuel S., Veziroglu, T. Nehat, & Kakaç, Sadik. 1976. Sustained and Transient Boiling Flow Instabilities in Two Parallel Channel Systems. *Pages 467–510 of:* Kackaç, S., & Mayinger, F. (eds), *Tw-Phase Flow and Heat Transfer,* vol. 1. Istanbul, Turkey: Hemisphere Publishing Corporation.

Moran, Michael J., & Shapiro, Howard N. 1993. *Fundamentals of Engineering Thermodynamics.* second edn. New York: John Wiley & Sons, Inc.

Perry, Robert H. (ed). 1984. *Perry's Chemical Engineers' Handbook.* sixth edn. Toronto: McGraw-Hill Book Company.

Porsching, T. A., Murphy, J. H., & Redfield, J. A. 1971. Stable Numerical Integration of Conservation Equations for Hydraulic Networks. *Nuclear Science and Engineering,* **43**, 218–225.

Rivkin, Solomon L., Aleksandrov, Aleksey A., & Kremenevskaya, Elena A. 1978. *Thermodynamic Derivatives for Water and Steam.* International Association of the Properties of Steam, U.S.A.

Shoukri, M. 1980. *Effect of Heat Addition on the Pressure Drop in Two-Phase Flow Systems.* Tech. rept. Ontario Hydro Research Division, Ontario.

Singer, Joseph G. (ed). 1981. *Combustion — Fossil Power Systems.* third edn. Windsor: Combustion Engineering Inc.

Stultz, S. C., & Kitto, J. B. (eds). 1992. *Steam — Its Generation and Use.* fortieth edn. U.S.A.: The Babcock & Wilcox Company.

Tong, L. S. 1965. *Boiling Heat Transfer and Two-Phase Flow.* New York: John Wiley & Sons, Inc.

Appendix A

Simulink Block Diagrams of the Dynamic Circulation Model

The simulink block diagrams for the dynamic circulation model is presented in this appendix.

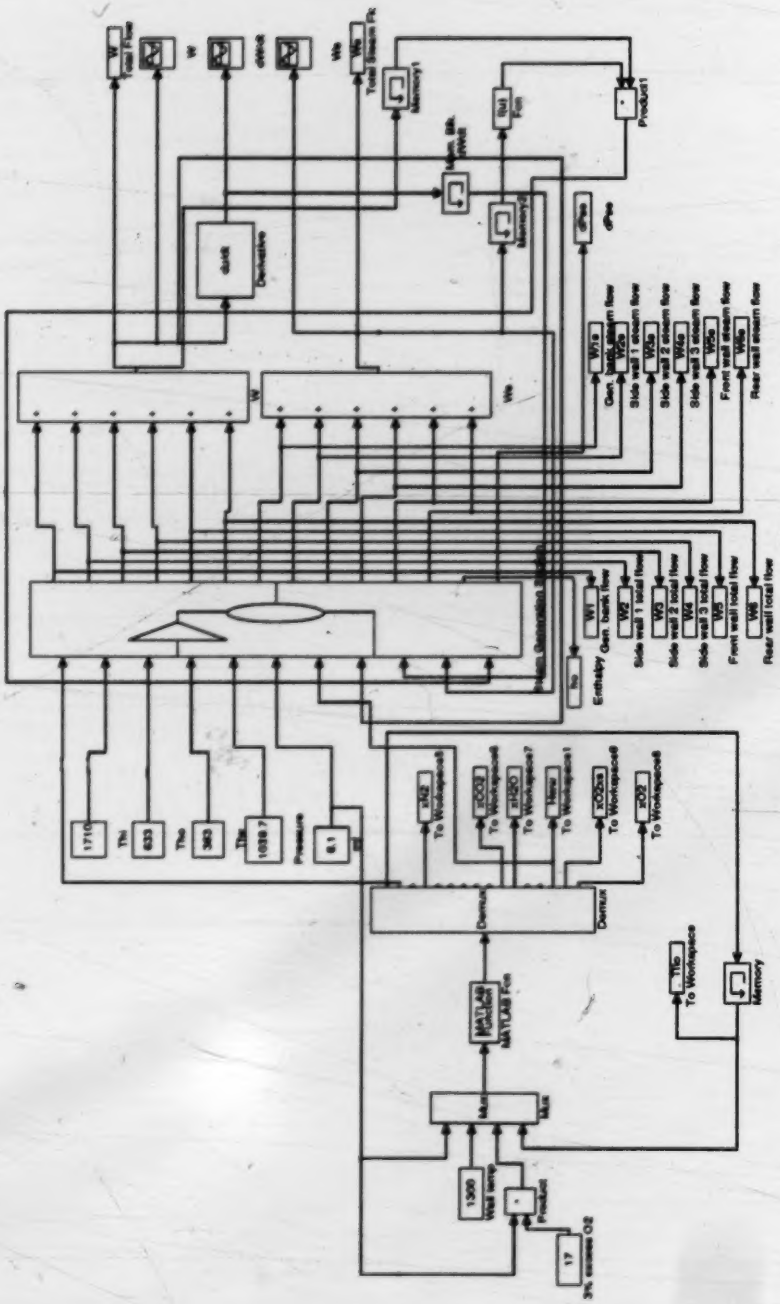

Figure A.1: First level of the model.

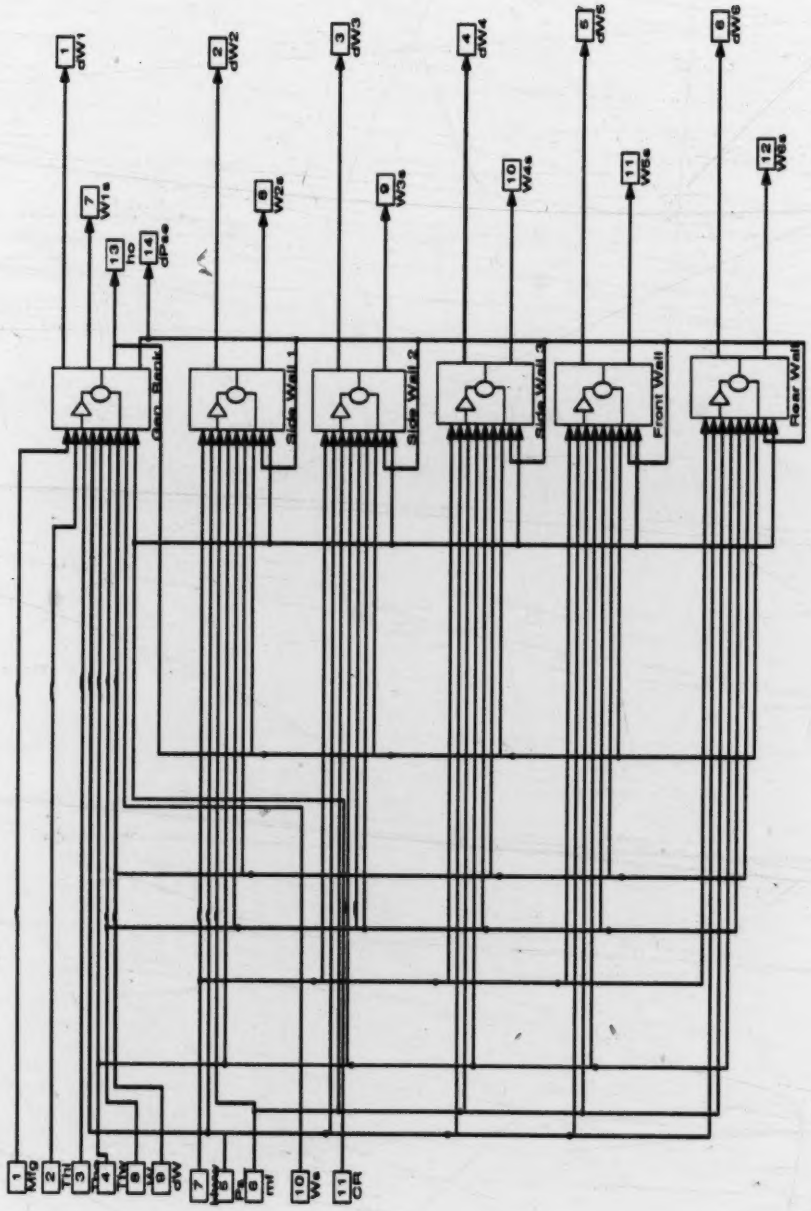

Figure A.2: Second level of the model.

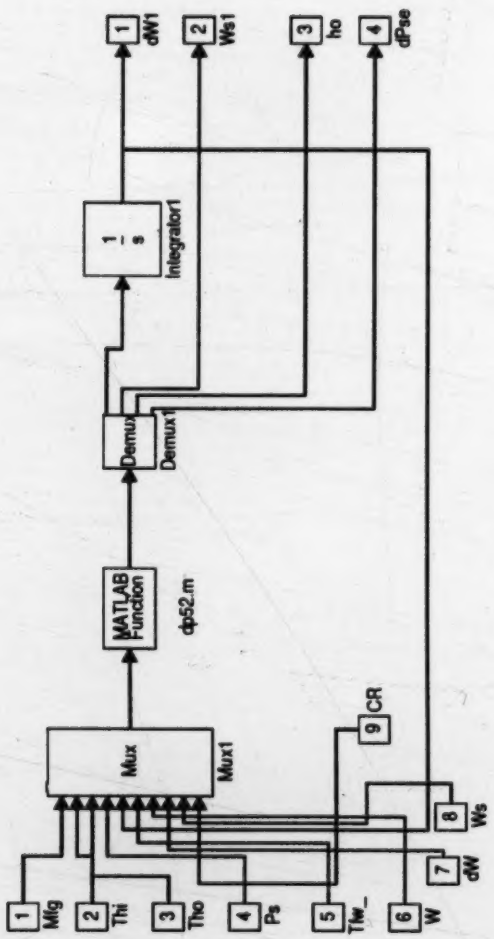

Figure A.3: Third level of the model.

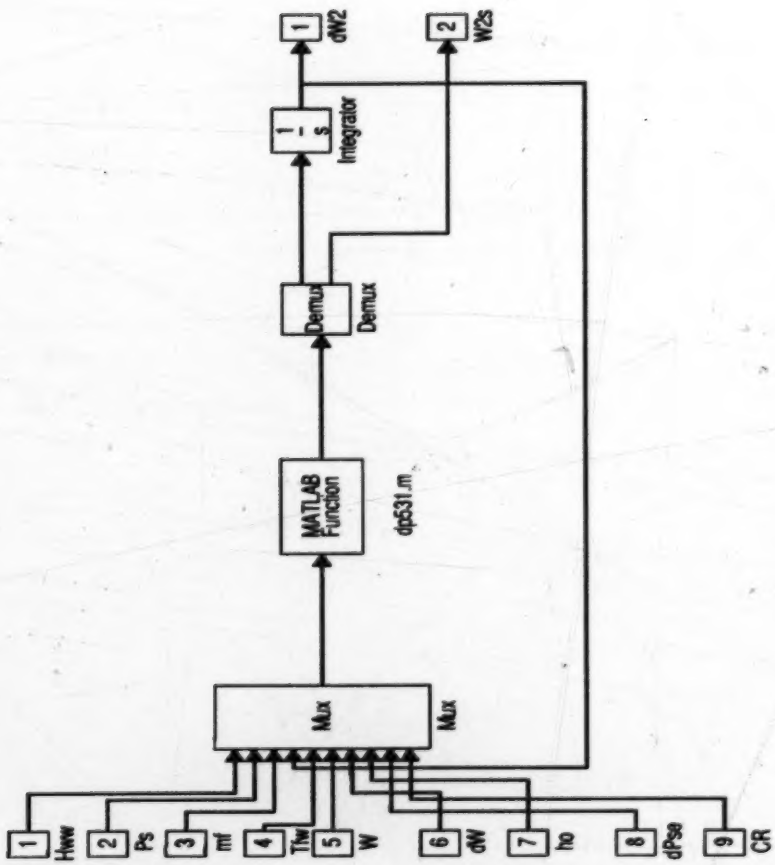

Figure A.4: Third level of the model.

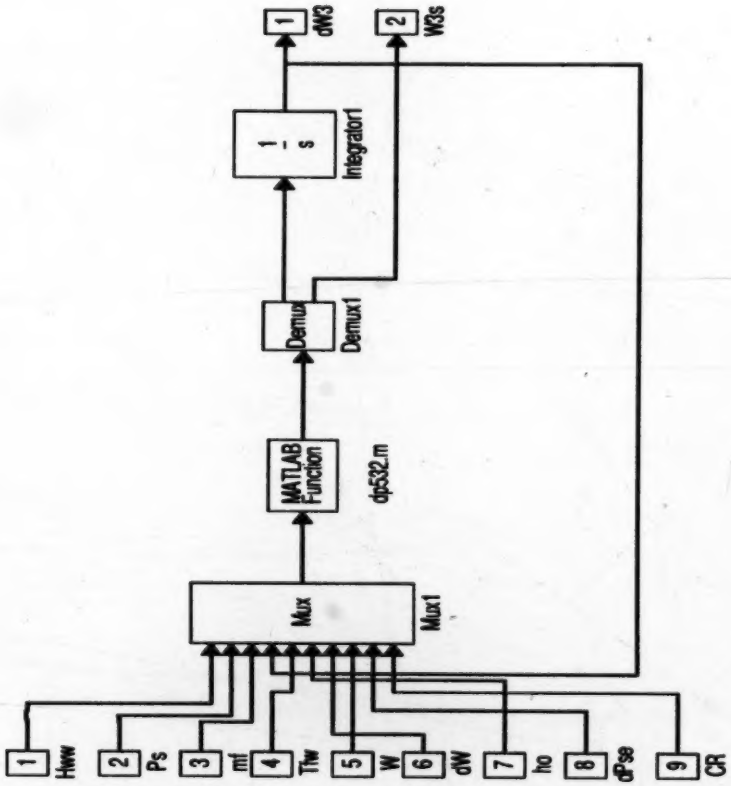

Figure A.5: Third level of the model.

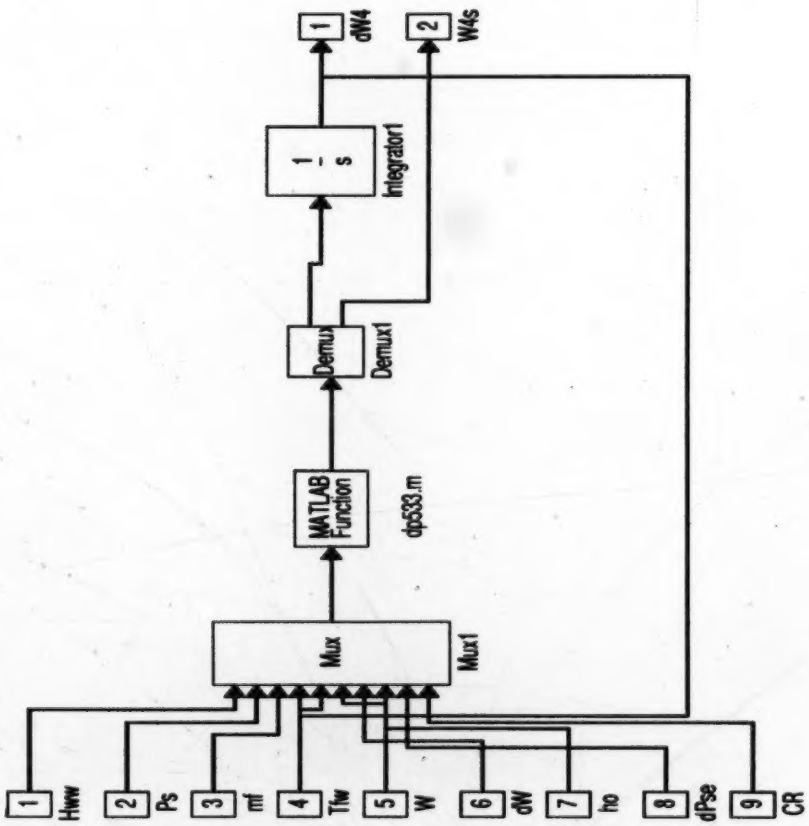

Figure A.6: Third level of the model.

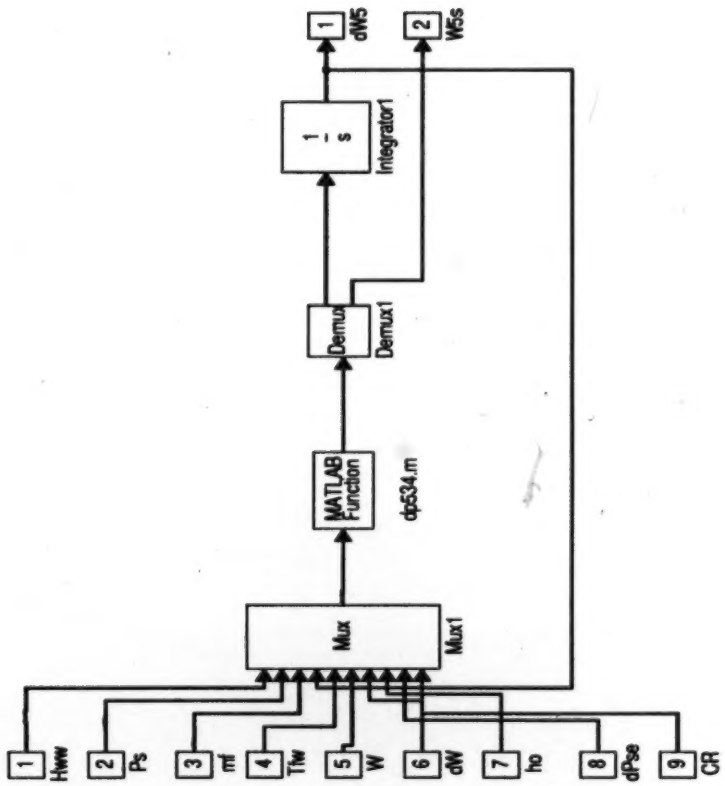

Figure A.7: Third level of the model.

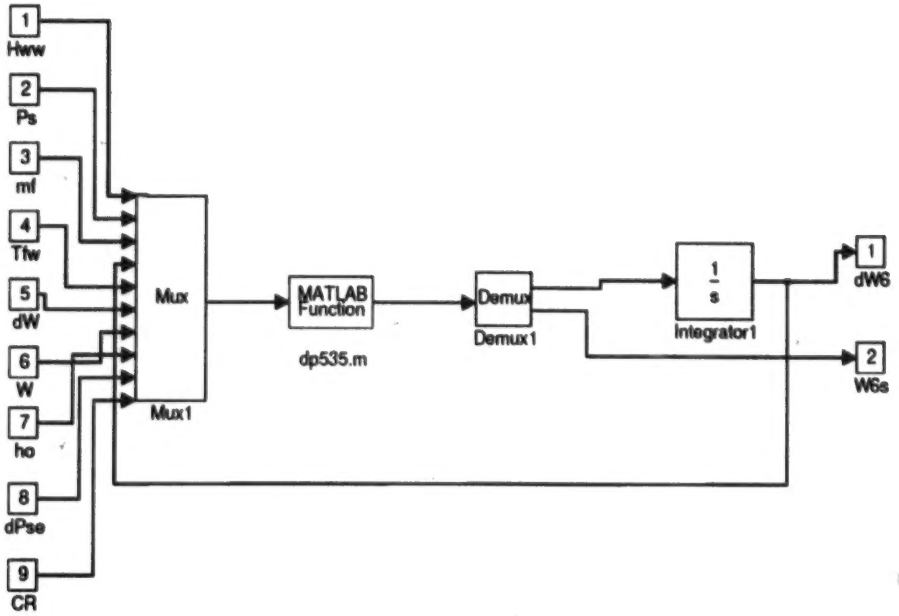

Figure A.8: Third level of the model.

Appendix B

The Derivation of the Homogeneous and Separated Flow Model

This appendix presents the derivation of the homogeneous and separated flow model mentioned in Chapter 3. The formulations used can be found in Ginoux (1978).

Consider the flow of a two-phase fluid in a channel of constant cross-sectional area, A, and constant periphery, S. The momentum balance over a length δl is as follows:

$$\int_A \left[p - \left(p + \frac{dp}{dl}\delta l\right)\right] dA = \int_S \tau_o \delta l ds + \int_A \frac{d}{dl}(G_f V_f + G_g V_g) dA + \int_A \rho g \delta l dA \quad \text{(B.1)}$$

For homogeneous model, the two-phase fluid is considered to be homogeneously mixed and travelling at the velocity through the channel. Therefore, the corresponding accelerational and gravitational terms for the homogeneous model are as follows:

$$-\frac{dp}{dl}_{acceleration} = \frac{1}{A}\int_A \frac{d}{dl}(G_f V_f + G_g V_g) dA \quad \text{(B.2)}$$

$$= \frac{d}{dl}[G(1-x)GV + GxGV] \quad \text{(B.3)}$$

$$= G^2 \frac{dv}{dl} \quad \text{(B.4)}$$

$$-\frac{dp}{dl}_{gravitation} = \frac{1}{A}\int_A g[\alpha\rho_g + (1-\alpha)\rho_f] dA \quad \text{(B.5)}$$

$$= \rho g \quad \text{(B.6)}$$

For constant shear stress wall, the frictional term is as follow:

$$-\frac{dp}{dl}_{friction} = \frac{\tau_o S}{A} \quad \text{(B.7)}$$

For separated model, the two phases are separated, but assumed to be in equilibrium. The accelerational and gravitational terms for the separated model

are as follows:

$$-\frac{dp}{dl}_{acceleration} = \frac{1}{A}\int_A \frac{d}{dl}(G_f V_f + G_g V_g)dA \tag{B.8}$$

$$= \frac{1}{A}\frac{d}{dl}\left[\frac{G^2(1-x)^2 V_f A_f}{(1-\alpha)^2} + \frac{G^2 x^2 V_g A_g}{\alpha^2}\right] \tag{B.9}$$

$$= G^2\frac{d}{dl}\left[\frac{(1-x)^2}{1-\alpha}V_f + \frac{x^2 V_g}{\alpha}\right] \tag{B.10}$$

$$-\frac{dp}{dl}_{gravitation} = \frac{1}{A}\int_A g[\alpha\rho_g - (1-\alpha)\rho_f]dA \tag{B.11}$$

$$= \frac{g}{A}[\rho_g A_g + \rho_f A_f] \tag{B.12}$$

$$= g[\rho_g\alpha + (1-\alpha)\rho_f] \tag{B.13}$$

The frictional term for separated model is the same as that of the homogeneous model.